A Comparative Study on the Influence of Obstacles on Flame Propagation in Dust and Gas Mixtures

An experimental study of confined and vented scenarios
in a 3.6 meter flame acceleration tube

Kjetil Lien Olsen

A thesis submitted in partial fulfillment of the
requirements for the degree of *Master of Science* in
the subject of Physics; Process Safety Technology

Department of Physics and Technology
University of Bergen
Bergen, Norway
June 2012

Preface

The present work is a master thesis that all the graduate students at the master program of Process Safety Technology at the Department of Physics and Technology (IFT) at the University of Bergen (UiB), have to submit as a part of the Master of Science degree. The experimental work has been done at the premises of GexCon AS at Fantoft in Bergen, Norway.

Acknowledgements

A great deal of thanks goes to various companies and people for helping me acquire different parts and equipment needed to do the experimental work. Special thanks go to Tine Meierier AS for providing an old dairy tank free of charge and to Kvaerner Stord AS for donating a stainless steel tube. Rolf Wee Transport helped with transportation when I was in dire need, and Fjell industrier supplied stainless steel parts for the dairy tank.

My superb supervisor Trygve Skjold supplied me with valuable input, encouragement and positive thinking throughout the work with the thesis. The highly skilled mechanics at the workshop at IFT deserve their share of gratitude for their precise craftsmanship that have supplied me with specially designed parts, which without, the experiments would not have been possible to perform.

The staff of the Labs department at GexCon AS have been helpful with answering stupid questions and made the days confined in solitude in the basement to a much more social thing than expected. The staff includes Knut Sømoe, Ivar Kalvatn, Gisle Andrè Enstad and Matthijs van Wingerden.

Special attention should be given to the people who used their precious time to read through my thesis, decorating with the red pen while providing valuable feedback and corrections. These include my brother, Andreas lien Olsen, Erlend Wangsholm, Ivar Kalvatn, Helene H. Pedersen, Camille Azzi, Kees van Wingerden and of course my supervisor Trygve Skjold. My brother also supplied his superb software coding skills to help me with processing the raw data from the experiments to something more useful.

Many people have made the years as a student at the University of Bergen to a special time, which I will remember for the rest of my life. Special attention should be directed to Linn Ringdal, Marianne W. Steiner, Eivin B. Larsen, Solveig Risøen and Kristian Gundersen for an unforgettable semester at The University of Western Australia. Natalja Pedersen should also be mentioned for her positive thinking and companionship. There are of course many, many more people who should be mentioned by name here, but unfortunately there is not enough room for everybody. Their share of the gratitude lives on in my spirit.

Finally, I would like to thank my parents, Bjørn Olsen and Aud Lien for their loving support and encouragement to acquire a higher education as well as financial help throughout the years as a poor student. I would have to live with an unforgettable shame if I did not express my gratitude to my brother Andreas and sister Ragnhild for their loving care and support throughout the years.

Cheers!

Kjetil Lien Olsen

II

Abstract:

This thesis describes an experimental investigation of flame propagation in a 3.6-meter Flame Acceleration Tube (FAT) with square 0.27m x0.27m cross section. The experiments in the FAT took place at the premises of GexCon AS at Fantoft, Bergen.

Constant volume and vented explosion experiments with initial turbulence were performed, with and without baffle plates to induce additional turbulence in the flow. Experiments with both maize starch and propane-air mixtures were conducted. The use of a dump tank with a water deluge system allowed vented experiments to be conducted inside. The previous data acquisition system was reviewed and a new pressure measurement system has been tested.

Plexiglas windows equally spaced along one sides of the FAT allowed flame propagation to be recorded with a high-speed video camera.

The unique design of the flame acceleration tube allows for comparative studies of flame propagation in gaseous mixtures and dust clouds under the same initial conditions. The experimental data has been analyzed with an aim to identify fundamental differences between gaseous flames and dust flames, suited for research purposes and validation work of computational fluid dynamic codes for both gas and dust explosions.

The introduction of additional obstacles in the tube resulted in enhanced flame acceleration for both gas and dust mixtures. The obstructions induced sufficiently high turbulence levels to give a strong indication of local quenching of the dust flames, since the denser obstacle configuration resulted in less flame acceleration than observed for the configuration with half the number of obstacles. The experiments performed with gaseous mixtures and obstacles produced such high explosion pressures that it was decided not to precede with the planned explosion series due to both safety reasons and the damage inflicted on the experimental apparatus.

The effect of the different venting areas was as foreseen, where reduced vent area resulted in an increase in the reduced explosion pressure, for both fuel types. In general, the gaseous mixtures produced the highest pressures and the fastest pressure build-up.

Flame propagation in a dust clouds can be characterized as premixed combustion with non-premixed substructures. Hence, the degree of volumetric combustion in clouds of maize starch, relative to rich propane mixtures, were investigated, and a clear difference in behavior during the early stages of flame propagation was found. A comparison between the measured pressure histories and recorded flame front positions suggested that the flame fronts of the dust clouds requires a certain induction length before a relative sudden increase in the rate of pressure rise takes place.

Table of Contents

Nomenclature:

Latin symbols:

p	Absolute pressure
S_L	Laminar burning velocity
S_T	Turbulent burning velocity
V	Volume of Enclosure
l	Turbulent length scale
n	Number of Moles of Gas
R	Universal gas constant
T	Temperature
K_{st}	Measure of reactivity for dusts
P_{red}	The maximum pressure that an enclosure can withstand without bursting
P_{stat}	The maximum static pressure inside an enclosure before the vent process starts
C_d	Dust concentration
u'_{rms}	RMS Turbulent Velocity Fluctuation

Roman symbols:

ϕ	Equivalence ratio
k	Turbulent kinetic energy
ε	Dissipation of turbulent kinetic energy
ν	Kinematic viscosity
δ_l	Laminar Flame Thickness.
λ	Detonation cell size

Dimensionless groups:

Re	Turbulent Reynolds number
Da	Turbulent Damköhler number
Ka	Turbulent Karlovitz number

Abbreviations:

UiB	University of Bergen
IFT	Department of Physics and Technology, UiB
CSB	Unites States Chemical Safety Board
CEN	European committee for standardization
CFD	Computational Fluid Dynamics
CMI	Chr. Michelsen Institute
CMR	Christian Michelsen Research
FLACS	CFD-code, Flame ACceleration Simulator
DESC	CFD-code, Dust Explosion Simulation Code
FAT	Flame Acceleration Tube
LFL	Lower Flammability Limit
UFL	Upper Flammability Limit
FA	Fuel-Air ratio

1. Introduction

1.1 Motivation

Flammable dusts represent a significant hazard in the process industry. Numerous explosions occur each year, resulting in severe damage to both personnel and equipment. More than 70 percent of the dusts handled in the industry are combustible[1]. Dust explosions are often hidden hazards, an extensive study conducted by the Unites States Chemical Board (CBS) [2] shoved that combustible dust used in the United States were only marked as hazardous in 41 percent of the cases. A dust explosion may occur if a sufficient amount of combustible dust is dispersed in air to form an explosive cloud and there is an ignition source present. The dynamics of a dust explosion are influenced by numerous factors, including chemical composition, particle size, dust concentration, moisture level and many more. The release of energy from the combustion process causes the reaction products to expand. This expansion induces flow and pressure waves ahead of the flame front, which promotes turbulent flow conditions. Flow past obstacles results in turbulent wakes, more turbulence, enhanced rate of combustion and hence more violent explosions.

1.1.1 Accidental dust explosions and hidden hazards:

In industrial countries, one dust explosion happens each day[3], and recent studies by the CSB shows that in the United States alone, there were at least 281 dust explosions between 1980 and 2005. In the reported explosions, there were at least 119 Fatalities and 718 injuries. An example of one of the reported accidents is the polyethylene dust explosion at West Pharmaceutical in North Carolina on January 29, 2003, where 6 people lost their life and 38 was injured[4]. The polyethylene dust came in a slurry to the plant and the material safety data sheet therefore did not mark the resulting dust as combustible. After it dried out, the dust became highly flammable. The production area was kept clean, but the suspended ceiling was not checked, hence allowing dust to sediment out on top of the work area with a catastrophic end result.

Dust explosions occur in a wide range of industries where different types of combustible dust are handled. These industries include[5]:
  i.   Wood processing;
  ii.   Grain elevators, bins and storage;
  iii. Fluor and feed mills;
  iv.   Manufacturing and storage of metals such as aluminum and magnesium;
  v.   Production of: plastics, starch, candy, spices, sugar, cocoa and many more;
  vi.   Coal handling and process area;
  vii. Pharmaceutical plants.

Abbasi[5] suggested that the number of reported dust explosions in developing countries, like India, may be severely underestimated. The reason for this is twofold: The term "explosion" often is used when incidents are being reported, not what caused the explosion, and most people have the perception that an explosion is what happens only when pressurized vessels burst or explosives are being used. This under-reporting of accidents could mean that the work done for prevent dust explosion does not reach the developing countries, thus allowing dust and powder explosions that otherwise could be prevented if the knowledge of the hazards were available.

1.1.2 Risk management

The risk of a hazardous event could qualitatively be described with the general function;

$$Risk = f(Probability, Consequence)$$

Hence, a frequent occurring low-consequence event may represent the same risk as a low probability high-consequence event. The risk of an event is often described using a risk matrix as shown in Figure 1.1. In a risk matrix, the consequence and probability of an event are normally graded on a scale from low to high. The criterion of how severe a risk might be, before actions to lower the risk have to be implemented, is set in each specific situation by the company or in reference to national or international guidelines.

CONSEQUENCE			
HIGH	MEDIUM RISK	HIGH RISK	IMMINENT RISK
MEDIUM	LOW RISK	MEDIUM RISK	HIGH RISK
LOW	NEGLIGIBLE RISK	LOW RISK	MEDIUM RISK
	LOW	MEDIUM	HIGH

PROBABILITY

Figure 1.1 : *The risk matrix.*

1.1.2.1 Prevention and mitigation of dust explosions

All fires occur when fuel in the presence of an oxidizer is exposed to a heat source (ignition source). If one of the essential elements above is removed, the possibility of a fire occurring gets eliminated. This is often illustrated with the fire triangle as shown in Figure 1.2.

Figure 1.2 : *The fire triangle* **Figure 1.3 :** *The dust explosion pentagon*
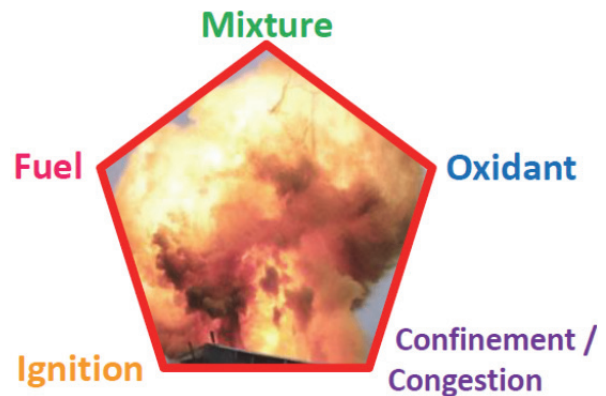
In order to get a dust explosion, there are two more essential elements needed: confinement/congestion and mixing. This was first emphasized by Kauffman[6] where he proposed the dust explosion pentagon as shown in Figure 1.3. Mixing of the reactants implies that the dust have to be suspended in the air as it burns. If a burning dust cloud is confined (partially confinement is sufficient) the pressure will build, potentially causing damage. Removal of either confinement/congestion or mixing will prevent an explosion, but a fire might still occur. One of the main differences between a fire and an explosion is the degree of mixing of the reactants. In a fire, the reactants are not mixed prior to

combustion, while a dust explosion might be categorized as a premixed combustion with non-premixed substructures[7].

There are two main strategies of reducing the risks associated with dust explosions, prevention and mitigation. Prevention or reducing the probability can be divided into subcategories: Prevent the formation of an explosible dusts cloud, and the elimination of an ignition source. Mitigation focuses on how to minimize the consequence if the explosible atmosphere gets ignited. Eckhoff [8, 9] presents a detailed description of how to implement the different preventive and mitigation strategies as shown in Table 1-1.

Table 1-1 : *Means of prevent and mitigating dust explosions: a modified schematic overview[8]*

Prevention		Mitigation
Prevent/Removing Ignition Sources	**Prevent Explosible Dust Clouds**	**Mitigation**
Smoldering combustion in dust, dust flames	Inerting by N_2, CO_2, and rare gasses	Partial inerting by inert gas
Other types of open flames (e.g. hot work)	Intrinsic inerting	Isolation
Hot surfaces	Inerting by adding inert dust	Vent
Electric sparks, arcs and electrostatic discharges	Inherent safety	Pressure-resistant construction
Heat from mechanical impact (metal sparks and hot spots)	Dust concentration outside explosible range	Automatic suppression
		Good housekeeping (dust removal and cleaning)

No two process plants are the same and the hazards may be significantly different in different plants, even if they produce the same materials. To prevent accidents, one should therefore try to classify the hazardous areas of the facility to identify the areas where special attention should be taken in reference to possible ignition sources. It is important to emphasize that the risk associated with a process might be significantly reduced by combining different methods. This is nicely illustrated in Figure 1.4, where both passive and active mitigation techniques have been installed on the different components in a production stream.
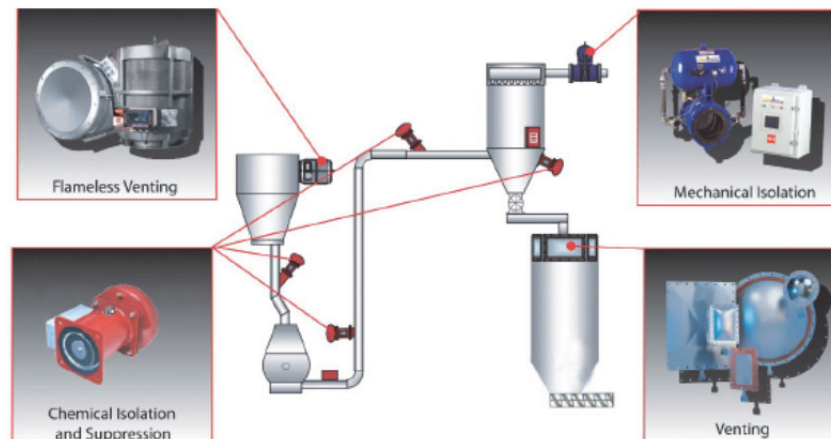

Figure 1.4 : *The use of numerous combined mitigation techniques to increase the safety associated with the process stream[10]*

Mitigation by explosion venting:

The maximum pressure obtained in an explosion may be significantly reduced if there is a possibility to vent unburned mixture and the hot combustion products from the enclosure. This is referred to as explosion venting. The basic principle of explosion venting is the competition between two processes[9]:

- Burning of the explosive cloud and generation of heat, which increase the pressure.
- The flow of burned and unburned mixture through the vent opening, which decrease the pressure buildup inside the enclosure.

It is possible to use vent of both gas and dust explosions, but it is most commonly used in the dust handling industries. There are several important physical and chemical parameters to take into account when designing an explosion protection system based on vent:

- The volume and aspect ratio of the enclosure.
- The maximum pressure that the enclosure can withstand without bursting, P_{red}.
- The opening pressure of the vent, P_{stat}.
- The mass of the vent cover.
- The reactivity of the mixture, normally described by the maximum pressure rise, $\left(\frac{dp}{dt}\right)_{max}$.

The design and installation of vent devices are specified in national and international standards. Norway has adopted the standards from the European Committee for Standardization (CEN). For gas explosion vent, NS-EN 14994[11] is the current standard, while for dust explosion venting the standard is NS-EN 14491[12]. These standards provide guidelines on how to design and implement vent in process facilities and equipment. This is done by use of empirical equations based on experimental data.

When designing a process facility, there may be situations where explosion venting is not the optimal solution. The substance causing the explosion might be toxic or harmful to people and the environment. In such situations, other means of explosion mitigation should be implemented. Certain precautions should be taken with respect to vent of enclosures[13]:

- There may be created a flammable cloud outside of the enclosure.
- It may cause short or long term health problems to personnel.
- Dusts could be an environmental pollutant.
- The vented material is lost from the production.
- It may be harmful in ways of public relations and the reputation of the company.
- National and international regulations may be broken in terms of pollution.
- There may not exist a way of controlling the spread of released materials.

To reduce the hazards of secondary explosions outside of the vented enclosure, specially designed vent systems, such as quenching tubes and vent ducts may be applied.

1.1.2.2 Computational Fluid Dynamics

Computers become more and more powerful. This increase in computer power has enabled the use of computational fluid dynamics (CFD). When applying CFD, the calculation domain (geometry) is sub divided in many cells (referred to as a control volume). In each of the cells, conservation equations are solved for conservation of mass, momentum, enthalpy, turbulent kinetic energy and dissipation of turbulent kinetic energy. The equations are solved by many finite steps[14].

FLACS (Flame ACceleration Simulator) is a CFD code which has been under development by the Christian Michelsen Institute (CMI), Christian Michelsen Research (CMR) and GexCon AS since the early 1980's. FLACS is extensively used around the world to predict the consequence of accidental

explosions. The code has been thoroughly validated against experiments for a wide range of scenarios, including release and dispersion of toxic and flammable materials.

The FLACS code is a three dimensional code which uses a finite volume method on a Cartesian grid. To simulate the fluid flow, FLACS solves transport equations for mass, momentum, enthalpy, fuel and mixture fractions. The turbulence is modeled with a k-ε model for the turbulent kinetic energy (k) and the dissipation of turbulent kinetic energy (ε). The distributed porosity concept is used to represent complex geometry on relative course computational meshes[15].

The Dust Explosion Simulation Code (DESC) is a special version of the FLACS code that was developed for predicting the potential consequences of industrial dust explosions in complex geometries[14]. One of the most important parameters with respect to explosion simulations is the turbulent burning velocity (S_T). There have been many attempts to model S_T, where typical correlations may be on the form:

$$S_T = f(S_L, \, C_d, \, u'_{rms}, l, p, T, \ldots \ldots)$$

S_L is the laminar burning velocity of the mixture (representing the reactivity). The dust concentration, C_d serves as a measure of how much flammable material there is in the system and whether the mixture is explosible or not. In a gaseous explosion this would be represented by the explosible limits and mixture fractions. The root mean squared value of the velocity fluctuation, u'_{rms} represents the degree of turbulent mixing in the system, l is a characteristic turbulent length scale, p is the pressure and T is the temperature.

This is a typical list of the different parameters used to calculate the turbulent burning velocities, and others might be added in specific simulations. A brief description of some of the parameters can be found in Chapter 2.

1.2   Aim of the Current Work

The motivation for the present work described here is to study how different obstacle and vent configurations influence flame propagation during dust explosions. The experiments were performed in a 3.6 meter Flame Acceleration Tube (FAT), inner cross-sectional area 0.27 x 0.27 m. The unique design of this experimental apparatus makes it possible to study the propagation of dust flames in a square channel with obstacles. Literature data on equipments in obstructed geometries involving dust are not easily obtained.

It is possible to mount obstacles along the entire length of the FAT, and vary the spacing between the obstacles to manipulate turbulence generation. Since there exist no possibility to measure turbulence directly during the experiments, reference tests with gaseous fuels were also conducted. A systematic comparison of dust and gas explosions in the same apparatus may lead to new knowledge on explosion phenomena such as the degree of volumetric combustion for dust flames compared to gaseous flames. The results from both the gaseous and dust experiments will be useful for model validation for the commercial computational fluid dynamics (CFD) codes FLACS and DESC.

Figure 1.5 : *The Flame Acceleration Tube and dump tank used in the experimental work*

The experiments consist of both constant volume and vented explosion experiments with either propane-air mixtures or mechanically suspended dust clouds of starch in air.

In the experiments, the flammable mixtures are ignited in the closed end of the channel, thermocouples at regular intervals measures flame propagation along the length of the tube, and piezoelectric pressure transducers measure the pressure development. A high-speed camera records the flame from a distance of approximately seven meters to visually observe the flame propagation through plexiglas windows located at the same distance from the ignition point as the thermocouples.

A dump tank of approximately 5m^3 was acquired and fitted with an entry tube and a water deluge system. This made it possible to conduct vented dust and gas experiments inside the test-facility hall where the apparatus is located.

2. Theory and Previous Work

2.1 Definitions and Basic Concepts

2.1.1 Combustion

Fire and the knowledge of how to control a flame is probably the main reason that we as the human race have managed to evolve and move out of the cave thousands of years ago. In spite of technological advancements and new thinking, combustion still represents about 90 percent of the global energy consumption[17]. To get a better understanding of the combustion phenomenon, it is helpful to first find a definition for combustion. This should be fairly straightforward, but apparently there is no generally accepted definition. There are many twists and turns in the literature about this, but there are some things that there seems to exist agreement about. This is stated by Babrauskas [18] in the "Ignition Handbook" that states that combustion is "*a self-sustained, high-temperature oxidation reaction*".

Combustion can be described as a self-sustained chemical reaction. This implies that there is no need for additional energy to support flame propagation when the reaction has been initiated. A simplified combustion reaction consists of two main reactants, a fuel and an oxidizer, where in most cases, the oxidizer is gaseous air.
A simple overall combustion reaction for a linear hydrocarbon may be expressed as:

$$C_{nc}H_{nh} + aO_2 \rightarrow ncCO_2 + bH_2O + \text{Energy(heat)} \qquad \text{Equation 2.1}$$
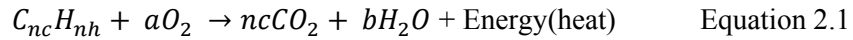
where the subscripted values indicate the total number of the different elements. The stoichiometry of a reaction refers to the exact amount of oxidizer to completely oxidize all of the fuel. A combustible mixture is said to be lean or rich in reference to the stoichiometric ratio. If there is an excess of air, the mixture is said to be *lean*, and if there is an excess of fuel, the mixture is said to be *rich*. The stoichiometric ratio of the oxidizer in reference to Equation 2.1 can be expressed as:

$$a = nc + \frac{nh}{4} \qquad \text{Equation 2.2}$$

For the combustion of propane (C_3H_8), which is the primary gaseous fuel in the present work, Equation 2.1 becomes:

$$C_3H_8 + 5O_2 \rightarrow 3CO_2 + 4H_2O + \text{Energy(heat)} \qquad \text{Equation 2.3}$$
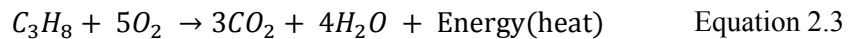
It should be emphasized that the above reaction is a crude simplification of the actual chemical reactions taking place in a combustion reaction, and can be considered as the reduced mechanisms of the reaction. A more detailed view of the different steps (elementary reactions) can be found in the literature and will not be discussed here, see e.g. Warnatz [17].

If the oxidizer is provided by gaseous air (oxygen), the fuel-air ratio and hence the equivalence ratio ϕ is commonly used to describe the stoichiometry of the mixture as:

$$(FA)_{mixture} = \frac{mass\ fuel}{mass\ air} \qquad ; \qquad \phi = \frac{(FA)_{mixture}}{(FA)_{Stoichiometric}} \qquad \text{Equation 2.4}$$

$\phi < 1$: Fuel lean mixture

$\phi = 1$: Stoichiometric mixture

$\phi > 1$: Fuel rich mixture

The nature of a flame is given by the initial condition and the fluid motion at the time of ignition. The fuel and the oxidizer may either be mixed prior to ignition (premixed) or the mixing and the combustion occur in the flame zone (non-premixed). If the mixture is not premixed, the diffusion of reactants controls the flame. This result in a somewhat more complex chemical composition across the flame zone compared to that of a premixed flame. This increased complexity comes from the different equivalence ratio (ϕ) across the flame, where the range of the ratio could go from zero at the oxidizer side to infinite on the fuel side[17].

Some examples of different flame types are given in Table 2-1, turbulent premixed combustion will be discussed in detail in section 2.1.3.

Table 2-1: *Examples of combustion systems with regards to flow type[17].*

Fuel \ oxidizer mixing	*Fluid motion*	*Example*
Premixed	Turbulent	Spark-ignited gasoline engine
	Laminar	Bunsen flame
Non-premixed	Turbulent	Compression-ignited diesel engine
	Laminar	Burning of a brick of wood

2.1.1.1 Laminar burning velocity, flammability limits and explosion pressure of gaseous fuel

As the concentration of flammable gas in a mixture increases or decreases away from the stoichiometric concentration at a given temperature and pressure, it will eventually reach two finite limits where the mixture will not be able to propagate a flame. These limits are called the lower flammability limit (LFL) and the upper flammability limit (UFL) for the given substance[8]. These values are obtained from standardized tests where the most commonly used is the test developed by the US Bureau of Mines[19]; flammability limits are quite easily available in the open literature.
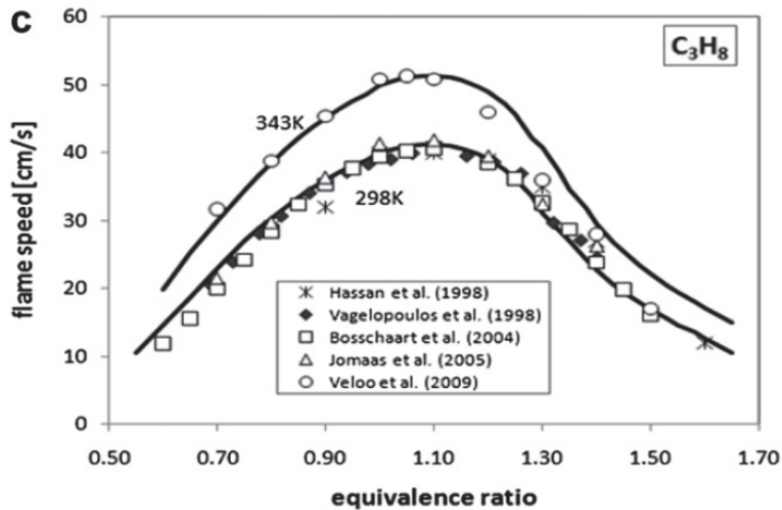
Figure 2.1 : *Laminar flame speed for propane at ambient pressure[20]*

Figure 2.1 illustrates the laminar flame speed for propane; the reactivity of the mixture is dependent on the stoichiometry of the mixture, where a slightly rich mixture will have the highest burning velocity. The velocities of the mixtures systematically decrease as the mixture fraction moves away from the stoichiometric mixture and approaches the flammability limits. The reaction zone e.g. the laminar flame thickness (δ), for common hydrocarbon mixtures usually have a thickness in the order of 1 mm[9].

The interdependence of various parameters which influence the explosion pressure is described by the equation of state for an ideal gas[5] as:

$$p = \frac{nRT}{V}$$

Equation 2.5

Where p is the pressure, V is the volume of the enclosure, n is the total number of moles in the mixture, T is the temperature in Kelvin and R is the universal gas constant. Different apparatus give varying peak pressures as shown by Razus [21] in Figure 2.2, where 3 different constant volume apparatuses are being used to find the maximum peak pressure for propane-air mixtures. The deviation between the peak pressures measured in the different apparatuses, may be explained by numerous factors such as heat loss to the vessel walls and turbulent conditions.
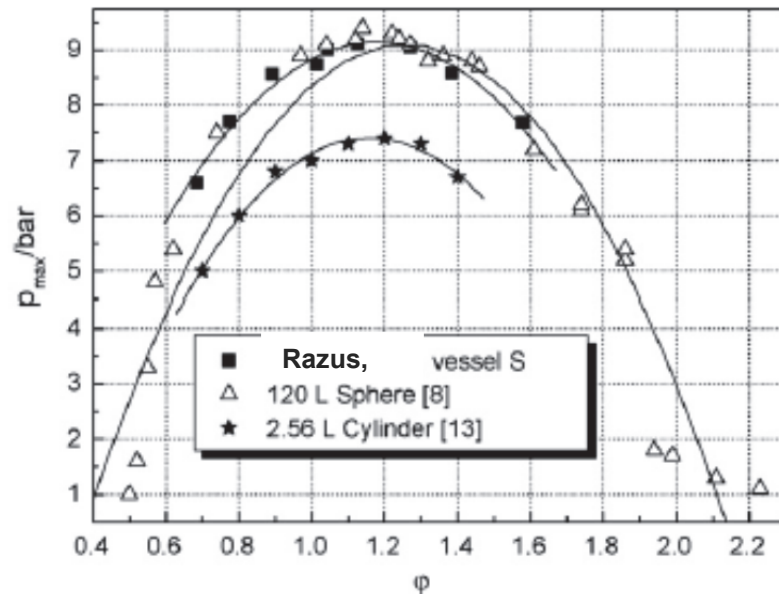
Figure 2.2 : *Peak explosion pressure of propane-air mixtures at ambient initial conditions [21]*

As shown by Razus, the maximum pressure is highest for slightly rich mixtures and decreases for leaner or richer mixtures. Common hydrocarbons have a peak pressure in the range of 8-9 bar. The maximum pressure reached in a constant volume explosion with an aspect ratio of 1 is proportional to the initial pressure. If two identical mixtures in the same apparatus of 1.0 and 1.5 bara initial pressure gets ignited, the resulting maximum explosion pressures would reach for instance 8 and 12 barg respectively. In interconnected vessels, the initiation of an explosion in one of the vessels might cause the initial pressure in the interconnected vessel to increase due to the expansion of combustion products. This effect is called pressure piling and may cause extremely violent explosions when the flame arrives in the interconnected vessel[8].

2.1.1.2 Dust explosions

A dust explosion may be regarded as rapid combustion of a dust cloud which results either in a rapid pressure buildup or a uncontrolled expansion[22]. Since the gas in which the dust is suspended in takes part in the combustion reaction, the gas is treated as a property of the dust explosion. There are many properties that affect the severity of a dust explosion, but the main contributors are as follows:
  ➢ The nominal dust concentration (amount of fuel).
  ➢ The particle size distribution of the dust (surface area).
  ➢ The chemical composition of the dust (heat of combustion).
  ➢ The moisture level in the dust.
  ➢ The confinement of the system in which the explosion takes place.
  ➢ The level of turbulent mixing in front of the flame and internally in the burning zone.

Dust concentration:
The combustion of a dust cloud can only happen if the concentration of dust is within certain limits. This concentration can be regarded as an analogue to the flammability limits of a flammable gas. Contradictive to most gas mixtures, the explosible range of dust clouds is of several orders of magnitude, with a normal organic dust having a explosible range of around 100 g/m^3 to 2000-3000 g/m^3 [9]. The stoichiometric concentration of dusts is often in the range between 100-300 g/m^3, but the most violent explosions tend to happen at concentrations of 2-3 times the stoichiometric value[23].

Particle size:

Any solid material which is combustible under normal ambient conditions may cause a hazard when divided into small pieces. This is illustrated by Eckhoff[8] in Figure 2.3, where the rate of combustion of wood are illustrated by the subdivision of the wood particles. In general, the intensity of which a particle burns and how easy it will get ignited increase with decreasing particle size. This statement is valid until the particles reach a small enough size at which the particles tend to lump together and form agglomerates. In general, particles with a greater size than 500µm do not represent an explosion hazard on their own, but it may burn in an explosible cloud if smaller particles are present. On the other side, particles with a size smaller than 10 µm will for most organic materials and coals no longer influence the explosion violence. This is because combustion of the volatiles becomes the rate controlling process in the flame propagation[24]. In reference to the size of these small particles, a human hair has a thickness in the range of only a couple of microns up to 500µm[25].

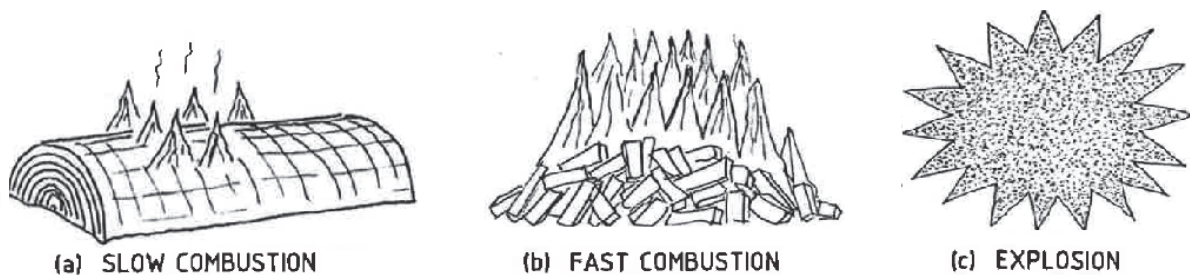(a) SLOW COMBUSTION   (b) FAST COMBUSTION   (c) EXPLOSION

Figure 2.3 : *Illustration of how particle size plays a role on the combustion rate of solid materials [8]*

Chemical composition:

The amount of heat liberated (thus the pressure buildup in reference to Equation 2.5) as a particle burns is given by the molar heat of combustion for the given specie. Eckhoff[8] argues that it is important to know the amount of heat liberated in a dust explosion in reference to how much oxygen it consumes. The reason is that in most dust explosions there is an excess of dust and the oxygen is the limiting agent. As seen in Table 2-2, metal dusts have the highest heat of combustion and therefore produce the most violent explosions. Volatile compounds in dusts tend to increase the explosion pressure, although there are little effect for volatile compounds below 10%[26]. Coal dusts tend to have a high concentration of volatile components.

Table 2-2 : *Heat of combustion of various solid substances per mole O_2 consumed [7].*

Material	Oxidation products	Heat of combustion (kJ/mol O_2)
Calcium	CaO	1270
Magnesium	MgO	1240
Aluminum	Al_2O_2	1100
Silicon	SiO_2	830
Chromium	Cr_2O_2	750
Zinc	ZnO	700
Iron	Fe_2O_3	530
Copper	CuO	300
Sucrose	$CO_2 + H_2O$	470
Starch	$CO_2 + H_2O$	470
Polyethylene	$CO_2 + H_2O$	390
Carbon	CO_2	400
Coal	$CO_2 + H_2O$	400
Sulphur	SO_2	300

Moisture level:
As the moisture level in a dust cloud increases, both the ignition sensitivity and the violence of the explosion are reduced significantly. A dust with a higher moisture level than 30% is not likely to cause a dust explosion, whereas concentrations below 10% do not tend to reduce the severity of an explosion[26]. Moisture affects the explosion by acting as an inert heat sink as the water gets heated up and vaporized, the water vapor then mixes with the reaction gasses and reduces the reactivity of the mixture. Moisture content increases the tendency to form agglomerates of particles due to the inter-particle cohesion of the dust[9].

Confinement:
Contrary to typical accidental gas explosions, dust explosions almost always start inside process equipment. The reason for this is that the dust concentrations needed for an explosion to occur usually only exist inside the production stream and transport systems. As the pressure builds because of combustion of a dust cloud, the vessel in which it is enclosed may burst. This often gives rise to secondary explosions as the flow and blast waves travels away from the enclosure. This domino effect is illustrated in Figure 2.4.
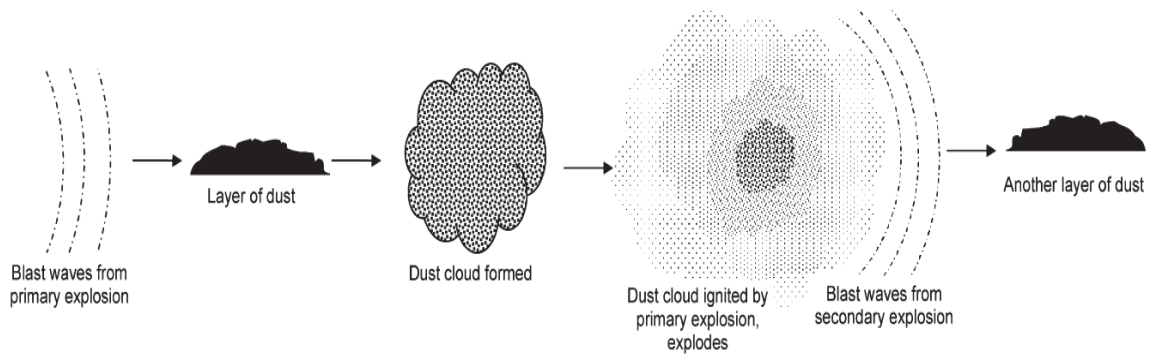

Figure 2.4 : *The domino effect for dust explosions, modified version[5]*

The blast wave from the primary explosion may disperse dust deposits. This secondary explosible dust cloud may severely damage the facilities and or harm workers. In order to prevent secondary explosions, good housekeeping is essential. To illustrate the dangers of dust deposits laying around a process facility, Eckhoff [8] used the following example:
Considering a situation with a blast wave from a primary explosion traveling over a 1 mm dust layer with a bulk density of 500 kg/m^3. If the deposits get suspended, it may cause a 1 meter high dust cloud with a concentration of 500 g/m^3 which is the worst case concentration for common organic compounds.

2.1.2 Dust explosion testing and scaling

The explosion violence for a dust sample is commonly defined by the K_{st} value. The concept of the K_{st}-value was first proposed by Bartknecht and describes the rate of the maximum pressure rise in a vessel in reference to the volume as follow:

$$K_{st} = constant = \left(\frac{dP}{dt}\right)_{max} V^{1/3} \qquad \text{Equation 2.6}$$

The K_{st}-value is commonly used as a input factor when assessing the requirements for vent and automatic suppression of vessels that may contain an explosible atmosphere[27].

It should be noted that the K_{st} value has some limitations when it comes to:
- The vessels in question should be geometrical similar.
- The flame thickness is negligible with reference to the radius of the vessel ($\delta \ll r$).
- The burning velocity and turbulence is the same in each of the vessels.
- The experiment is initiated with a point ignition in the center of the vessel (this is hard to accomplish since the usual ignition source is a chemical igniter).

Different experimental apparatus give values with several orders of magnitude in between them[8], it is therefore essential to use standardized constant volume explosion vessels for determining the K_{st}-value[5]. Such standardized tests include the ISO $1m^3$, Siwek and USBM 20liter vessel, and the 1.2 liter Hartman bomb. Dusts are categorized in reference to the Kst value as seen in Table 2-3.

Table 2-3 : *Classification of the explosibility for combustible dusts [5].*

K_{st}-value	Group	Severity
	St 0	Non-explosible
$0 < K_{st} < 200$	St 1	Weak
$200 < K_{st} < 300$	St 2	Strong
$300 < K_{st}$	St 3	Very strong

2.1.3 Turbulent combustion regimes

Turbulence is something that everyone has a relationship to, either in the form of the wind outside or the waves in the ocean. In this context, the main motivation of understanding turbulence is the effect it has on the combustion process. Eckhoff [9] stated that the turbulence in a medium is a state of rapid internal, more or less random movement in all of the directions. In an explosion, the turbulence enhances the heat and mass transfer, causing enhanced combustion rates.

Turbulence is an inherent property in dust explosions, without turbulence it would not be possible for the dust to get suspended in air, and it would not stay suspended, but settle down as dust deposits. The turbulence may be initially present at the time of ignition, or it can be induced as the flame travels away from the ignition point. As the flow travels past objects it creates turbulent wakes and eddies. In a turbulent flow, the largest eddies are governed by the size of the geometry, while the smallest are controlled by the viscous diffusion. As shown in Figure 2.5, Borghi[28] developed a diagram to describe the relation between the turbulent scales and the reaction rate of a premixed flame.

In the diagram, the intensity of the turbulence is given on the y-axis as the ratio between the laminar burning velocity S_l and the fluctuation in the turbulent flame velocity $u^{'}$. The turbulent length scales are given on the x-axis by the ratio of the integral length scale L and the laminar flame thickness δ_l.
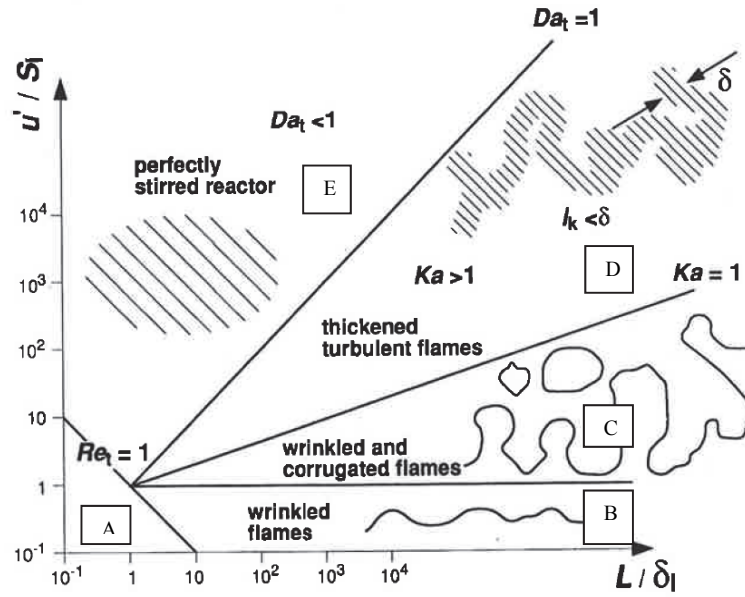
Figure 2.5 : *Borghi diagram[16], after Borghi[28]*

The Borghi diagram is separated into different combustion regimes lines. The separation lines in are a function of the non dimensional turbulent Reynolds number Re_t, The turbulent Karlovitz number Ka, and the turbulent Damköhler number Da.

The Karlovitz number describes the ratio between the chemical time scale (τ_c) and the Kolmogorov time scale (τ), where τ is the dimension at which diffusion of the specie takes the same time as half a revolution of the turbulent eddy (the fastest eddies).

$$K_a = \frac{\tau}{\tau_c} = \left(\frac{u'}{S_l}\right)^{3/2} \left(\frac{L}{\delta_l}\right)^{-1/2} \qquad \text{Equation 2.7}$$

The Damköhler number (Da) describes the ratio between the turbulent time and the chemical time. The chemical time can be estimated as the time needed for the flame to propagate a distance equal to the flame thickness. The turbulent time is the ratio of the turbulent length scale and the velocity fluctuation:

$$t_{turbulent} = \frac{L}{u'} \quad : \quad t_{chemical} = \frac{\delta_l}{S_l} \quad : \qquad \text{Equation 2.8}$$

$$Da = \frac{t_t}{t_{ch}} = \left(\frac{u'}{S_l}\right)^{-1} \left(\frac{L}{\delta_l}\right) \qquad \text{Equation 2.9}$$

The Damköhler number has a high value for fast reactions (small t_{ch}).

The turbulent Reynolds number is defined by the turbulent length scale, kinematic viscosity and the velocity fluctuation (turbulent length scale) as:

$$Re_t = \frac{u'L}{\nu} = \left(\frac{u'}{S_l}\right)\left(\frac{L}{\delta_l}\right) \qquad \text{Equation 2.10}$$

The different turbulent combustion regimes in the Borghi diagram are:

A. **Laminar combustion** with a smooth flame surface. $Re_t < 1$.

B. **Wrinkled flame**. If the turbulent velocity fluctuation are less than the laminar burning velocity ($u' < S_l$), the flame will have a wrinkled or laminar flame profile The transition between the laminar and wrinkled flame are governed by the physical size of the system at $Re_t = 1$.

C. **Wrinkled and corrugated flame**. If the turbulent velocity fluctuation are higher than the laminar burning velocity ($u' > S_l$) but the chemical reactions are faster than the transport caused by the turbulence ($Ka > 1$). In this regime, the turbulence will wrinkle the reaction surface and cause formations of pockets that burn individually. The reaction front will still have a continuous surface.

D. **Thickened turbulent flames**. In this regime the turbulence disturbs the reaction surface and the reaction zone will be thickened: $Ka > 1$, $Da > 1$.

E. **Perfectly stirred reactor.** The turbulent mixing happens faster than the chemical reaction and there is no clear flame front: $Da < 1$.

2.1.4 Deflagration and detonation

There are in essence two different modes of flame propagation that can drive an explosion[26]. The most common is deflagration, where a flame propagating at subsonic velocities relative to the unburned reactants ahead of it. A compression or shock wave is generated and travels ahead of the flame front[29], the strength of this front depends on the rate of chemical reactions in the reaction zone. In a deflagration front, the dominating driving mechanisms are the diffusion and turbulent convection of heat and mass over the flame front which heats and ignites the reactants in the front of the reaction zone. For hydrocarbon-air mixtures, the typical deflagration happens at flame speeds below 300m/s [26].

The second mode of flame propagation is a detonation where the flame front travels as a shock wave closely followed by the reaction zone that sustains the detonation front. The driving mechanism of a detonation wave is compression of reactants that increases the temperature up to the auto-ignition temperature of the mixture. In a detonation, the reaction front appears as a cellular structure where the front is characterized by the detonation cell size (λ). The more reactive the mixture, the smaller the cell size. In a square channel, the height of the channel has to be larger than the cell size for a detonation to occur[30]. For propane, the detonation cell size is between 5 and 10 cm dependent on the equivalence ratio[31, 32]. The detonation velocity is given by the velocity of sound in the hot combustion products and is typically of the order 2000-3000m/s for hydrocarbon-air mixtures[26].

The peak pressure reached in hydrocarbon explosions is in the order of 8-9 bar for a deflagration, and for a detonation up to 20 bar[26]. The relationship between the burning velocities for the different combustion regimes can be seen in Figure 2.6, where the velocities are represented on a logarithmic scale. As seen in Figure 2.6, the combustible concentration range for the different combustion regimes decreases as it goes from laminar burning trough turbulent and then detonation.
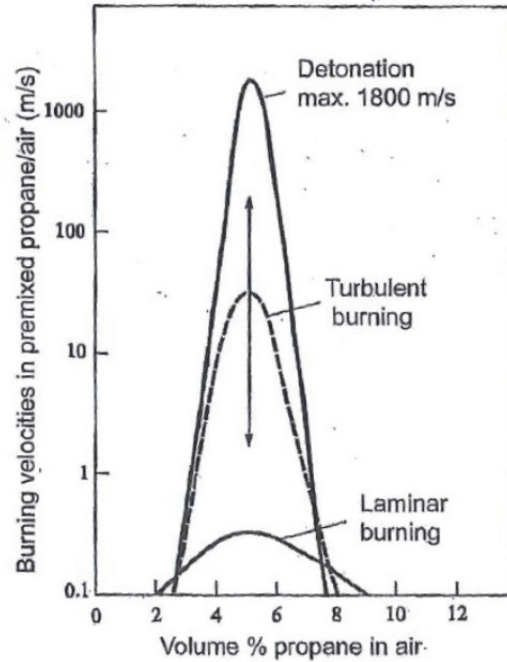
Figure 2.6 *: Burning velocities the different combustion modes for premixed propane-air mixtures at ambient temperature and pressure [9].*

2.1.4.1 Flame acceleration in tubes and channels:

If a quiescent premixed combustible mixture is ignited in the closed end of a tube or a channel, the flame will propagate away from the ignition point. As the flame propagates away, the initial laminar flame front will be curved and stretched as it travels into the reactants. The main contributors to the flame curvature and stretch are the Kelvin-Helmholtz (KH) and Rayleigh-Taylor (RT) instabilities[33]. In closed or obstructed vessels, generation of acoustic waves may interact with the flame front and cause pulsations in the flame. The most dominating effects on the flame front are the KH instability, which is caused by shear forces, and the RT, which is developed as the flame travels towards the unburned gas. As the flow passes an obstruction or through a vent opening, the KH and RT instabilities start to dominate in the flame front. This can be seen in Figure 2.7 where a stoichiometric methane-air flame is propagating through an obstructed channel with two different blockage ratios. Where the blockage ratio is the ratio of the original area versus the obstructed area.
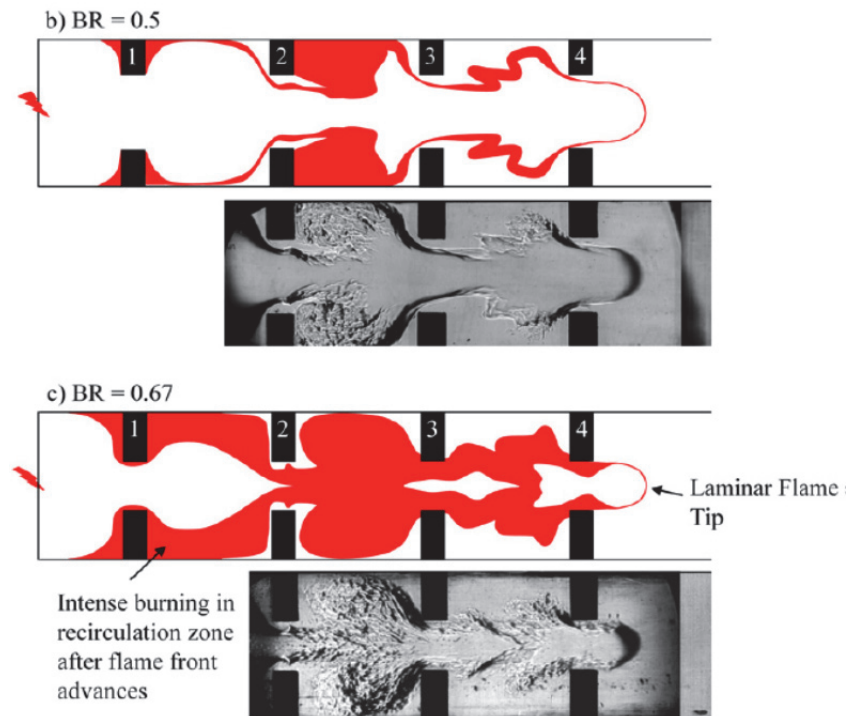
Figure 2.7 : *The influence of obstacles on flame acceleration in a square channel with two different obstacle configurations. Red area indicating the reaction area of the flame. Stoichiometric methane-air at 0.47bara initial pressure. Photograph taken by Schlieren photography[34]*

As seen in Figure 2.7, the obstacles greatly increase the surface area of the flame, thus resulting in a much higher energy release rate, which leads to acceleration of the flame front. Again increases the surface area and causing a positive feedback in terms of more turbulence generated which further increases the area of the flame.

In channels with significant wall roughness, the flame propagation may form a turbulent boundary layer in front of the reaction zone. This results in a higher degree of mixing along the walls of the tube/channel and may result in a tulip shaped reaction zone as shown in Figure 2.8.
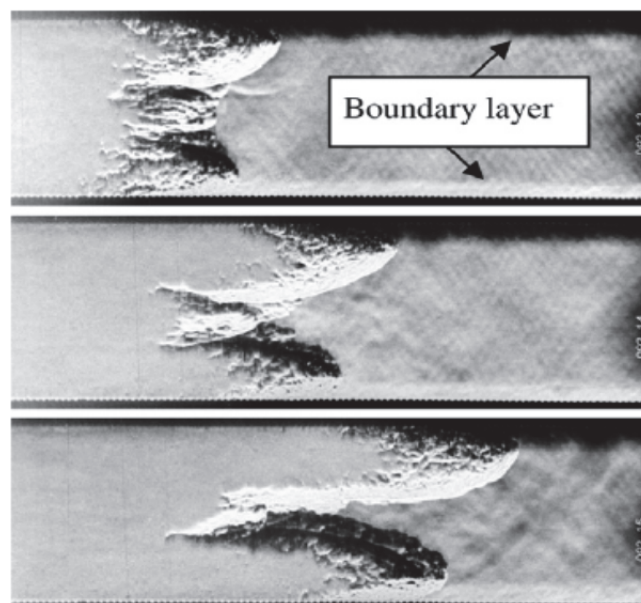

Figure 2.8 : *Shadow photographs showing the characteristic tulip shape of a stoichiometric hydrogen-air mixture traveling at 320m/s with a time resolution of 0.1 ms[33]*

While the flame front burns, turbulence is also generated in wakes and sheer layers, resulting in an unstable front that may change shape as the flame propagates trough the channel[33]. Depending on the mixture properties and the boundary conditions, the influence of obstacles in an obstructed channel may either result in weak or strong flame acceleration. Weak flame accelerating often results in relatively slow unstable flames while strong flame acceleration may lead to supersonic velocities relative to a fixed observer[33].

2.1.4.2 Deflagration to detonation transition

Given strong flame acceleration, as shown in Figure 2.7, a deflagration wave can transform into a detonation wave if the conditions are favorable. The transition often takes place when the deflagration front reaches a velocity in the order of half of the Chapman-Jouguet (C-J) velocity (i.e 1000m/s)[19]. The C-J velocity is the velocity of a detonation front where auto-ignition of the reactants are able to sustain the velocity of the combined reaction and pressure front. Since a detonation wave propagates by a different driving mechanism than a deflagration, there will not be a continuous acceleration, but a sudden increase of the velocity at the onset of the deflagration to detonation transition (*DDT*).

The possibility of a deflagration front undergoing DDT is strongly dependent on the turbulence generated. Thus, long galleries and channels are especially exposed to the hazards of detonations. These include coal mines, where fatal accidents have been initiated by a methane explosion, where the shock wave has suspended the coal dust that lies in the channel. As a result, the explosion may transform into a hybrid explosion with both gas and dust as the fuel.

2.2 Previous Work

2.2.1 Previous work on turbulent flame propagation

Many experiments on various scales have been conducted with the aim of understanding the role of different parameters on flame propagation in explosions. Pioneering work done by researchers such as Bartknecht, Palmer, Eckhoff and many more have all contributed to increase the knowledge and understanding of explosion phenomena.

Limited attention has thus far been directed to investigating the effect of obstacles on the propagation of dust flames. Almost all the data available in the open literature today concerns flame propagation in smooth long tubes of large length/diameter ratio or silo experiments. The effects of obstacles on gaseous mixtures have received a great deal more attention.

Such experiments include the experiments conducted by Moen et al.[35], where they conducted large scale methane-air experiments in a 50 m³ tube with a length of 10 meters. To induce turbulence in the tube, different orifice plates with blockage ratio in the range of 0.16-0.84 were mounted along the flame path. They found that the steel baffles drastically increased the overpressure reached inside the tube. No obstructions inside the tube gave an overpressure of 0.15 barg. By introducing baffles with a blockage ratio of 0.3, they measured pressures of 0.6, 3.5 and 8.0 barg, for 1, 3 and 6 rings respectively. They also found that the flame accelerated strongly in the first part of the tube, until, it reached a terminal speed in the range of 300-500 m/s.

Chao et al.[36] studied mixtures of methane, propane, ethylene and hydrogen in a 7 meter long channel of square cross-section. A 1.1 meter acceleration tube filled with orifice plates with a stoichiometric hydrogen-air mixture was used to initiate the explosion. This ensured that mixtures of different fuel and equivalence ratio inside the main channel would reach sufficient velocities where the transition between fast deflagration and quasi-detonation could be studied. Inside the main channel, there were cylindrical rods placed vertical to induce turbulence. The obstacles had a blockage ratio of 0.19 and 0.41. It was found that in obstacle filled channels, the transition between fast deflagration and detonation could be a gradual process without a clear change in the propagation mechanism. Chao proposed that the rapid turbulent mixing of hot combustion products and reactants, caused by the obstructions in a high speed deflagration could lead to adiabatic auto-ignition. This is in contrast to the classical ZND-detonation mechanism where detonation is caused by adiabatic compression of the reactants by the shock wave[36]. Figure 2.9shows the experimental apparatus used by Chao et al.
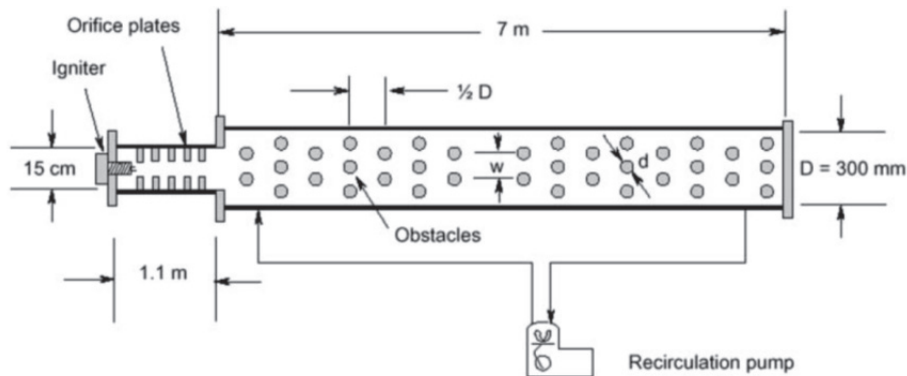

Figure 2.9 : *Schematics of the experimental apparatus used by Chao et al.[36].*

Johansen and Ciccarelli [34] studied the influence of obstacles on flame propagation in experiments with stoichiometric methane-air mixtures at low initial pressure (0.47bara) in a 2.44 meter square channel with a cross section of 7.6x7.6 cm. To characterize the impact of the obstacles, they used a small amount of helium gas injected into the channel prior to ignition to be able to use as a tracker for the Schlieren photographs taken of the early stage of the flame acceleration. The pressure was monitored by eight piezoelectric pressure transducers and the flame position was monitored by eight ionization probes. They found that the flame velocity along the centerline of the channel fluctuated with the spacing of the obstacles with an accelerating and decelerating effect each time the flow passed an obstacle. They used three different obstacle sizes with BR 0.33, 0.5 and 0.67 respectively. Obstacles with 0.5 BR produced the highest flame velocities, with recorded values approaching 800m/s. They found that in the early stages of flame propagation, the larger blockage ratio had the most dramatic impact on flame acceleration. Photos from the experiments can be seen in Figure 2.7 in section 2.1.4.1.

Eckhoff et al. [37, 38] performed large scale vented dust explosion experiments in a 22 meter high silo, volume of 236m^3. To predict how the current guidelines for dust explosion vent performed for different scenarios, they varied the ignition position and mode of pneumatic filling. Four different positions were used: 1.5, 7.3, 12.0 and 21 meter from the bottom of the silo. The flame arrival was measured by use of six specially designed probes that measured both dust concentration and flame arrival. The pressure was measured by 3 pressure transducers. They found that ignition close to the top of the silo produced overpressures in the range of 10-20 mbar and flame speeds around 5 m/s. When igniting the dust cloud near the bottom of the silo, overpressures of 0.8-1.2 bar, and flame speeds exceeding 100m/s were recorded. The most violent explosions were recorded in the range of 400-500g/m^3.The fuel used was maize starch of type *Meritena A*. Maize starch from the same batch are used in the experimental work in this thesis.

These experiments have later on been used for validation of DESC by Skjold el at [39]. Skjold also conducted test of the *Meritena A* maize starch in a modified USBM 20l-vessel where the laminar burning velocity was estimated to 12.6cm/s and the K_{st}-value estimated at 150 bar m/s, thus placing it in the St 1 dust class in reference to Table 2-3. The particle size distributions of the dust were determined by laser diffraction where the standard percentile readings was 6, 13 and 20 μm for the 10, 50 and 90 percentile, respectively[39]. An electron microscope picture of the *Meritena A* maize starch is shown in Figure 2.10.
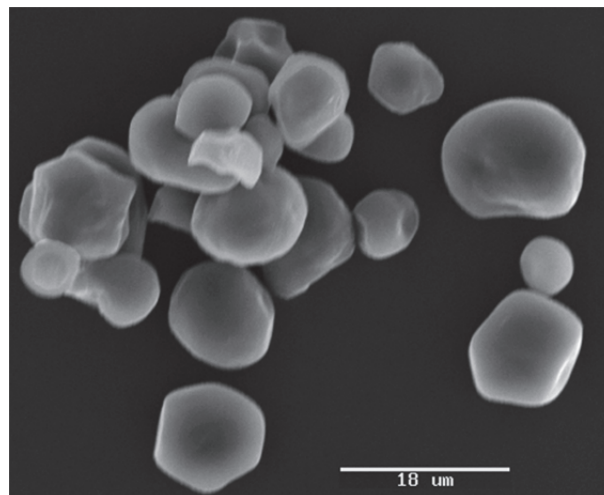

Figure 2.10 : *SEM picture of maize starch particles (Meritena A)[39].*

Pu et al.[40] investigated the influence of obstacles in lean methane-air and corn starch-air mixtures. They used two different flame acceleration tubes of 1.0 and 1.86 meter with a cross section of 0.05x0.05meter and a diameter of 0.19meter, respectively. The smallest channel was made out of glass to allow visual observations of the flame with Schlieren photography as it propagated upwards towards the open end. The dust was introduced by a vibrating dust feeder on top of the tube. The obstacles were placed symmetrically on both sides of the channel and could be varied in size to obtain blockage ratios of 0.2, 0.4 and 0.6. The bigger apparatus was a closed volume tube fitted with a piezoelectric pressure transducer to monitor the pressure and 8 ionization probes to detect the flame arrivals. Dispersion of the dust cloud was through two linear perforated pipes, based on the principle used by Bartknecht in the 1m^3 ISO bomb. Twelve concentric rings placed half a diameter apart with a blockage ratio of 0.392 were used to induce turbulence as the flame propagated trough the tube. It was found that the flame propagation for lean methane-air mixtures (5.5%) had velocities in the same region as cornstarch-mixtures of 550g/m^3. The pressure achieved for the methane-air experiments, showed that the introduction of obstacles in the tube reduced the maximum pressure. This is the opposite case as for the dust explosions, where the obstacles increased the maximum pressure. The reason for this was thought of as a compensation of the heat lost to the walls of the obstructions, by the additional heat released from the wider burning zone of the dust. The experiments performed by Pu were one of the motivating factors for the construction of the FAT and the experimental results found by Pu have later on been used in the validation work for the DESC code[41].

Skjold et. al.[42] investigated dust explosion under near constant pressure conditions in a balloon experiment inspired by the classical soap bubble experiments used for gaseous fuels. The aim of the experiments was to try to illustrate the challenges of dust explosions by comparing the flame thickness of turbulent dust flames and gaseous flames. Experiments with both quiescent and turbulent propane mixtures as well as turbulent mixtures of *Meritena A* maize starch and Lycopódium spores were conducted. The experiment did not succeed in determining the turbulent burning velocity or an approximation of the flame thickness. However, the results illustrate the challenges of accurately describing the mechanisms of turbulent dust flame propagation, and the characterization of the reaction zone in a dust flame. Further details can be found in Appendix D : .

2.2.2   Experiments in the flame acceleration tube (FAT)

Enstad[43] and Kalvatn[44] developed a probe for detecting dust flames in the FAT.

Enstad focused on flame detection with an impedance method with a measurement principle based on how the plasma in the reaction zone of the flame change the dielectrical constant and the resistance of the medium between two capacitive plates.

Kalvatn focused on optical flame measurements after the principle of Lambert Beers law. He used a light emitting diode (LED) to emit light at a certain wavelength, while a photodiode registered the intensity of the signal from a fixed distance. As the medium (dust cloud, flame front etc.) in between the photodiode and the LED change, the attenuation of light change and it is possible to estimate properties such as the concentration of a dust cloud by the light adsorbsion of the dust in question.

The general outcome of this work was that the optical method detected the flame arrival prior to the impedance method, while flame arrival from thermocouples gave arrival times in between the above methods. A spark generator and thermocouples mounted on rods with corresponding amplifiers were made for the ignition and temperature measurements; these have been used in the present study.

Skjold and Castellanos[45] studied the turbulent flame propagation with different mixtures of propane-air and mechanically suspension of maize starch in air under constant volume. The main aim of the work was to find a reliable and robust way of detecting flame arrival in a dust explosion using thermocouples and visual observations with a high speed video camera, located at a fixed distance from the FAT. To identify the flame, a criterion based on the derivative of the temperature, recorded in the range of 400-2000 °C/s and temperature measurements at 100, 200 and 300°C, was used. It was found that the methodology of finding the flame arrival with the thermocouples, estimated the flame arrival prior to the visible flame, but there did not seem to be an easy way of correlating the time difference. This is shown in Figure 2.11, where there are some discrepancies between the estimated (red triangles) and visually observed (Yellow circles) arrival of the flame for a lean and close to stoichiometric concentration of propane in air.
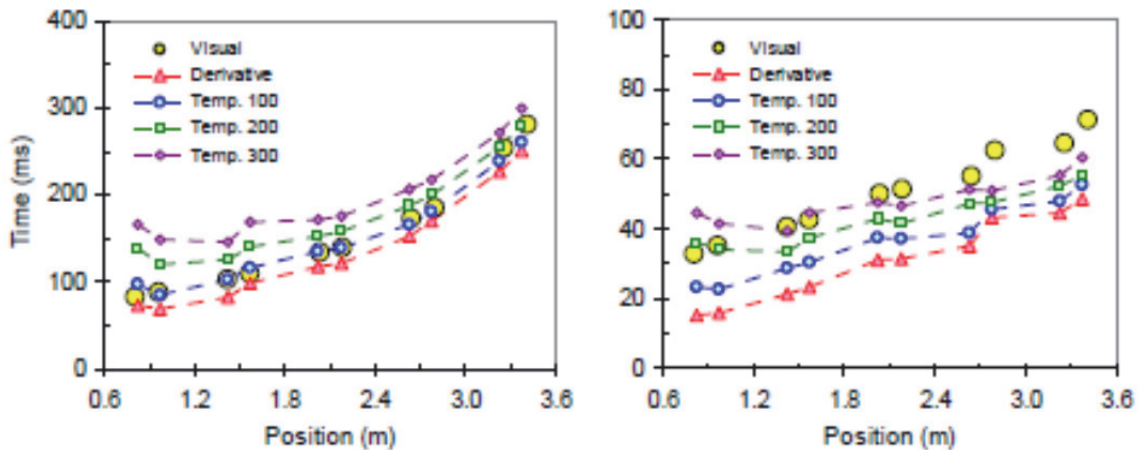

Figure 2.11 : *Estimated flame arrival for two tests of 3.0% and 4.5% propane in air [45]*

3. Experiments

This chapter describes the experimental equipment and experimental procedures. The same approach is followed in all the experiments in the FAT. The approach is based on previous work by[43-45], with some adaptations for vented scenarios.

Experiments with both gas (propane) and dust (maize starch) are included and the experimental results are then compared to each other. For propane, four different fuel concentrations are tested: 3.0%, 4.5%, 6.0% and 7.5%. Experiments with dust used a nominal dust concentration of 500 g/m^3, which is close to the worst-case concentration for the *Meritena A* maize starch[37, 38].

3.1   The Flame Acceleration Tube (FAT)

The flame acceleration tube consists of three equal 1.2 meter long ducts with internal cross-section 0.27x0.27 meter, giving a length-to-diameter (L/D) ratio of approximately 13.3. The first of the three sections is fixed to a frame, which is bolted to the concrete floor. The other sections are fitted on wheels that run on the frame. This allows access to the entire interior of the tube for easy cleaning as well as the possibility to mount obstacles and instrumentations. Each section is basically identical with a dispersion nozzle in the middle and circular Plexiglas windows on one of the sidewalls and in the roof. This allows visible observation of the flame as it propagates through the channel. The ignition is positioned near the closed end of the tube either as a spark-gap or a chemical igniter. The tube is also fitted with ten type K thermocouples and three Kistler 701A piezoelectric pressure transducers. To ensure atmospheric conditions at the time of ignition, a vacuum pump is used to evacuate the channel prior to the injection of air from three high-pressure air reservoirs. The pressures in the reservoirs are monitored with three pressure transducers from PCB during the injection of air into the main channel.

3.1.1   The data acquisition and control system

Two computers running on Windows XP were used to control the experiment. The first computer controls a NI USB-6529 data acquisition card via a USB port, which in turn controls both the triggering and the logging of the experiment. The digital output ports on the card are being used to control the triggering of the high-speed valves, the camera, the ignition, the piezoelectric sensors and a LED-light. The logging is done by use of the analog input channels.

The second computer is used to control the Phantom v210 high-speed video camera.

The high speed camera

In order to be able to record the flame propagation, the camera was set at a 90 degree angle to the FAT, at a distance of 7.33 meter. The sensitivity of the camera to detect light is dependent of the framing rate of the recordings, and this dictates the accuracy of the visible flame speeds recorded. The detection of the visible flame was done manually by the author, and is to some extent subjective. The typical frame rates used were 4000 fps for experiments without obstructions, and 7800 fps for experiments with obstructions. This results in time resolutions of $2.5\text{x}10^{-4}$ s^{-1} and $1.28\text{x}10^{-4}$ s^{-1}, respectively. The limitation of the time resolution became a problem when conducting vented explosions with high flame speeds.

The pressure measurement system

The pressure measurement system is divided in two parts. The first system consists of three piezoelectric sensors, fitted opposite to the second observation window in each section of the FAT. The sensors send signals to the amplifiers, who amplify the signal by a factor of 1.5, before it is sent to the NI-CAD card. Both the sensors and the amplifiers are manufactured by Kistler.

The second pressure measurement system consists of three piezoelectric sensors and a signal amplifier from PCB Piezotronics. These were used to measure the pressure history in the high-pressure reservoirs during the air injection into the FAT.

The temperature measurement system
The flame arrival along the length of the FAT was detected by ten thermocouples. The thermocouples were positioned in the centre of the FAT, at the same radial distance from the closed end as the edge of the last 5 windows. The thermocouples are of type K, with a wire thickness of 0.3 mm, and cover a temperature measuring range up to 1100°C for short pulses.

Because of problems regarding the data acquisition and camera control, as well as operational errors when conducting experiments, some of the experimental data have been lost or become corrupt, thus they are not suited to be presented in the results and discussion chapter.

3.2   The Dump Tank

An old dairy tank was acquired and fitted with a water deluge system and an entrance tube with a diameter of 50cm. This was done to collect the dust from the vented explosions and limit the secondary dust explosion outside of the FAT. Thus the explosions inside the FAT could be vented in the process hall. The dump tank is made out of stainless steel and has a volume of approximately $5m^3$. The deluge system consists of a Bete P40 nozzle placed on the top of the tank (details in Appendix D : , and a high pressure washer. The washer delivers water with a pressure in the range of 60-70 bar, with a rate of about five liter per minute. The position of the dump tank in reference to the flame acceleration tube is shown in Figure 3.1.

3.3   Experimental procedure for the operation of the FAT

The experimental approach is described in according with the schematics of the FAT in Figure 3.2, from Enstad[43] and Kalvatn[44] and is reproduced below.

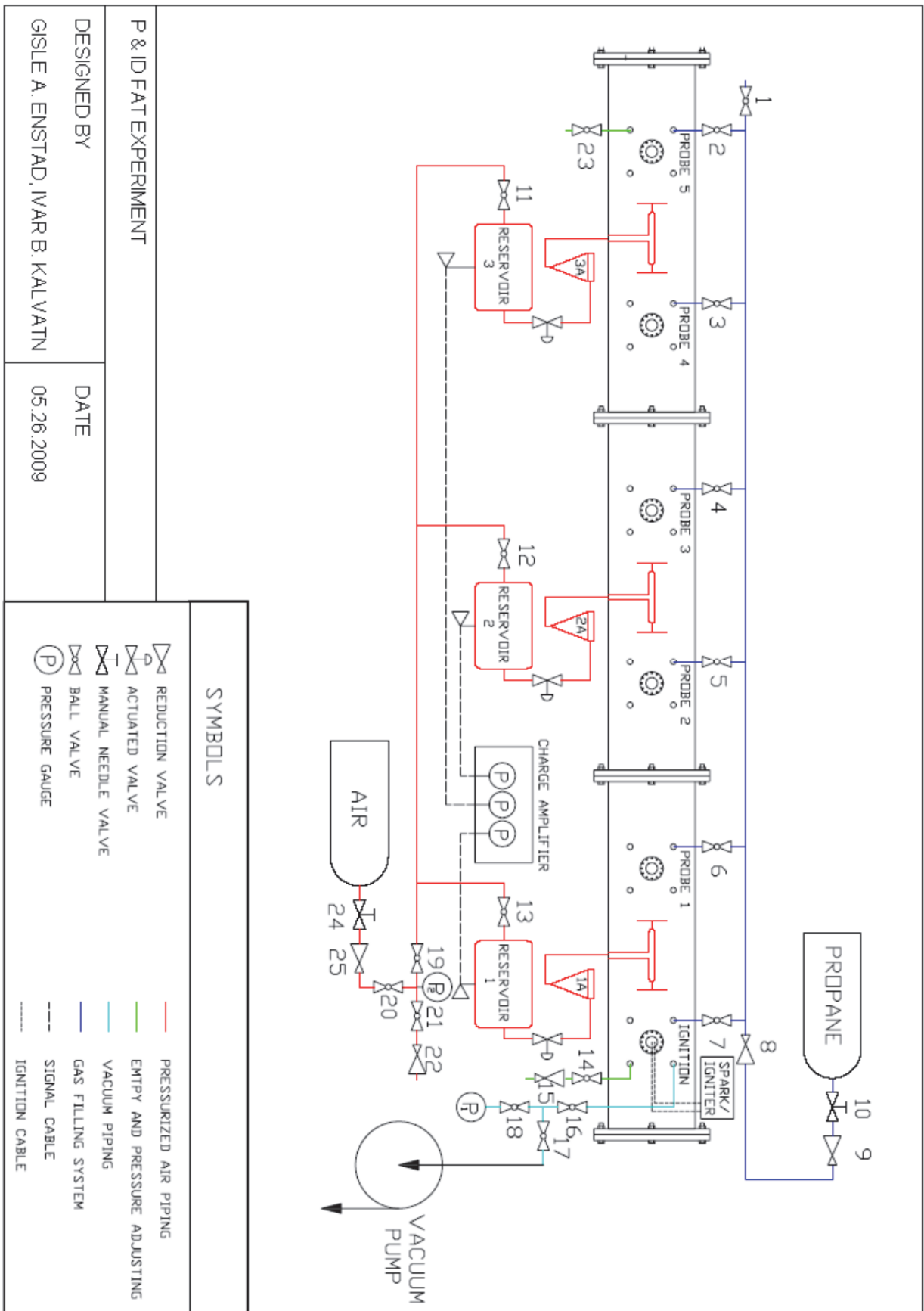**Figure 3.1 :** *The Flame Acceleration Tube and the dump tank*

Figure 3.2 : *Schematics of the FAT [43, 44]*

1)   Open the end flange and inspect the igniter;

> ➤ Chemical igniter for dust experiments
> ➤ Spark gap for gaseous experiments

2)   Close the end flange.

3)   Check that valve 14 is closed.

If dust experiments;

Place a weighted sample in each of the dust reservoirs, 1A, 2A, 3A and tighten the sealing cap.

4)   Start the vacuum pump and open valves 16, 17, 18.

5)   *If ventilated experiments;*

Make sure that the seal on the vent panel is airtight. Use manual force or the clamp to apply pressure until the vacuum is strong enough to hold the panel in place.

6)   Evacuate the FAT to the desired pressure by monitoring the pressure with pressure gauge P_1, then close valve 17 and stop the vacuum pump.

7)   Open valve 24, 20, 19, 11, 12 and 13 to fill the air reservoirs to the desired pressure, monitor with pressure gauge P_2. When the desired pressure is reached, close valve 11, 12, 13 and 19.

*If gaseous experiment*s;

Connect the propane hose to valve 8, then open valve 10.

Gently flush the Propane system to make sure that there is only propane in the pipes, and then start injecting propane into the FAT. This is done by gradually filling propane from one of the valves at a time from valve 2-7 while monitoring the pressure on pressure gauge P_1.

Close valve 8 and 10.

Close valve 16 and 18.

Disconnect the propane hose from valve 8.

8)   Turn on the camera and make sure that the program is ready to be activated by the NI-CAD card.

If ventilated experiments;

Activate the deluge system.

9)   Secure the area.

10)   Activate the LabView program and open the "sotralogger.vi" file.

11)   Check that the test number is correct and that the correct configuration file is being used.

12)   Make sure that all the connections on the NI-CAD card are properly connected.

13)   Activate the siren three times to warn people about the coming explosion.

14)   Start the explosion.

15)   Activate the siren to signal that the experiment went as planned without any destruction.

3.3.1   Gas injection and dust dispersion.

For experiments with flammable gas, the mixing was done on the basis of the method of partial pressure. This is done by connecting a pressurized bottle of flammable gas (propane) to a system connected to the FAT via a choke valve. The mixing system consists of a line of six manual ball valves distributed along the length of the FAT, and 3 needle valves to bleed the system of air. To get the right concentration, a vacuum pump is used to evacuate the FAT prior to the injection of gas. During the evacuation and filling of gas, the pressure is monitored by a Druck digital pressure indicator.

For vented explosions, the vent panel fitted with an o-ring is initially pushed tight against the FAT, to ensure an airtight seal. This is done either manually, or by the use of a specially manufactured clamping device. The gas is evenly distributed along the length of the FAT by the use of the six valves to ensure that the mixture becomes homogeneous. Pressurized air from the dust dispersion system is used to mix the gas, and ensure close to ambient conditions at the time of ignition.

When conducting dust explosion experiments, a weighted dust sample is placed in each of the dust reservoirs. To reduce the moisture content of the dust, the dust was dried in a laboratory drying oven at 105 °C overnight prior to the experiments. The dust is dispersed inside the FAT through three pneumatic valves, controlled by the computerized signal system. To ensure that the turbulent intensity is the same for both gas and dust explosions, the experiments were performed with the same signal sequence, with an ignition delay of 1 second from the activation of the valves. This implies that the flow field is turbulent at the time of ignition.

3.3.2   Vented explosions

The vent of the FAT is done by the use of a hinged vent panel. It is possible to vary the vent area to investigate the effect on factors such as the maximum explosion pressure and flame acceleration. There are three different vent areas: $441cm^2$, $327cm^2$ and $210cm^2$, corresponding to opening ratio of 0.395, 0.551 and 0.712, respectively. The vent areas as illustrated in Figure 3.3 will sometimes be referred to as either large (vent area #1), medium (vent area #2) or small (vent area #3).

There is no fastening mechanism for the panel in the closed position, thus the panel is kept in place by the pressure difference of 0.4 bar (under-pressure inside the FAT). It is not straightforward to achieve an airtight seal around the vent opening. To achieve this, a special clamping device was designed. This clamp made it possible to apply force to the panel until the pressure difference was strong enough to suck in the panel. Because of the variation in force applied to the panel, the hinge occasionally opened prior to ignition.

The sheer weight of the vent panel is quite large compared to other industrial vent solutions. This causes a limitation of the efficiency of the panel since the inertia forces that have to be overcome before the vent through the opening can start. This inertia caused an upwards diversion of the flames for the most reactive mixtures.
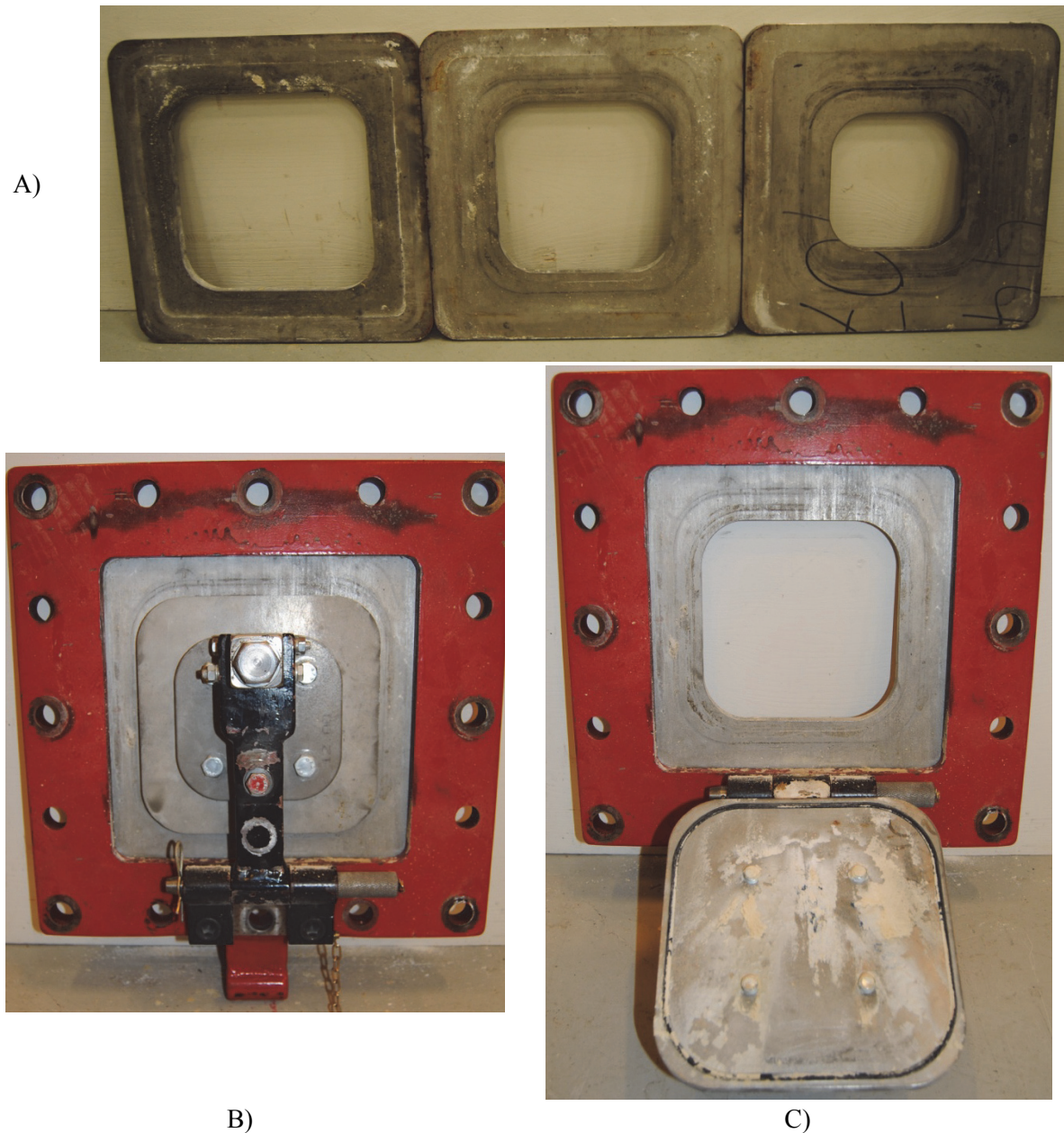
Figure 3.3 *: The vent areas and the fastening mechanism for the vent panels. A) From the left, vent panel 1, and 3, respectively. B) End flange of the FAT with vent panel 2 in the closed position and C) vent panel in the open position (covered in residual maize starch after a dust explosion).*

3.3.3 Explosions with obstructions

To introduce additional turbulence as the flame propagates through the tube, obstructions in form of baffle plates with a blockage ratio of 0.4 were mounted along the propagating direction. Experiments with both gas and dust were conducted.

Two different obstacle configurations were used, where the distance between obstacles were varied. In the first configuration, there were used a total of 20 baffle plates, while in the second configuration, there were only 10. The distance between the obstacles was set to either 15cm (approximately half of the height of the FAT) or 30cm. The obstacles were aligned on rods with the desired spacing as shown in Figure 3.4 and Figure 3.5, and mounted inside the FAT as shown in Figure 3.6.
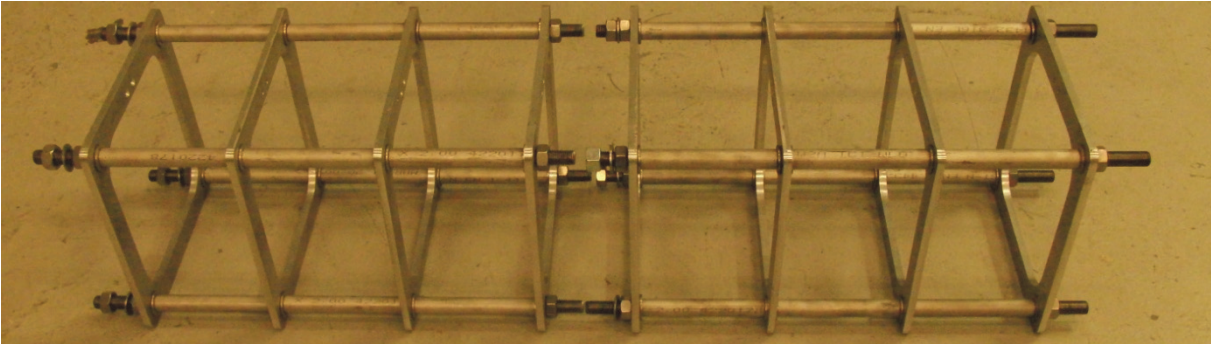
Figure 3.4 : *Obstacle configuration #1, 20 baffle plates 15 cm apart, blockage ratio of 0.4.*
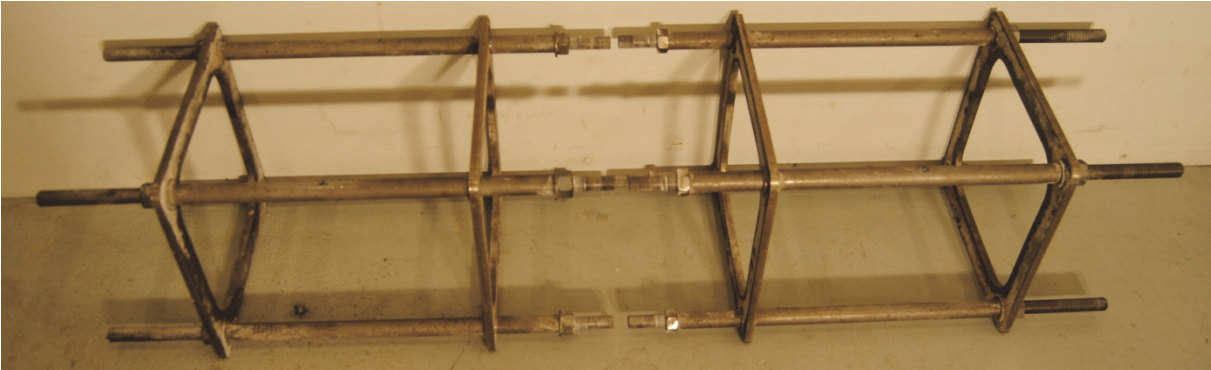

Figure 3.5 : *Obstacle configuration #2, 10 baffle plates 30 cm apart, blockage ratio of 0.4.*
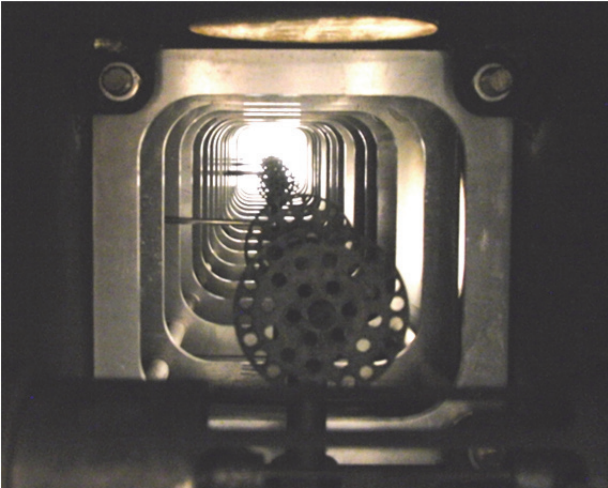

Figure 3.6 : *The interior of the FAT, without and with obstacle configuration #1, mounted inside the FAT*

3.4   Simulation of the experiment in FLACS

Attempts to simulate the experiment with FLACS failed due to inherent limitations of the code in the current version, and also due to limited time available. The problem can be divided into two parts.

Firstly, in FLACS it is possible to define one (and only one) high pressure region with a given composition. This region is then possible to use as either the conditions inside the tube or in the high pressure reservoirs. In order to simulate vented experiments, it would be necessary to define multiple high pressure regions (tube and reservoirs in addition to the atmospheric conditions outside the FAT).

Second, when the air from the reservoirs gets injected into the FAT, there is an expansion of the air as the pressure decreases from approximately 17.4 bara to 1 bara. This results in a cone shaped "expansion-area" in front of the nozzles. With regards to the pressure difference and the physical real life shape of the nozzle, this "expansion-cone" has a shape with a diameter of at least 8 cm across. This becomes a problem when creating the grid for the simulation volume, because the "expansion-cone" needs to be within one grid-cell. With this approach, the only grid cell size appropriated for the 27x27x360cm internal volume of the channel is a 9cm cubic cell. This in turn gives only 3 cells across the height and width of the channel. Given the guidelines of FLACS and the normal practice of experienced users, there should be 10-15 grid cells in each direction inside the simulation volume.

One of the possible solutions to this problem, would be to simulate the injection as a surface-leak (to be released in the next version of FLACS), which can cover many grid-cells. A second solution would be to divide the leaks into smaller leaks, and place the leaks inside smaller grid-cells. This solutions would most likely work, but it would result in either 30 or 54 different leaks, given the physical real life scenario, thus resulting in a great deal of time consumed to define the scenario. Hence, the simulations of the experiments were left for further work.
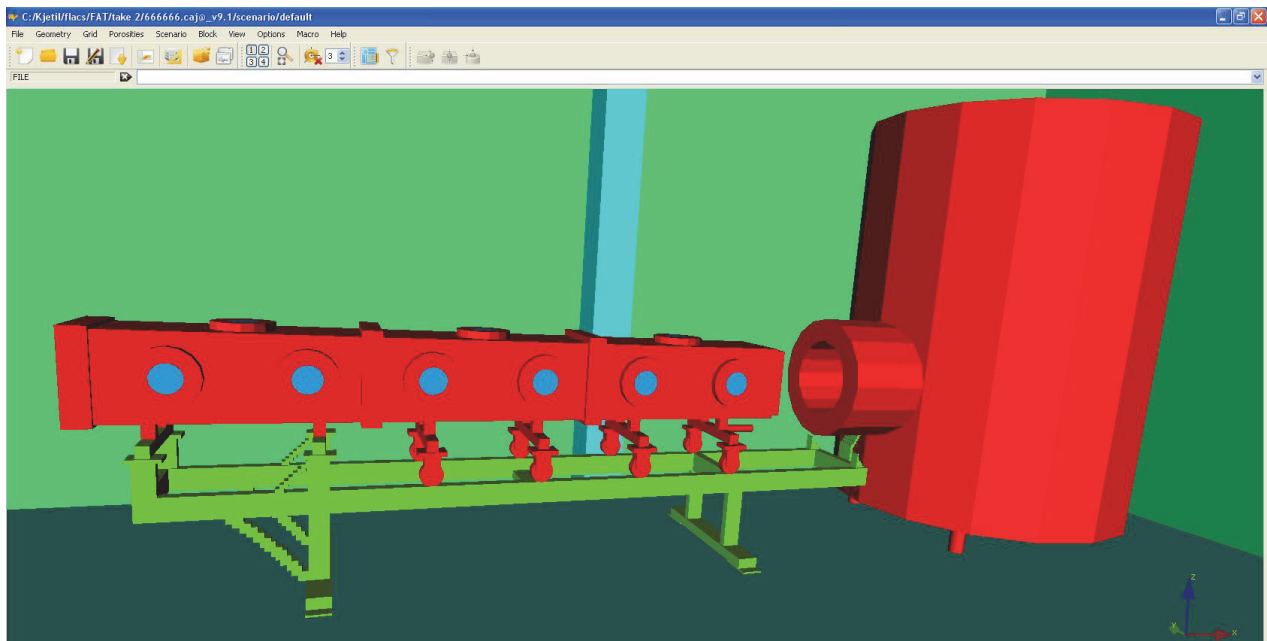

Figure 3.7 : *Geometry built in CASD to simulate the experiment*

The geometry of the experiment as shown in Figure 3.7, was built in CASD (Computer-Aided Scenario Design), which is the visualization tool in FLACS for the geometry and scenario files.

3.5   Methodology

3.5.1   Analysis of high speed video recordings

The videos recorded with the high speed camera have all been manual analyzed by the author. In order to get a clear and consistent picture of how the flame propagates trough the channel, some fine-tuning of the videos has been done. All of the analyses were done in the Phantom Camera Control software, version 9.3.689.

In cases with lean gas mixtures and for dust explosions, it was not always straightforward to identify the flame front. In order to get a clearer view, some adjustments were made with the built-in image processing features in the software. The same methodology did not work for all the cases, but the typical approach resembles the following procedure:

1)   The "automatic white balance" option was the first one to be used; this was done with reference to the white section around the test number. This ensures that the colors are correct.
2)   Then the "sharpen" filter was applied to sharpen up the edges and creating a better contrast between the colors.
3)   The brightness, gain, gamma and hue were increased to make the image appear brighter.
4)   Manually adjustment of the white balance in order to get the clearest flame possible.

The difference between original recordings and the manually processed pictures can be seen in Figure 3.8 and Figure 3.9

Figure 3.8 : *Test nr. 30, 3.0% propane, flame at 94 ms after ignition, original and with image processing.*
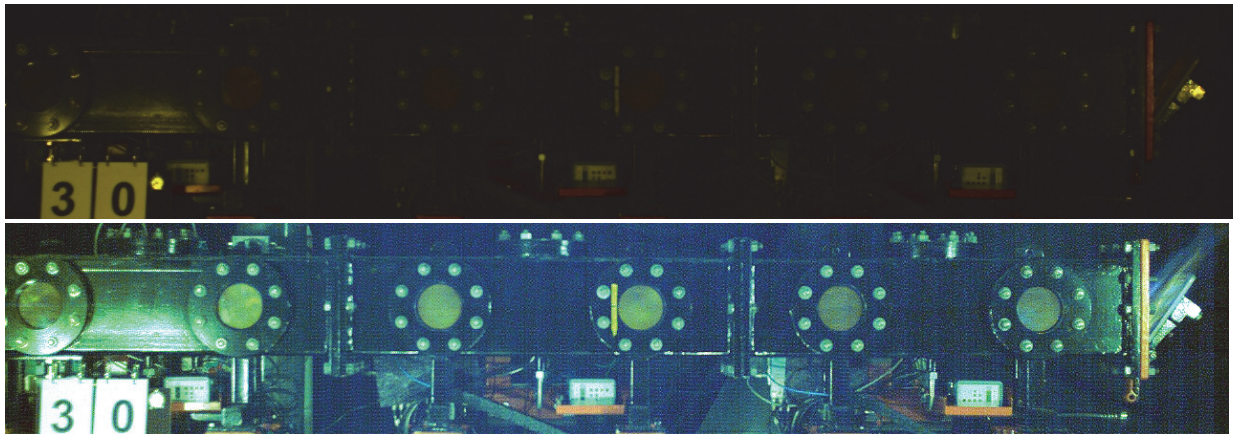

Figure 3.9 : *Test nr. 30, 3.0% propane, flame at 118 ms after ignition, original and with image processing.*

In the analysis of the video, the flame arrivals at the windows and at the vent opening were registered for further use in the analysis.

As the flame accelerates towards the opening, the accuracy of the measurement decreases due to the limited time resolution. Within the first half of the tube, it was in most cases possible to determine the arrival at the windows to within one frame. However, in the second half it of the tube, the flame speed made the detection at the fixed measuring points difficult due to the speed of the flame front. This often resulted in the flame propagating a couple of centimeters into the view of sight before there was possible to visually observe the flame. When this was the case, the arrival was estimated in between the two frames of which the flame was visible or not. This is illustrated in Figure 3.10 where window number 2 is zoomed in on. Here there are 11 frames from the flame arrival at the window until it reaches the end. Where as in Figure 3.11 at window number 6; there are only 3 frames to cover the same distance.

| a) 38.23ms. | b) 39.73ms. | c) 40.98ms |

Figure 3.10 : *Flame propagation in the first section of the tube. Selected frames from test nr. 33, 4.5% propane, Flame arrival at window nr.2, 11 frames from start to end.*

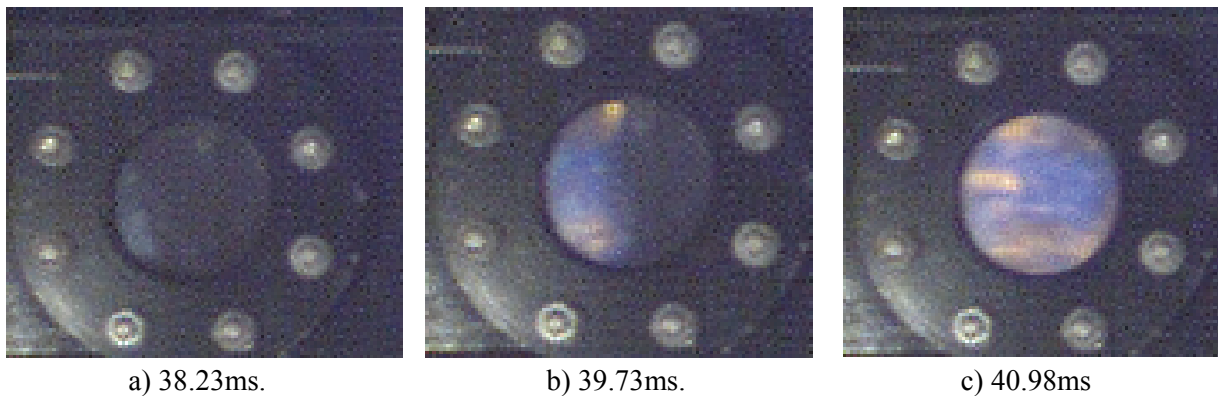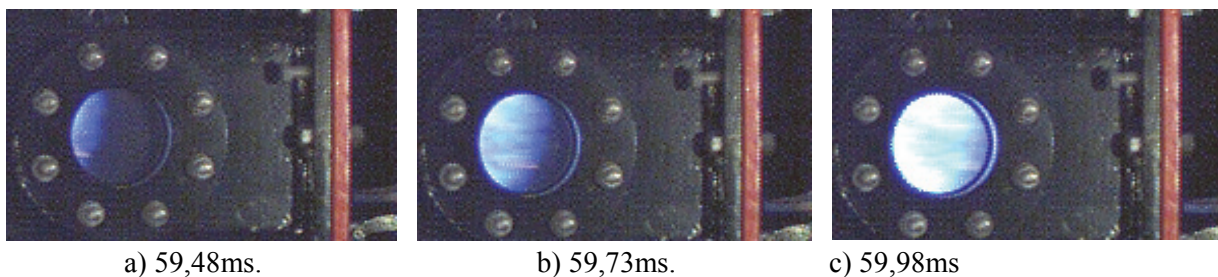| a) 59,48ms. | b) 59,73ms. | c) 59,98ms |

Figure 3.11 : *Flame propagation in the last section of the tube. Selected frames from test nr. 33, 4.5% propane, Flame arrival at window nr.6, 3 frames from start to end.*

3.5.2 Adjusting the time of ignition in the raw data

The NI-CAD card did not always start saving of the signals from the measuring systems at the same time. The reason for this was not found, but a possible reason is that the logging frequency of 50 kHz was too high. This resulted in some loss of data in the beginning of the logging period, typically 21 ms. There is reason to believe that this systematical error in the detection time, may have been present in earlier experiments conducted in the same apparatus. This may explain the data presented by Skjold and Castellanos[45] as seen in Figure 2.11, where a 21 ms time difference in the detection time would explain the discrepancy between the thermocouple and visual data. Skjold and Castellanos had an average observation delay time of 18 ms.

Because of the initial lack of data, the time of ignition for each experiment had to be manually adjusted in the MatLab program that processed the data. This was done to allow the pressure and temperature data to be in agreement with the visual observed flame. As seen in the original data from test number 78 in Figure 3.14, the pressure is highest at around 68ms. In comparison with the video recordings from the test, this corresponds to the flame at a distance of less than one third of the entire length of the FAT, shown in Figure 3.12.
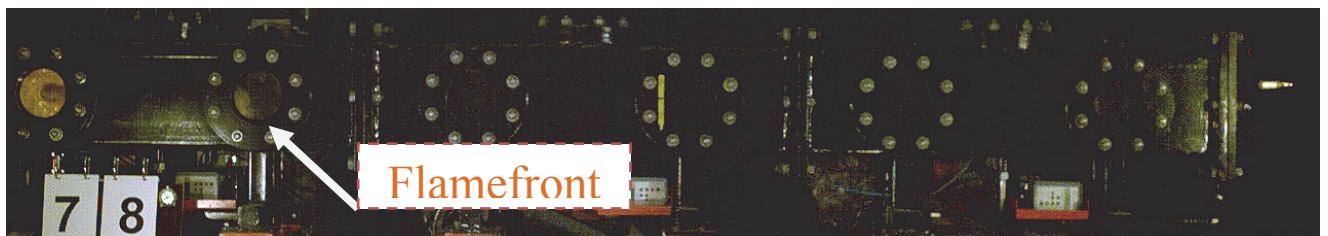
Figure 3.12 : *Test number 78, image from the video recording after 68.1ms.*

The process of finding the correct delay between the pressure and flame arrival data and the video recordings is done by use of the pressure history inside the reservoirs. As seen on the upper part of Figure 3.14, there are some disturbances (data points) of the signal at -20ms. It is reasonable to assume that this disturbance is due to the noise generated by the electrical signal used to ignite the mixture in the spark gap or with a chemical igniter. When adjusting the time of ignition in accordance to the disturbance, the peak pressure is adjusted from 68 ms to 88ms as shown in Figure 3.15. This correlates nicely to the recordings shown in Figure 3.13, showing that the flame at this point has just reached the end of the FAT. The ignition time on the video recordings is validated by the LED light which signals the time of ignition in the spark gap. The ignition in the spark gap was also investigated by separate tests, it was found that the spark was initiated without any delay.
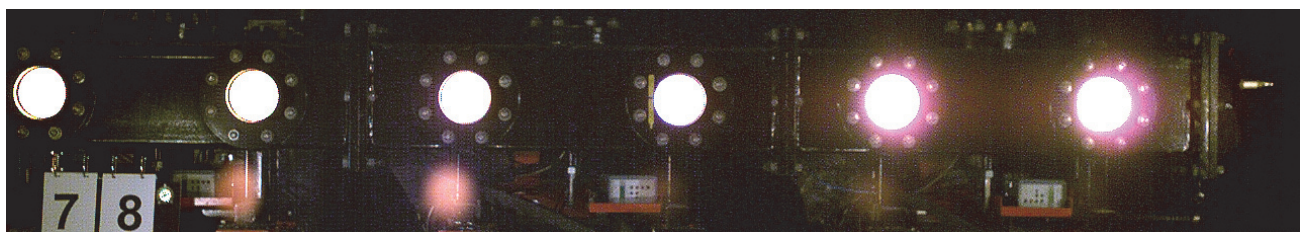
Figure 3.13 : *Test number 78, image from the video recording after 88.2 ms.*

34
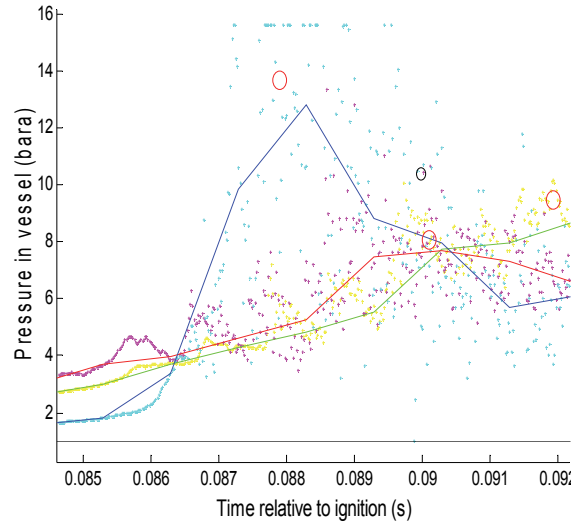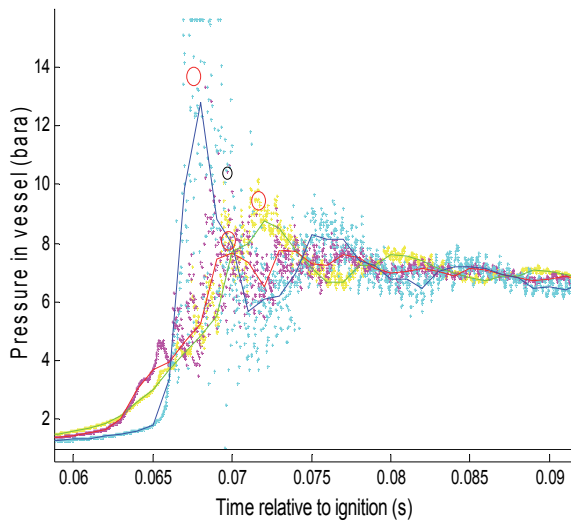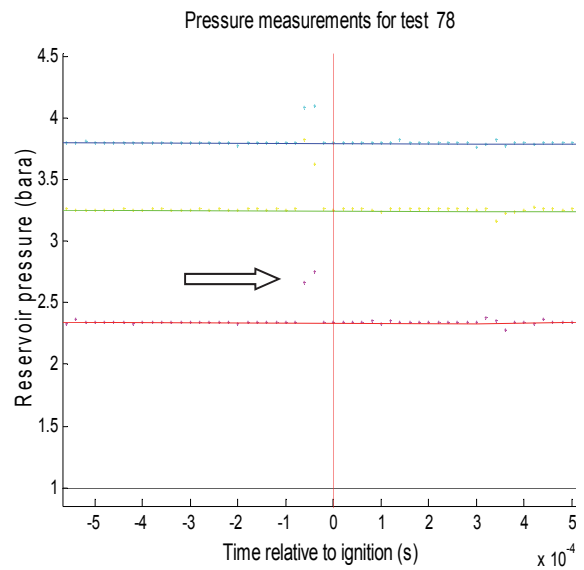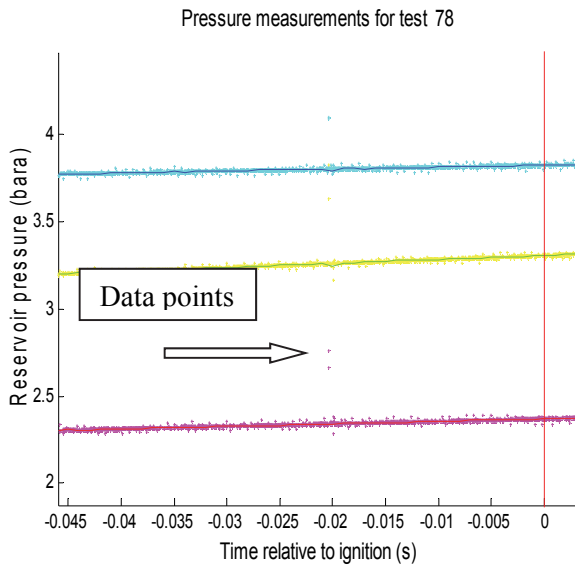
Figure 3.14 : *Original data from test number 78, reservoir pressure above and FAT pressure below.*

Figure 3.15 : *Adjusted data from test number 78, reservoir pressure above and FAT pressure below.*

The pressure measured inside the FAT, as seen in the lower part of Figure 3.14 and Figure 3.15 will be discussed in section 4.1.3.

3.5.3 Flame arrival from the thermocouple data

The flame arrival times were measured internally by means of thermocouples. The onset of flame arrival were set to the time where the derivative of the temperature reached 1500 °C/s, as shown in the lower section of Figure 3.16. This criterion worked well for identifying the flame arrival for experiments without obstructions. For some of the experiments with obstructions, the amplitude of the fluctuation of the curves were higher than shown in Figure 3.16, thus requiring a higher criterion, typically in the range of 2000-2500 °C/s. The new criterion was then used as an input in the MatLab script for the interpretation of the data. As seen below, where the black circles indicate the detection time for the flame arrival, the criterion for the onset of flame arrival works quite well for determining the sudden temperature change associated with the reaction zone of the flame.
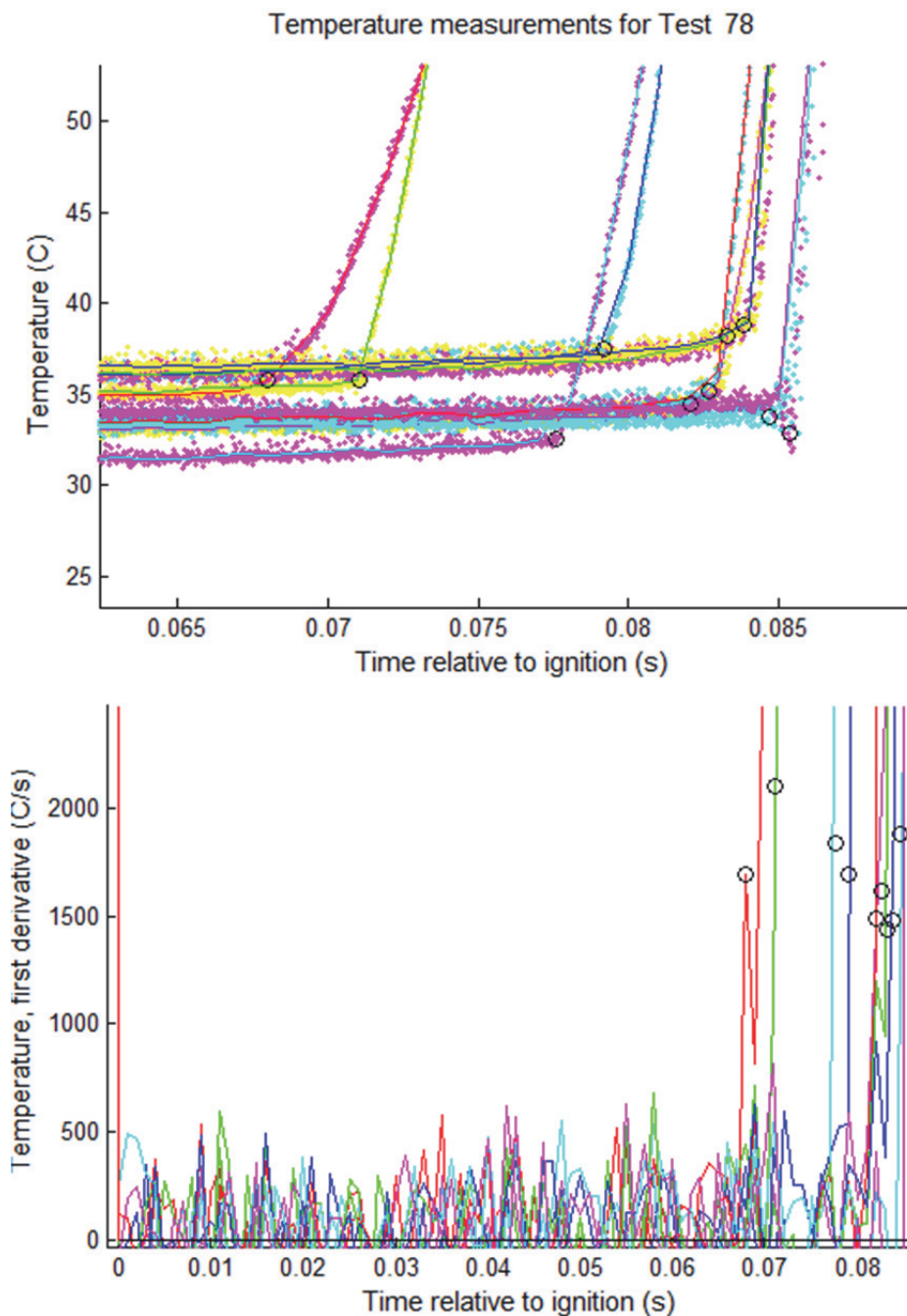
Figure 3.16 : *Temperature (above) and the derivative of the temperature (below) for test number 78, 3.0% propane, closed volume with obstruction configuration #2 Each color represents a measuring position.*

4.   Experimental Results and Discussion

The experimental results are presented and discussed. The chapter is divided in four sections.
Section 4.1 presents the initial conditions and measuring methods.
Section 4.2 presents the results for the vented experiments.
Section 4.3 presents the results for the obstructed experiments.
Section 4.4 presented an overview of the most important data and new findings from the previous sections.

4.1   Initial Conditions and Comparison of Different Measuring Methods

4.1.1   Initial pressure and fluid motion inside the FAT

The initial conditions varied due to the performance of the pneumatic valves. Since the valves did not have the exact same timing in each test, the amount of air that was released into the tube prior to ignition varied. The residual pressure inside the reservoirs was measured after each test. In some extreme cases, the pressure inside the reservoirs after the explosion was considerably higher than planned (8.1 bara in test number 16). This resulted in some inconsistencies regarding the initial pressure. The average pressure inside the reservoirs prior to injection was 17.39±0.18 bara, while the average pressure after was 2.63±0.09 bara.

If we assume that the temperature was the same before and after, and that the air behaves as an ideal gas. The average initial pressure inside the FAT is given by;

$$p_{F,f} = \frac{(n_{F,i} + n_{R,i} - n_{R,f})RT}{V_F} = \frac{\left(\frac{p_{F,i}V_F}{RT} + \frac{(p_{R,i} - p_{R,f})V_R}{RT}\right)RT}{V_F} = 0.959 bara \qquad \text{Equation 4.1}$$

This is 5.4% below the ambient pressure. This will in turn affect the stoichiometry of the experiments with gaseous fuel, as summarized in Table 4-1.

Table 4-1 : *Calculated experimental concentrations for gaseous fuels in reference to the initial condition.*

Propane concentration		Equivalence ratio	
1.0 bara	0.959 bara	1.0 bara	0.959 bara
3,00 %	3,13 %	0,74	0,77
4,50 %	4,69 %	1,12	1,17
6,00 %	6,26 %	1,52	1,59
7,50 %	7,82 %	1,93	2,02

A correlation of the initial pressure at the time of ignition was not conducted, hence there could be an inherent mixture error for each of the experiments performed. This will also mean that the maximum theoretical pressure for the mixture will be decreased or increased in reference to the actual pressure at ignition. This varying injection of air would possibly affect the turbulence level at the time of ignition.

The initial conditions inside the tube at the time of ignition, for both the gas and dust mixtures were turbulent as a consequence of the injection of air. The level of turbulence was not measured, but the same triggering sequence was used to ensure as identical as possible initial conditions for the gas and dust mixtures.

4.1.2   The pressure time history inside the reservoirs

The pressure-time history inside the reservoirs was monitored by three pressure transducers from PCB, Figure 4.1 shows a typical signal from the high pressure reservoirs. The curves shown are as follow, red (reservoir #1), green (reservoir #2) and blue (reservoir #3).

There is a rapid decrease in the pressure after the pneumatic valves open and the air leaves the reservoirs. However, the signals were not in agreement with the measured residual pressure inside the reservoirs after the injection. This discrepancy was investigated by some comparison tests with the pressure measuring system based on the Kistler transducers (yellow curves).
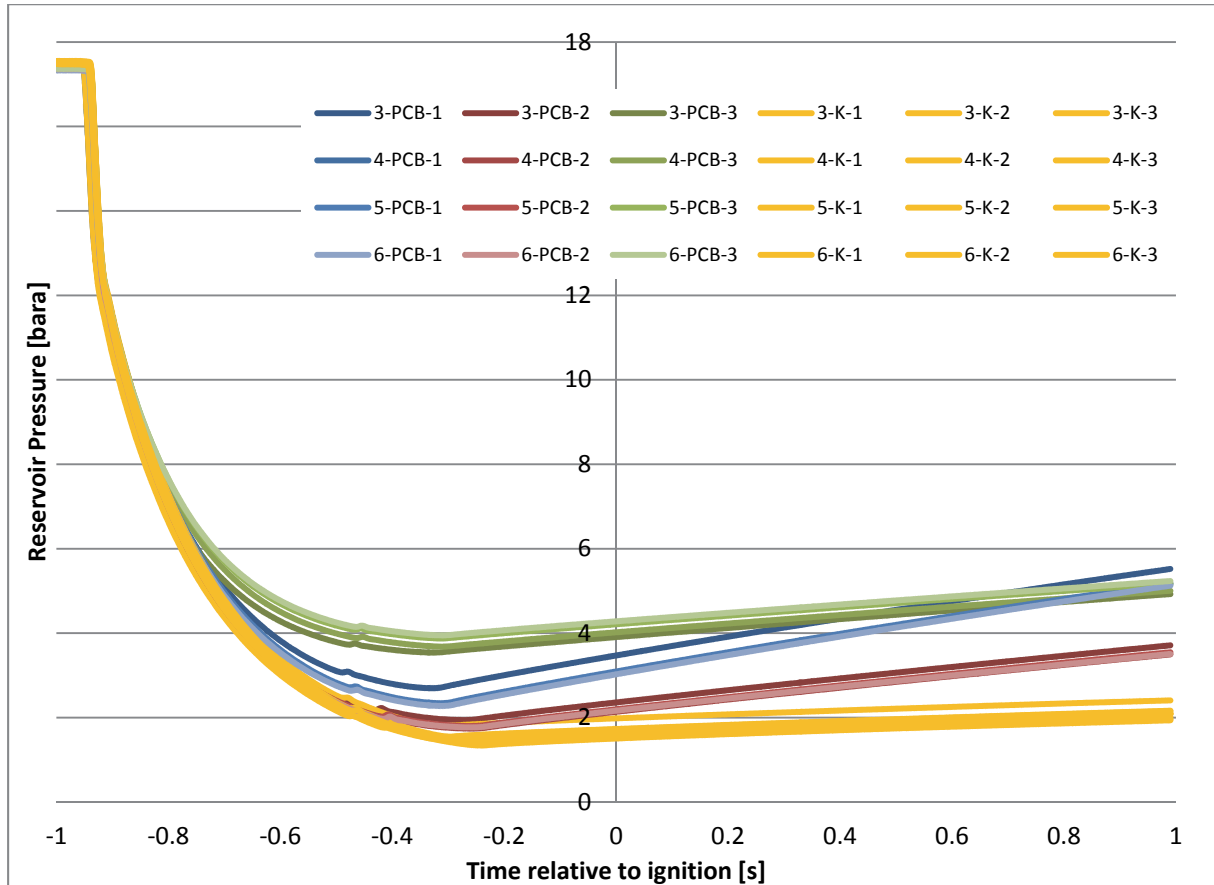
Figure 4.1 : *Comparison of the pressure history curves for different pressure measurement equipment inside the high pressure reservoirs for 4 different evacuation tests.*

While the reservoir pressure measured with the system from Kistler (yellow) give a consistent pressure curve, the signals from the PCB system drift significantly. The most likely reason is a too short discharge time constant (DTC) of the PCB sensors and the charge amplifier. The DTC is basically the time required for the amplitude of a pulse to decrease to a given value (typically 10% of the amplitude maximum). In the pressure measuring system, this value is the voltage of the initial signal. In a resistor-capacitor circuit as we have, the DTC (50 seconds for the sensor and 5 seconds for the amplifier) will add up like resistors in parallel, resulting in a DTC shorter than the shortest DTC of the components, as shown in Equation 4.2.

$$DTC_{total} = \frac{1}{\frac{1}{DTC_{sensor}} + \frac{1}{DTC_{amp.}}} = \frac{1}{\frac{1}{50} + \frac{1}{5}} = 4.5 \ seconds \qquad \text{Equation 4.2}$$

This decay time of 4.5 seconds resulted in the signal "loosing" strength early in the evacuation process and not reaching the pressure both measured manually and with the Kistler system. The DTC for the Kistler sensor was not found in the manual, but the amplifier has an adjustable DTC, where the medium setting of 10.000 seconds was used. Based on this discrepancy between the Kistler and PCB systems, the pressure data from the reservoirs were not further analyzed.

4.1.3   Comments regarding the pressure measuring system in the FAT

The experimental data for the pressure development inside the channel was recorded at a logging rate of 50.000Hz. This signal is then smoothed and resampled in a MatLab script as seen in Appendix C : . An example of raw and resampled data is shown in Figure 4.2 and Figure 4.3. The smoothing is done by a Savitzky-Golay filter, which, for each data point, fits a second order polynomial to a certain interval of surrounding points. This method works fine for the least violent experiments. However, when the pressure rise is at the highest, the noise generated decrease the accuracy of the method to the point where the accuracy could be taken into question. In the MatLab script, the number of data points before and after each of the points can be varied to alter the degree of smoothing. Unfortunately, this was not done in the present work. This results in poor representation of the pressure curves for some of the most reactive explosions.
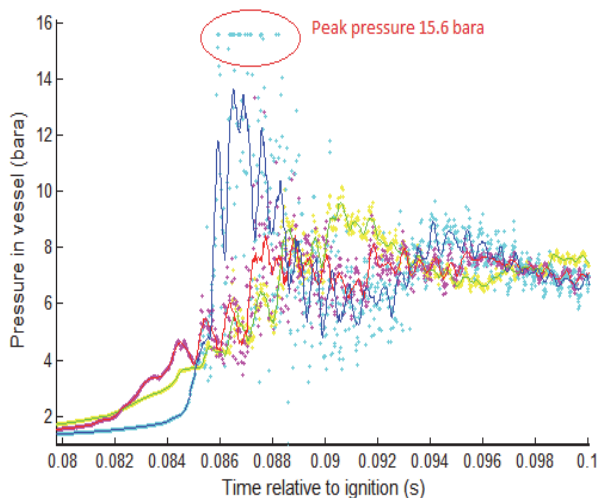
Figure 4.2 : *Adjusted pressure data from MatLab for test number 7. Curves indicating the resampled signal.*
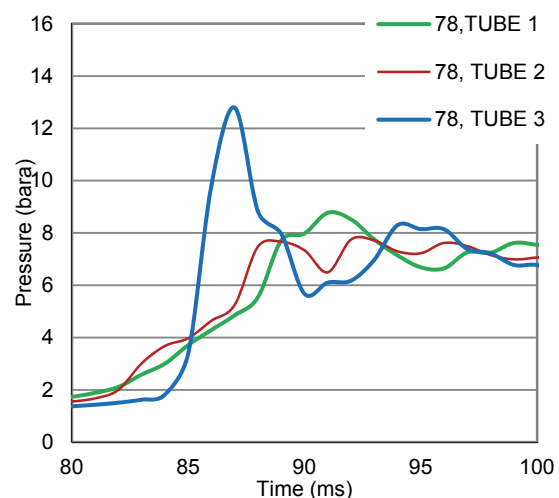
Figure 4.3 : *Adjusted pressure data from test number 78. The smoothed and resampled data plotted in Microsoft Excel.*

The red circle in Figure 4.2, indicates the upper threshold for the pressure measurements, resulting from the amplification of the charge amplifiers. The received signal on the NI-CAD card is limited to ±10V, where the amplification from the Kistler amplifiers gave +1V for a pressure of 1.5bar. Hence, any pressure difference above 15 bars would not be detected by the NI-Cad card. Resulting in a upper pressure measurement limit of 15.6 bara (15 bar explosion pressure + 0.6 4bar initial pressure). As a consequence, the pressure represented in the present work for the most violent explosions are most likely under predicted.

An approximate solution to this would be to assume that the distribution of the noise in the signal is symmetrical around an average value. An equal amount of points could be excluded on the lower end of the signal for a given time interval. Assuming a limited fraction of the data points within a

specified, and relatively narrow, interval, exceed the 15.6 bar threshold, this approach would most likely result in a better estimate for the average value.

4.1.4   Comparison of visually observed data and the thermocouple readings

The deviation between the data logged by the NI-CAD card and the visually observed was compared and a visual representation of the results with vent panel 1 can be found in Figure 4.4. The dotted lines in Figure 4.4 represent the arithmetic average and the standard deviation of the detection times as shown in **Table 4-2**. The visually observed time is set to zero, thus giving negative value if the thermocouples detect the flame after that of the video analysis. Each of the data points symbolizes the measuring points as shown by the arrows in Figure 4.6.
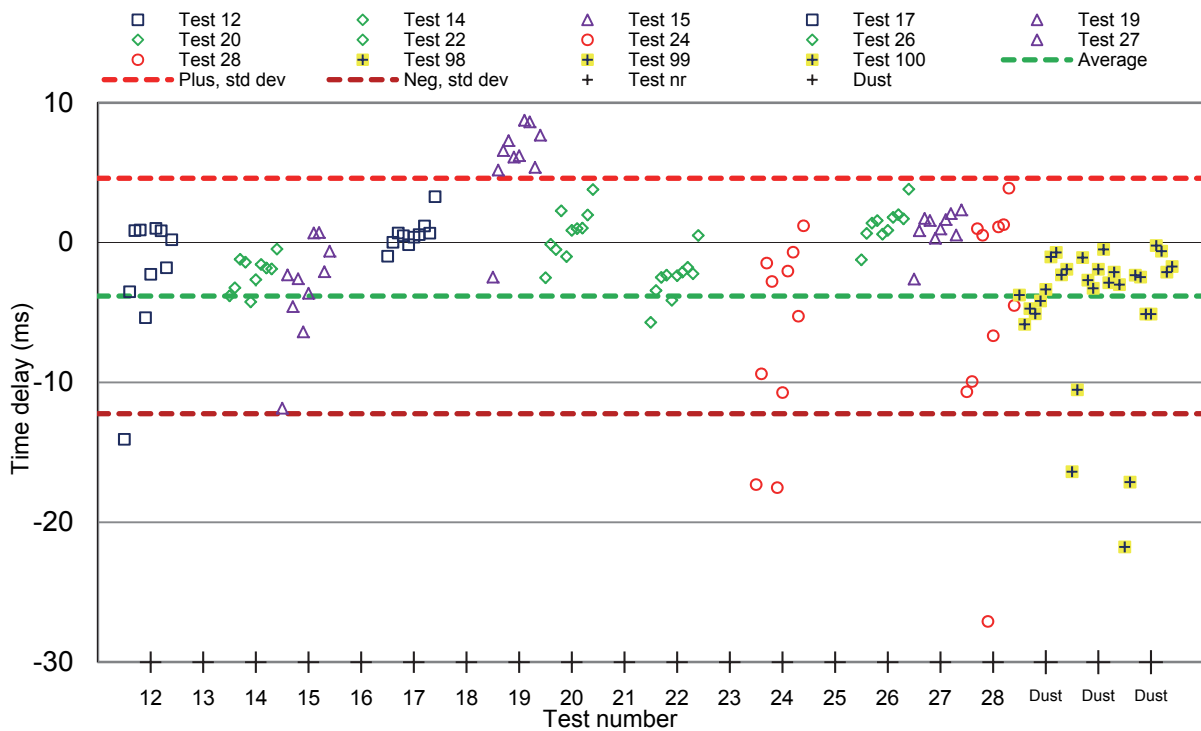
Figure 4.4 : *Comparison of the Visual observed flame and the detection of flame arrival from the thermocouple data for selected tests with vent panel 1. Each point represents the data for one of the measuring positions. Blue =3.0%, Green =4.5%, Purple =6.0%, Red = 7.5%, Yellow =500g/m³ maize starch.*

The largest deviation was found for the experiments with the lowest flame speeds. This is illustrated in Figure 4.4, where the tests with 7.5% propane (red circles) show the largest scatter. The different configurations of either closed volume/vented and smooth surface/obstructed affected the deviation as shown in **Table 4-2**.

Table 4-2 : *Deviation between the different flame arrival methods for the different physical configurations*

	Total number of test	Average delay time [ms]	Standard deviation [ms]
Smooth, Vent area #1	20	-3.8	8.4
Smooth, Vent area #2	13	-1.3	5.5
Smooth, Vent area #3	11	-2.2	6.7
Obstructions #1,Closed and vented	18	-3.6	8.3
Obstructions #2, Closed	21	0.9	6.6

40

Figure 4.5 illustrates how the deviation between the data varied as the flame propagated through the tube for some selected gaseous tests with vent area number 2. The first two thermocouples tend to detect the flame prior to the visual observation. As the flame accelerated through the tube, the deviations do not follow a consistent pattern, with visual observations both before and after the thermocouple readings.
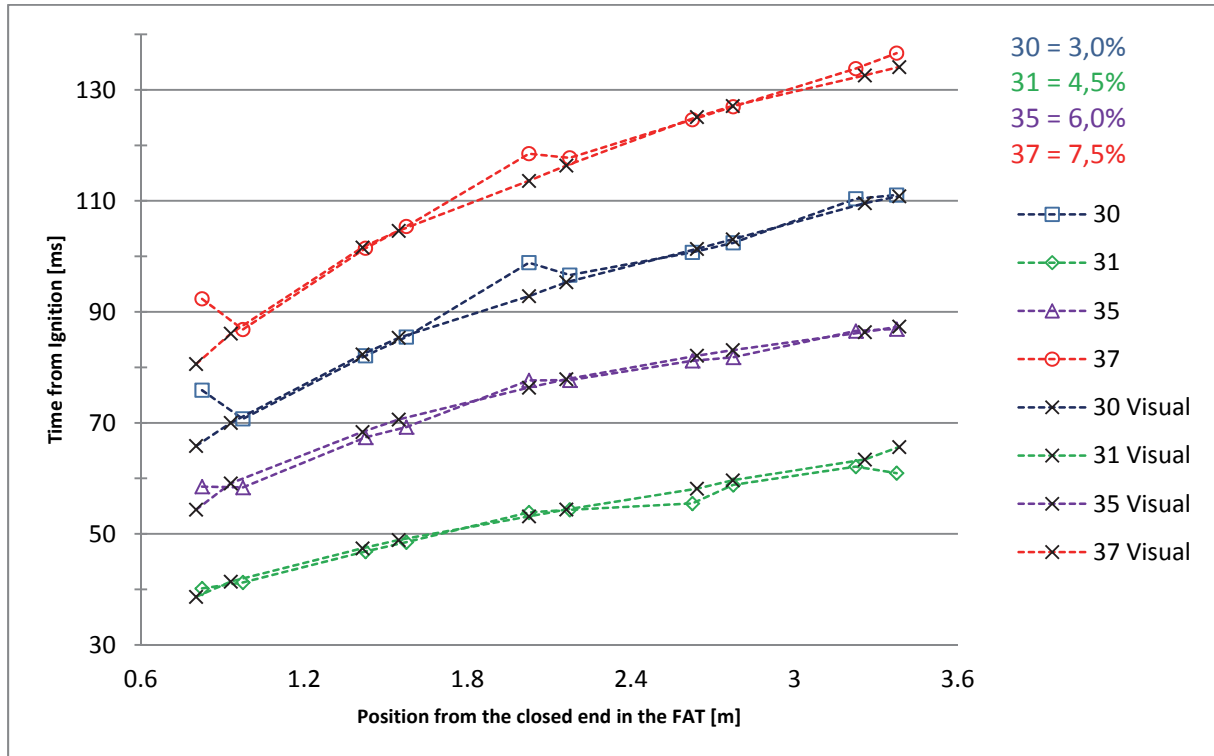
Figure 4.5 : *Comparison of visual and recorded data for selected propane-air tests with vent panel 2.Visual observation marked by crosses, thermocouple data by geometrical figures.*

Table 4-3 : *Visual observation and thermocouple readings for test 31, 4.5% propane. All numbers in milliseconds.*

Time relative to ignition [ms]	Position									
	TF1_2a	**TF1_2b**	**TF2_1a**	**TF2_1b**	**TF2_2a**	**TF2_2b**	**TF3_1a**	**TF3_1b**	**TF3_2a**	**TF3_2b**
Thermocouple	40.1	41.2	46.8	48.5	53.9	54.3	55.5	58.8	62.1	60.9
Visual analysis	38.7	41.4	47.4	48.9	53.2	54.4	58.2	59.7	63.4	65.7
Deviation	-1.5	0,2	0.6	0.4	-0.7	0.1	2.7	0.8	1.3	4.7

Table 4-3 summarizes the data, while Figure 4.6 illustrates the comparison for test number 31, 4.5% propane and vent panel number 2. As shown here, the deviation between the flame arrival data is in the order of milliseconds. In order to appreciate the significance of the millisecond deviation, it is useful to create a visual picture of the situation. In a perfect world, the flame front would be located at the tip of each of arrow as shown in Figure 4.6 at the different times indicated by the thermocouples. Unfortunately, this is not the case, resulting in flame speed measurements from the thermocouple data which look even worse than the visual observed as shown in section 4.2 and 4.3. The test shown here is one of the tests with the smallest deviation. Hence, for less reactive mixtures, the visualization of the thermocouple data would not present the same accuracy as shown in Figure 4.6. Flame speeds recorded by the thermocouples are therefore not included in the results.
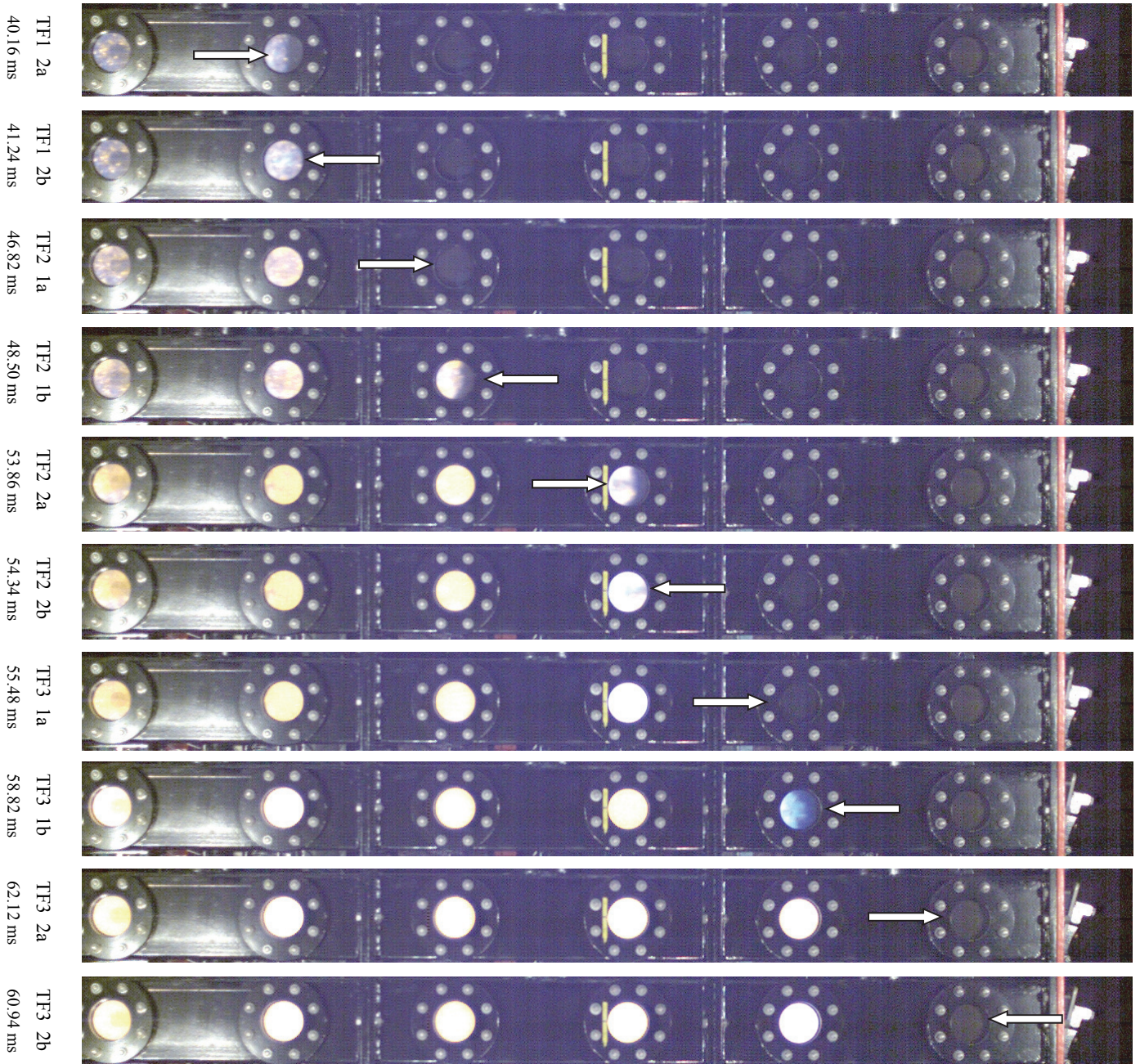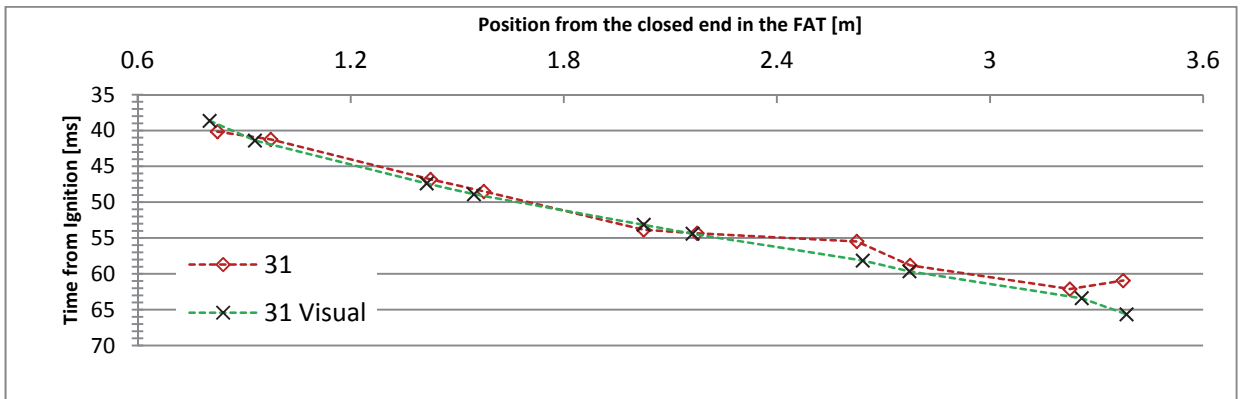
Figure 4.6 : *Selected frames from test 31, 4.5% propane, showing estimated arrival time by the thermocouples (red line in graph), arrows indicating measuring point, arrival times in reference to Table 4-3.*

4.2   Vented Experiments without obstructions

Vented experiments with both gas and dust were conducted and then compared to each other.

4.2.1   Flame speed

The flame speed (S_f) along the length of the FAT is calculated from visual observations of the flame front. The accuracy of these measurements is limited by the temporal resolution of the high-speed video recordings as well as inherent uncertainties in the identification of a well-defined flame front. Given the physical dimension of the Plexiglas windows, speeds exceeding 450 m/s are not possible to measure accurately for the first 55 tests, but for the remaining tests, this limit is increased to around 850 m/s. In the figures presenting the results, the test number is included as the first number in the legends. The flame speed is calculated as the distance the flame travels between the observed points, divided by the elapsed time.

Since the detection of flame arrival is conducted by the author, the observations are somewhat subjective. This is especially the case for the observation when the flame front exits the FAT through the vent area. At this point, the flame is no longer confined by the walls, thus propagate in all the directions. The position for flame observation outside of the FAT is along the centerline, 7.1 cm from the end wall.

To appreciate the actual speed of the flame front, it may be helpful to place it in a familiar context, such as driving in a car or a bus. In Norway the normal speed limit outside populated areas is 80km/hour, which might be considered a high velocity. However, 80 km/h, or about 22 m/s, corresponds to a slow deflagration. The flame speeds observed in the FAT reach speeds approaching 1000m/s or 3600km/h for some of the most extreme situations.

A summary of the experiments with vent panel number 1, 2 and 3 are shown in Figure 4.7, Figure 4.8 and Figure 4.9, respectively.
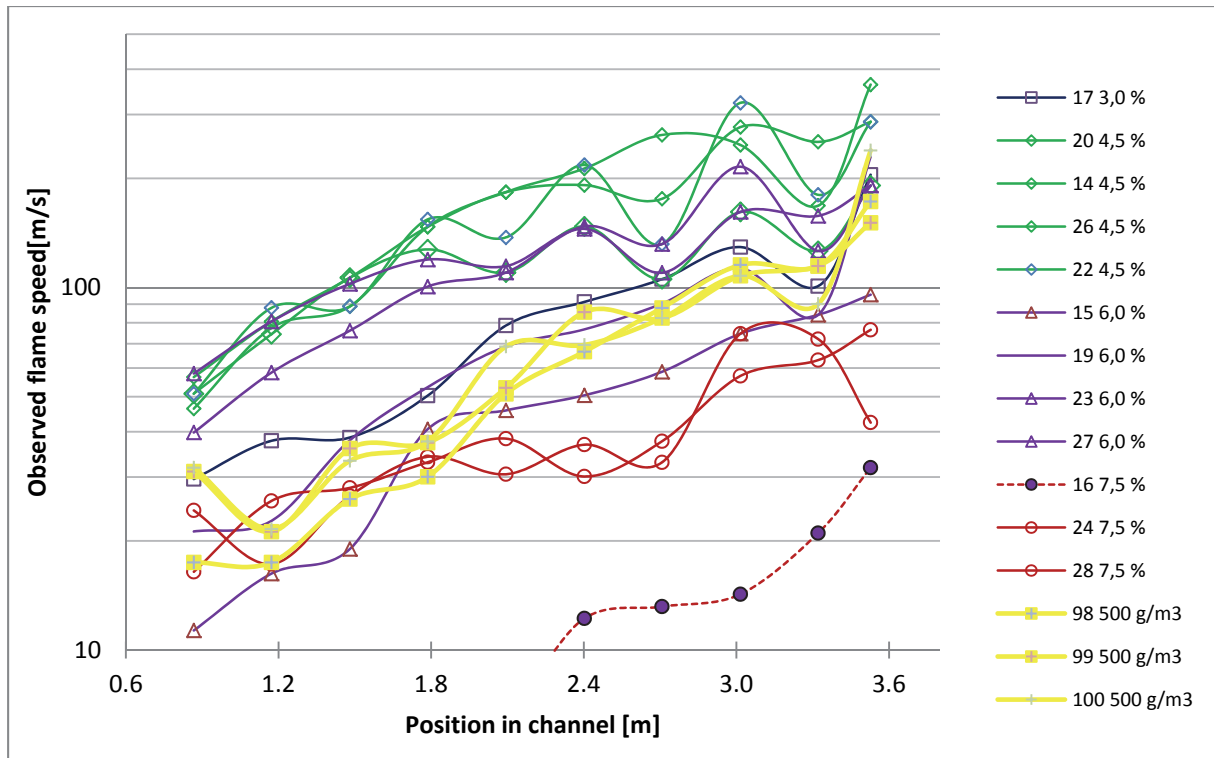
Figure 4.7 : *Visually observed flame speed in vented experiments with gaseous and solid fuel. Vent area #1 (large). The results for test number 16 deviates from the other results due to a problem with the pneumatic valves.*

The expansion of combustion products combined with the increased turbulent combustion accelerates the flame front as it approaches the vent opening. The flame front reached the highest speeds, approaching 400 m/s, for gaseous experiments at concentrations slightly above stoichiometric. Flame speeds were observed.

The visually observed flame speeds for maize starch seem to have a similar profile as the gaseous experiments. For vent opening number 1 (large), the maize starch experiments reached speeds resembling that of a 6% propane-air explosion. This is in contrast to the smaller vent sizes shown in Figure 4.8 and Figure 4.9, where the profile of a 7.5% propane-air mixture seemed more appropriate. A possible explanation for this might be that dust starts to fall out of suspension and thus decreasing the explosibility (500 g/m^3 is said to be the worst case scenarios) of the mixture as the flame speed decreases with decreasing vent area. The maize starch experiments had flame speed in the last section of the channel of approximately 180, 100 and 70 m/s for vent panel 1 (large), 2 (medium) and 3 (small), respectively.

For test number 16 as shown in Figure 4.7, the pneumatic valves that control the inflow of air from the reservoirs malfunctioned. This resulted in a lower initial pressure around 0.9 bara in the FAT. This decrease in pressure resulted in a change in the stoichiometry of the mixture, from the intended 7.5% to around 8.3% propane, which has the lowest laminar burning velocity of the mixtures. The decrease in the inflow from the reservoirs would also result in a lower level of turbulence.
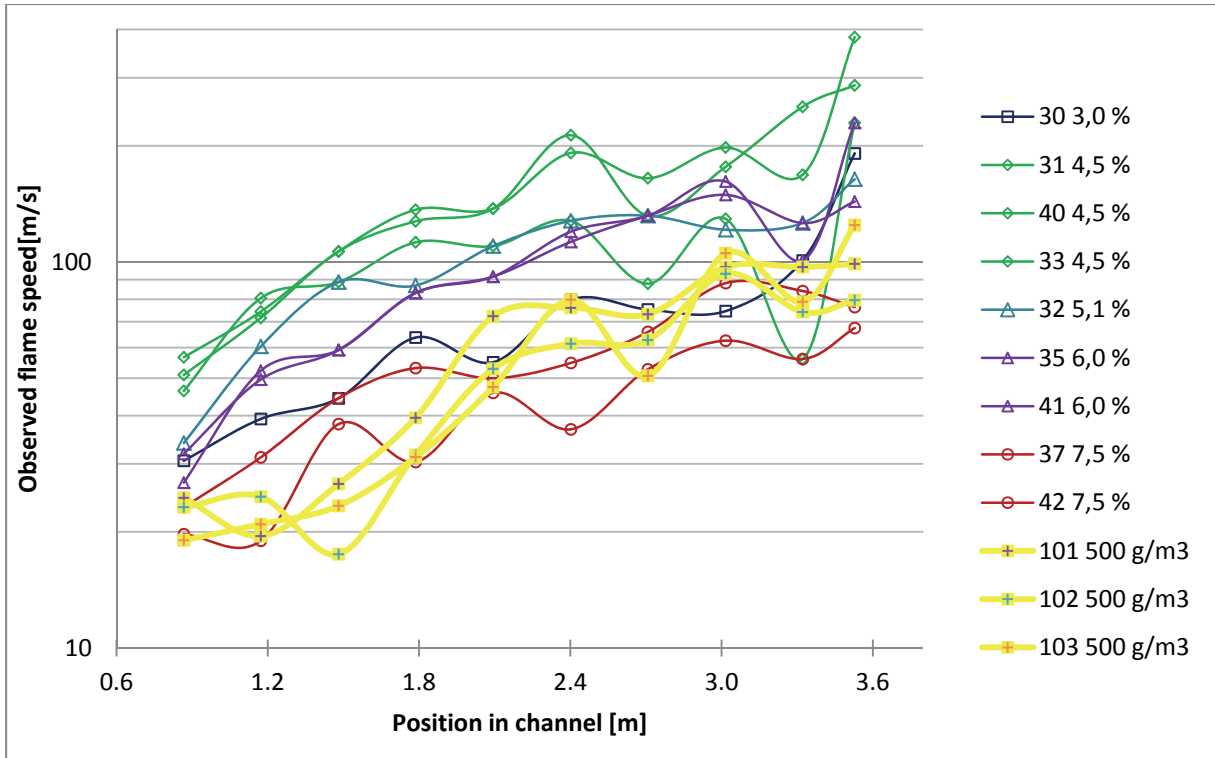
Figure 4.8 : *Visually observed flame speed in vented experiments with gaseous and solid fuel Vent area #2 (medium). Logarithmic flame speed.*
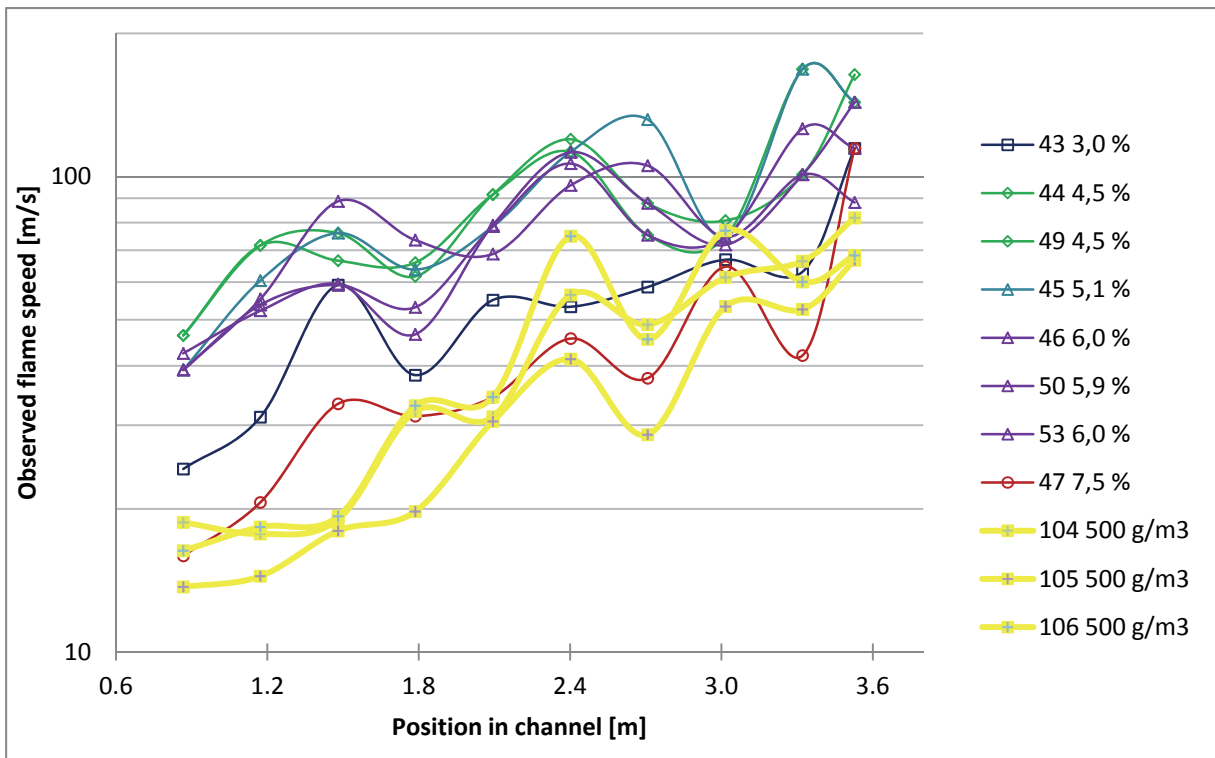
Figure 4.9 : *Visually observed flame speed in vented experiments with gaseous and solid fuel. vent area #3 (small). Logarithmic flame speed.*

As shown in Figure 4.9, the visual flame speeds recorded for the experiments conducted with vent area number 3(small) seem to approach more or less the same flame speed, 69±8 m/s, before the last two windows. This is in contrast to the rest of the tube, where the flame speeds are "scattered" all over the place. In between the measuring positions, a dust dispersion nozzle and eight fastening brackets for the obstructions are located. No explanation of this odd phenomenon has been found, but some interactions between the flame front, vent opening and the dispersion nozzle, might influence the flame front at this location.

4.2.2   Pressure measured with piezoelectric transducers

The maximum pressures reached as the flame propagated through the FAT varied with the different mixture compositions and vent areas. The highest pressures were reached for slightly above stoichiometric propane concentrations and the smallest vent area. Typical pressure curves for vented explosions with vent area number 1(large) and rich gas and dust are shown in Figure 4.10.
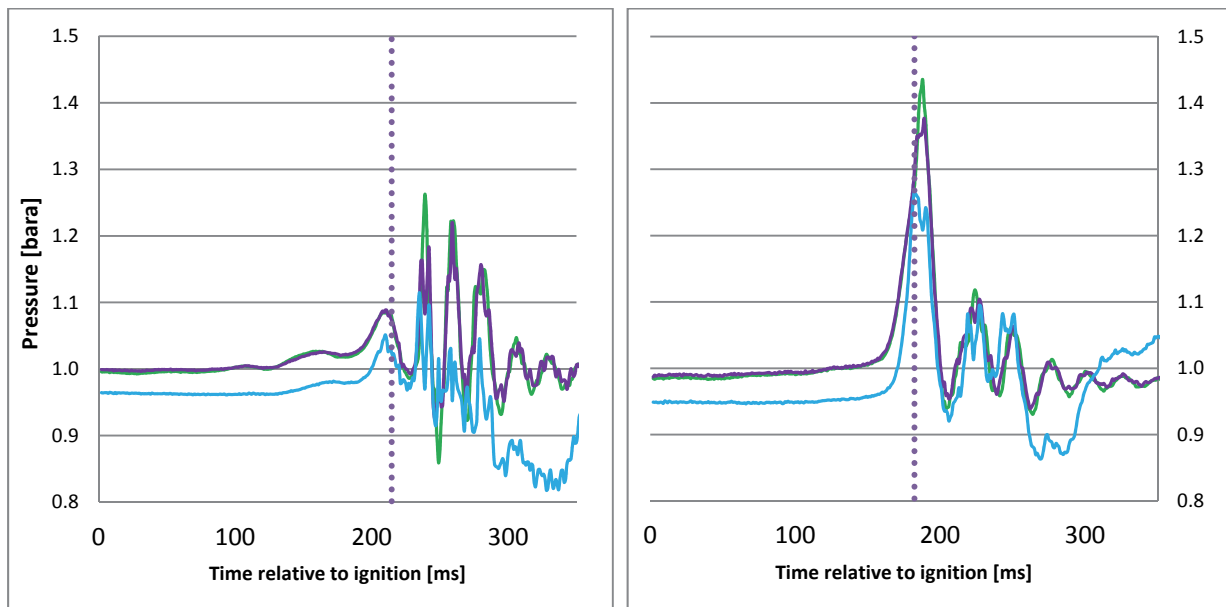
Figure 4.10 : *Pressure history with vent area 1.Vertical dotted line represents the time of arrival of the visually observed flame front at the vent opening. Green, Purple and Blue represents sensor 1, 2 and 3 respectively. A) Test number 24, Spark ignition of 7.5% propane-air. B) Test number 98, 40J chemical ignition of 500g/m³ maize starch.*

As seen in Figure 4.10, the pressure measured at the different sensors in the FAT have similar pressure history curves. The sensor located near the closed end, commonly measures the highest pressure, and the peak pressure decrease closer to the vent opening. The peak pressure used to describe the different experiments will refer to the highest pressure, regardless of the position in the channel. In vented experiments, the expansion of hot products pushes unreacted mixture out of the channel, where a secondary explosion may take place.
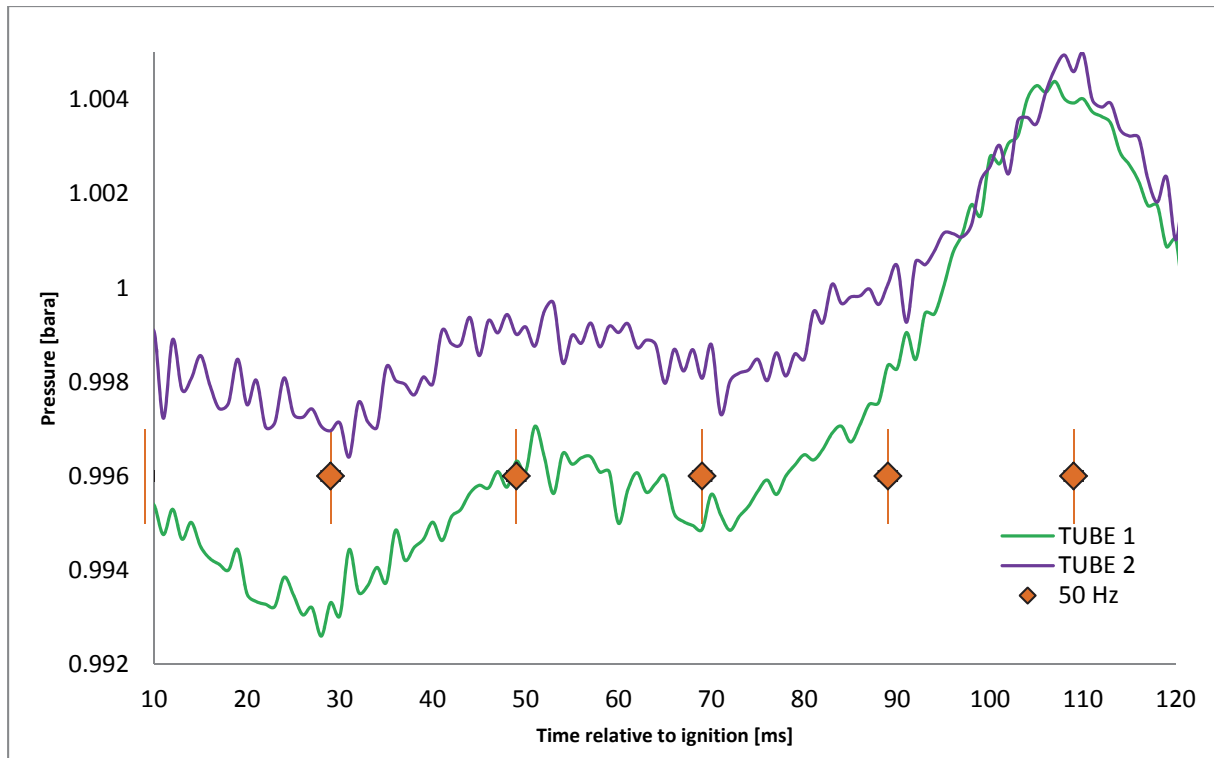
Figure 4.11 : *Fluctuations in the measured pressure signal from the Kistler System, Test number 24. A 50 Hz disturbance is indicated by use of some data points.*

As illustrated in Figure 4.11, there are some fluctuations in the measured pressure. The amplitude of this fluctuation is approximately 50 Hz for many of the experiments, thus introducing the possibility that this noise might originate from the 50Hz, 240V powered equipment used in the FAT. As seen above, the signals are influenced by many different frequencies, thus making it hard to identify the various disturbances. One of the possible sources of the disturbance in the signals may originate from acoustic waves, which could travel back and forth in the tube. This behavior is observed in earlier work in the FAT with closed volume experiments. Acoustic waves cause the flame front to vibrate back and forth as it approached the end wall. This disturbance is most pronounced for the least reactive mixtures, thus the rich 7.5 % propane-air and the dust clouds.
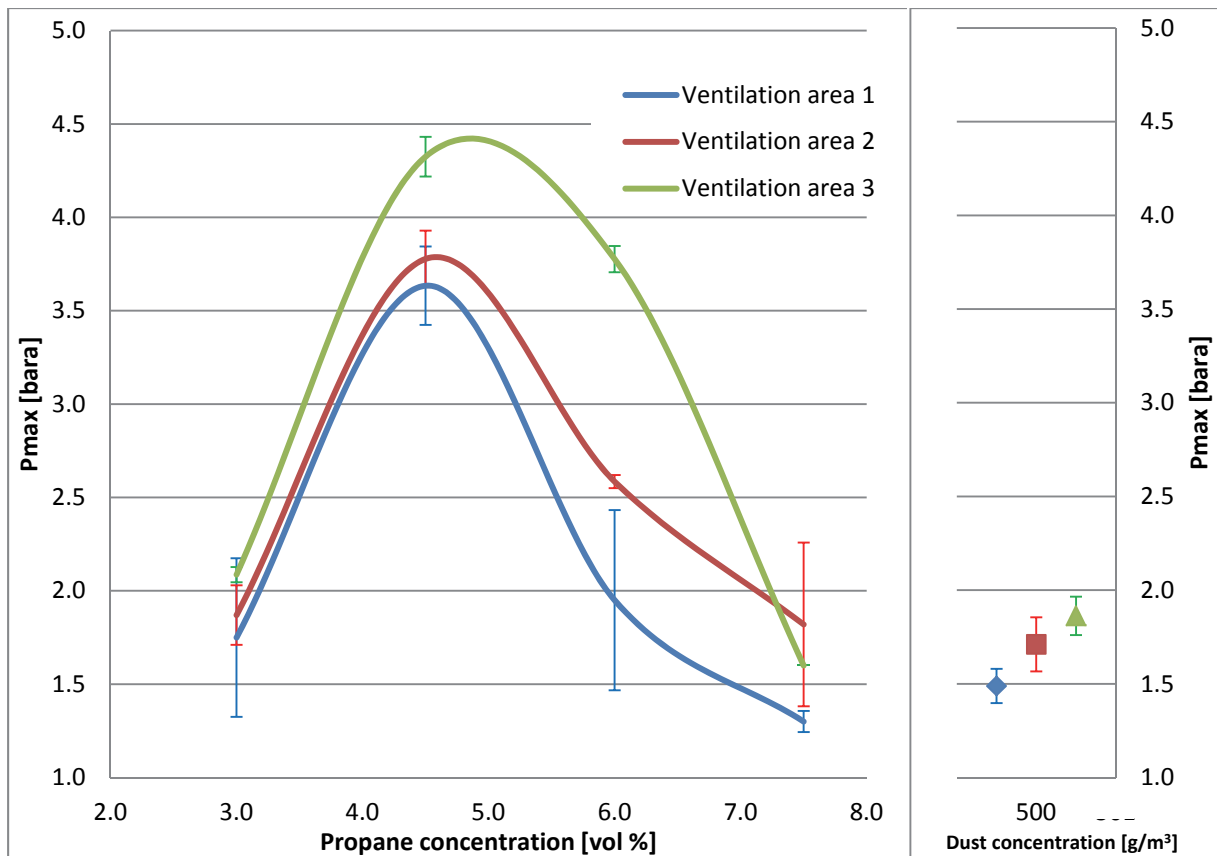
Figure 4.12 *: Maximum pressure for vented experiments without obstructions for both gaseous and solid fuel. The curves represent the average value, including the standard deviation at the given concentrations.*

Figure 4.12 shows that the results from propane, for the different vent configurations, resemble the pressure curves obtained in closed vessels by Razus as shown in Figure 2.2. The rather large standard deviation at some of the concentrations for gaseous experiments presented in Figure 4.11, shows that many more experiments should be conducted at the given configurations to ensure a representative illustration of the peak pressure in the vented explosions.

However, decreasing the vent area seems to increase the pressure developed. The reason for this can be explained with an example from the daily life. Consider the situation of manually pumping air into a football. After first trying to pump one time without the needle attached to the end of the pump, and then attach the needle, one can feel the increased resistance applied to the piston by the air inside the pump. The same effect is reasonable to expect in the vented experiments conducted in this work.

As seen on the right side in Figure 4.12, the decrease in vent area had the same positive effect on the maximum pressure for the dust explosions. The pressure for dust explosions did not reach the same maximum values as the stoichiometric gaseous experiments, but rather similar to the rich 7.5% and lean 3.0% propane-air mixtures at the given vent areas.

This, although the energy release is not exactly the same , is in contrast to the maximum pressure reached in closed volume explosions, where the maximum pressure for maize starch dust clouds of nominal dust concentration 500g/m³ (8-8.5bar)[39] is in the same region as slightly rich mixtures of propane, while the rich 7.5% (3.7bar) and lean 3.0% (5-7bar) are lower as shown in Figure 2.2. However, the pressure for a dust explosion seems more likely to be compared to the rich mixture.

A possible explanation for this discrepancy in pressure for the dust and rich mixtures is the speed at which the reaction front is moving through the FAT. Contrary to a gas explosion, where fuel and oxidizer are mixed on a molecular level, combustion in a cloud of maize starch reacts by devolatilization and subsequent mixing prior to combustion. This causes an induction time for each particle, thus resulting in a thicker reaction zone. This thickened reaction zone, and the extensive radiation as the dust burns, cause problems with the detection of flame arrival at the windows. The problem with visually observing a flame front in a dust was also experienced in the balloon experiment[42] as shown in Appendix E : .

4.3   Obstructed Experiments

Experiments with the obstructions shown in section 3.3.3 were conducted and are discussed in this section. For safety reasons, and also to limit damage to equipment, vented gas explosions were not conducted with obstructions after initial tests with 3.0% propane resulting in flame speeds exceeding 1000m/s and maximum pressures measured of 15 bar (extreme value for a vented explosion indoors). Some of the damages to the equipment caused in these experiments are shown in Figure 4.13.
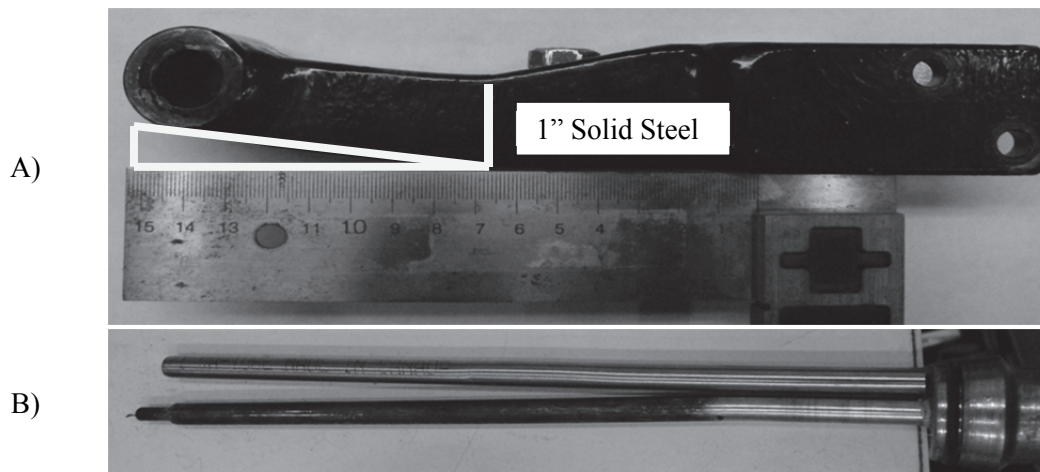
Figure 4.13 : *Damage to experimental equipment caused by vented gas explosions, 3.0% propane, with obstacle configuration number 1. A) Vent hinge. B) Thermocouple, the actual deformation was more severe, but the rod had to be straightened by banging on it with a club before physically removing it from the casing in the sidewall of the FAT.*

As a consequence of the extreme conditions with gaseous fuel, only vented dust explosions were conducted with obstructions eliminating the possibility to compare gas and dust explosions for vented scenarios.

4.3.1   Flame speed

4.3.1.1   Obstruction configuration number 1:

The flame speeds for dust explosions with obstruction configuration number 1(20 baffle plates) are presented in Figure 4.14. It should be noted that finding the flame arrival time for dust experiments with obstructions is not an easy process due to the intense radiation in the flame front that lights up the dust in the cloud in front of the burning zone.

Flame speeds approaching 500 m/s was observed for dust experiments with obstruction configuration number 1. By comparing the flame speeds obtained without obstructions as presented in Figure 4.7,

Figure 4.8 and Figure 4.9 to those obtained in the presence of obstructions as shown in Figure 4.14, one can observe that the obstructions have a strong accelerating effect on the flame front with speeds in the range 100-300 m/s on a general basis with obstructions, compared to 70-180 m/s from the experiments without obstructions.
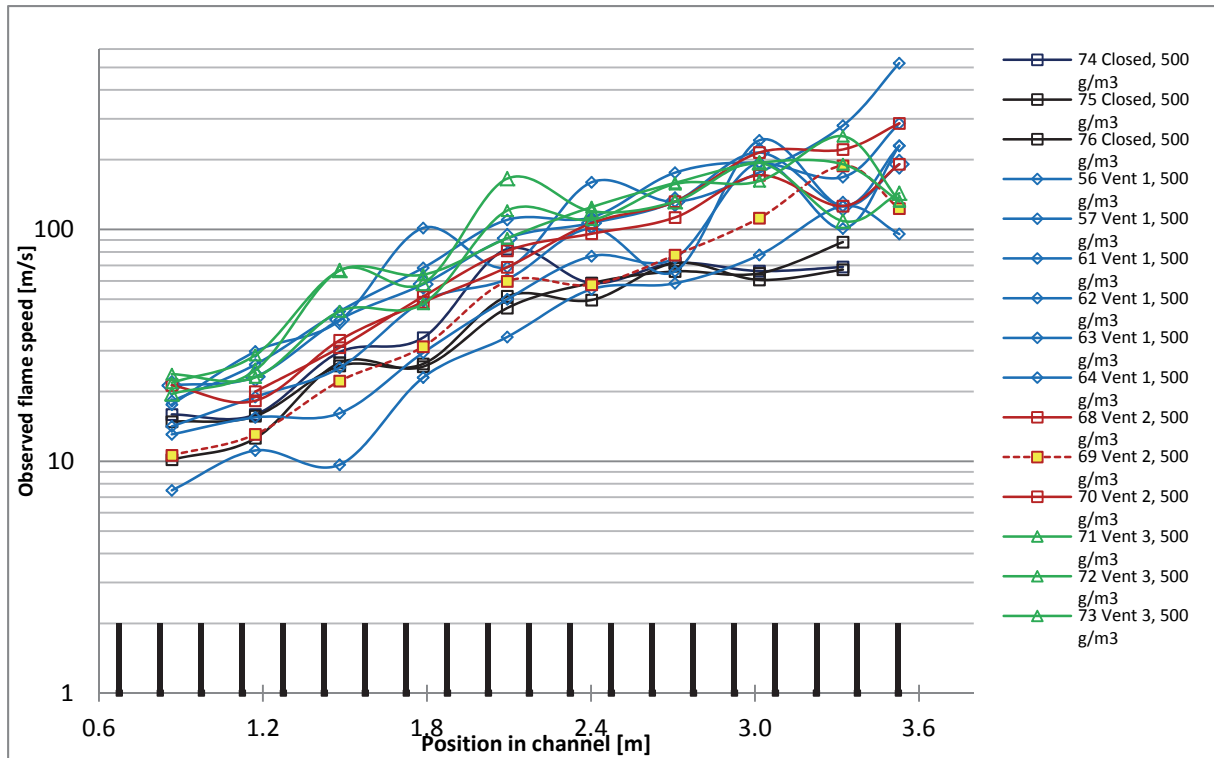
Figure 4.14 : *Flame speeds from visual observations in experiments with 500g/m3 maize starch and obstacle configuration #1 (position of obstructions indicated by vertical bars). Logarithmic flame speed, Test number 69 explained especially in the text.*

The experiments performed with constant volume (black lines) accelerate up to a near constant flame speed of about 70 m/s over the first 2.0-2.5 meter. This might be caused by the same effect seen in the experiments with smooth inner surface and vent area number 3(Figure 4.9). The reason for this observation still remains a big mystery, and further work on this observation might enlighten the mystery. Since the obstructed experiments were performed under constant volume conditions, the constant flame speed is of special interest since the flame propagates into a compressed but turbulent area without losing its speed. This scenario could be of great interest for the validation work for DESC since closed volume simulations of the FAT are quite easy to simulate compared to a vented scenarios as outlined in section 3.4.

Vented experiments with vent area number 1(large)(blue lines) received the most attention during this work. However, the poor repeatability of the experiments made it difficult to interpret.
The effect observed without obstructions, where a decrease in the vent area had a significant decelerating effect, is not seen for the dust experiments with obstructions.

However, the tests with vent area number 2(medium) (red lines) seems to have a constant acceleration trough the FAT. Test number 69 (red dotted line with yellow filled boxes) as seen in Figure 4.14, have a sudden decrease in the speed as it reaches the vent opening. The reason for this, and most likely many of the different curves with the characteristic drop in the last point, is that the vent panel still had not opened fully as the flame reached the vent. This observation was a common one when interpreting

the video recordings. This suggests that the inertia of the panel was too high, and a lighter panel should be used in further work.

The tests with vent area number 3(small) (green lines) have a characterizing drop in the acceleration in the last section of the FAT, with speeds around 200 m/s, which is still significantly higher than without obstructions (70m/s). Hence, one can conclude that the introduction of obstructions in the tube have a strong accelerating effect on the flame propagation.

4.3.1.2 Obstruction configuration number 2:

To evaluate whether gaseous experiments could be conducted or not, with obstruction configuration number 2 (10 baffle plates), the same approach as for obstacle configuration number 1 were used. It was concluded that gaseous experiments could be conducted only in closed volume scenarios. The visually observed flame speeds for both gas and dust explosions with obstruction configuration number 2 are presented in Figure 4.15.
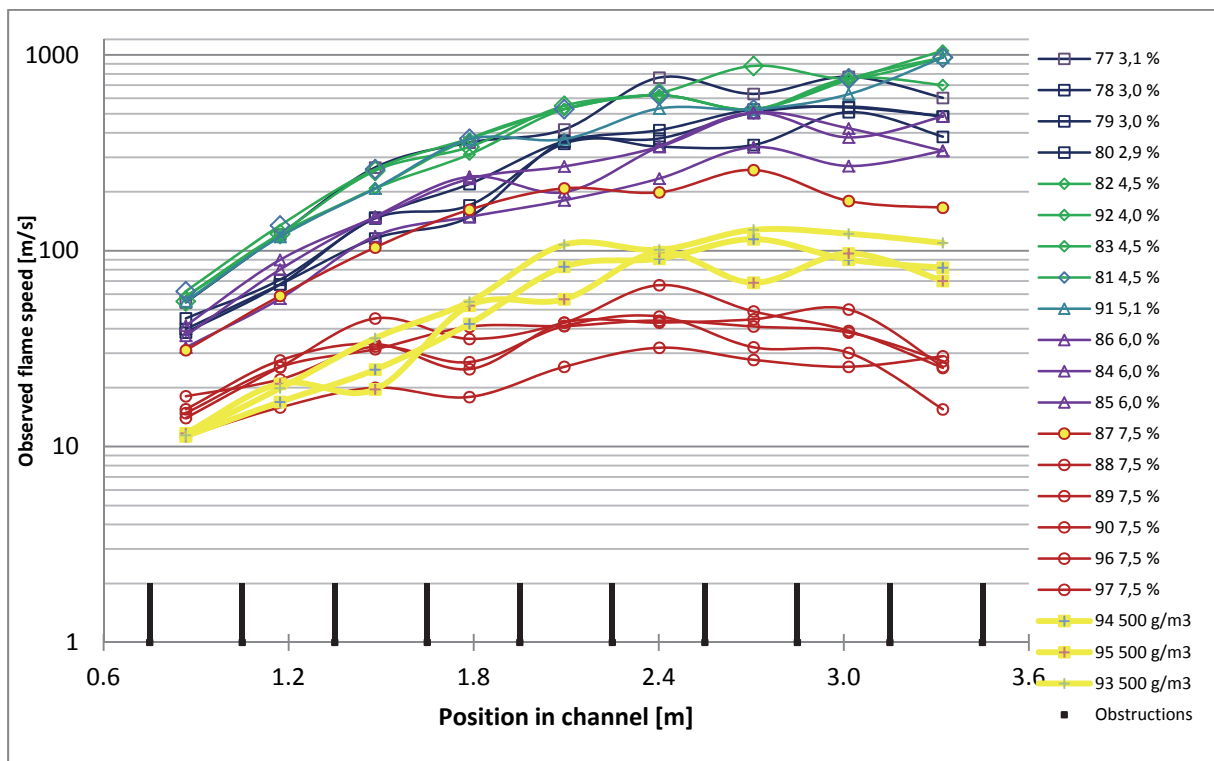
Figure 4.15 : *Visually observed flame speed in gaseous and dust experiments with obstacle configuration #2 shown as vertical bars. Logarithmic flame speed.*

As illustrated in Figure 4.15, the slightly rich mixtures of 4.5 and 5.1% produced the most violent explosions, with flame speeds approaching 1000 m/s. This is further discussed in section 4.3.2.

The 7.5% propane experiments seem to behave differently, with relatively slow flame speeds compared to the other mixtures. However, test number 87 does not seem to follow the general trend as the other experiments for the same concentration. This experimental repeatability, for the flame speeds at the given concentration, makes it difficult to quantitatively describe the rich mixture. However the main batch (5 out of 6) of the 7.5% propane experiments seems to have similar flame speeds. This observation suggests that the turbulence generated by the introduction of obstacles in a closed elongated volume, on the rich propane mixtures, do not result in the same flame propagation than the

more reactive mixtures experience. To quantitatively describe the mixture, attempts were made to find the laminar burning velocity for such high equivalence ratios in the open literature, sadly, this was not found. However, by estimating a modified Kg-value (obtained by the maximum pressure rise in a modified USBM-vessel, with an ignition delay of 60 ms) from the results of Skjold[46], the reactivity of the mixtures can be compared to the average flame speed as shown in Table 4.4, and illustrated in Figure 4.16.

Table 4.4 : *Comparison of the reactivity of propane and maize starch explosion in the FAT, with obstruction configuration number 2, the last observation has not been included in the calculated values.*

	K$_{st}$ and modified K$_g$ [bar m/s]	Average flame speed [m/s]	Standard deviation [m/s}
3.0%	330	456	86
4.5%	700	675	118
6.0%	520	371	95
7.5%	130	41	11
500 g/m^3 maize starch	150[39]	101	18
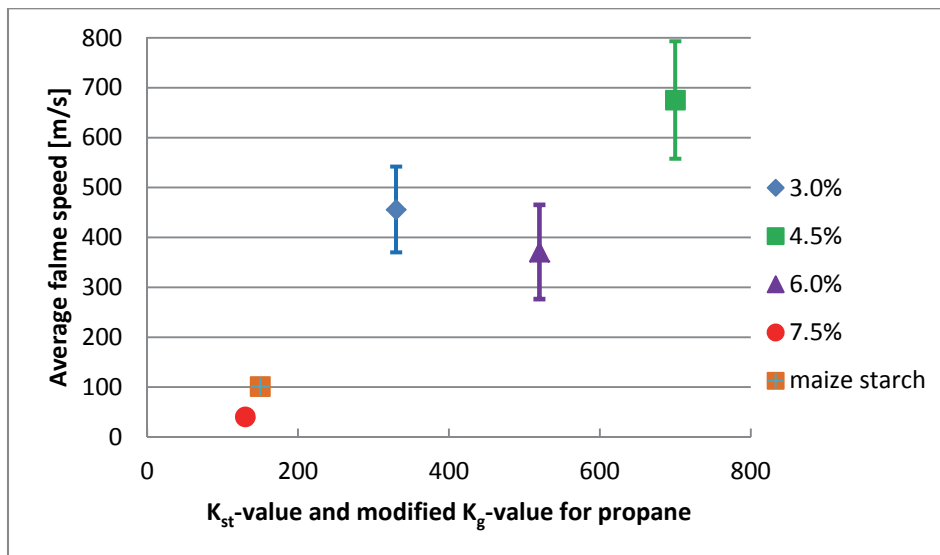
Figure 4.16 : *Calculated averaged flame speed in the last section of the FAT for experiments with obstruction configuration number 2,*

A modified K$_g$-value would be especially suited for the comparison, since the initial fluid motion inside the tube is turbulent at the time of ignition. As seen in Figure 4.16, no clear assessment can be made out of the data. However, the lack of correlations could indicate, as stated by numerous authors throughout the years, that the use of the K$_{st}$-value, may not be the best possible solution for safe design in process plants, since as shown in Figure 4.16, the flame speed and hence the violence of an explosion seem to decrease for the 6.0% mixture compared to the 3.0% mixture, regardless of the higher modified K$_g$-value.

The reactivity of the different mixtures and fuels shown in Figure 4.15, indicates that when modeling dust explosions with the *Meritena A* maize starch, the laminar burning velocity should be lower than those for the 3.0%, 4.5% and 6.0% propane mixtures.

The constant volume dust explosion experiments conducted with obstruction configuration 2 (10 baffle plates) gave higher flame speeds than the ones conducted with configuration 1(20 baffle plates), regardless of the fact of that there were only half the number of obstructions. However, the repeatability of the experiments with configuration number 1 seems to be better, suggesting that additional repetitions would be required for both configurations to qualitatively get a description of the possible propagating mechanisms that control the flame speed of a dust flame in an obstacle laden path.

The reactivity of propane is clearly visible when conducting experiments in near stoichiometric mixtures. With flame speeds in the range of 1000m/s, the possibility of reaching deflagration to detonation transition (DDT) starts to become an issue. This possibility is further examined in the next section, where the pressure and flame speeds are compared.

4.3.2   Pressure measured with piezoelectric transducers

The extreme speeds of some of the experiments conducted with gaseous fuel with obstacles generated such high levels of turbulence that the pressure rise in the last section of the FAT reached maximum rates of pressure rise of the order 10.000 bar/second. This intense pressure rise caused mechanical deformation of both obstructions and thermocouples. To illustrate the shear violence of the explosions, Figure 4.17 might be of interest. As seen here, the 1 cm thick aluminum baffle plate on the left side have experienced an intense shock which have deformed it quite severely. The orientation of the deformation suggests that the pressure wave has come from the right side e.g. the closed side. This might serve as an indication that the mixture trapped by the confinement of the end wall and the approaching flame front have reached such high temperatures that the mixture developed hot-spots and auto-ignition. The pressure time history from one of the candidates (test 91, 5.1% propane) to which explosion caused this deformation can be seen in Figure 4.18.

Figure 4.17 : *Deformation to the last obstruction caused by high local overpressure in experiments with propane and obstacle configuration number 2(10 baffle plates). Flow direction from left to right, with the end wall 15 cm from the right baffle plate.*
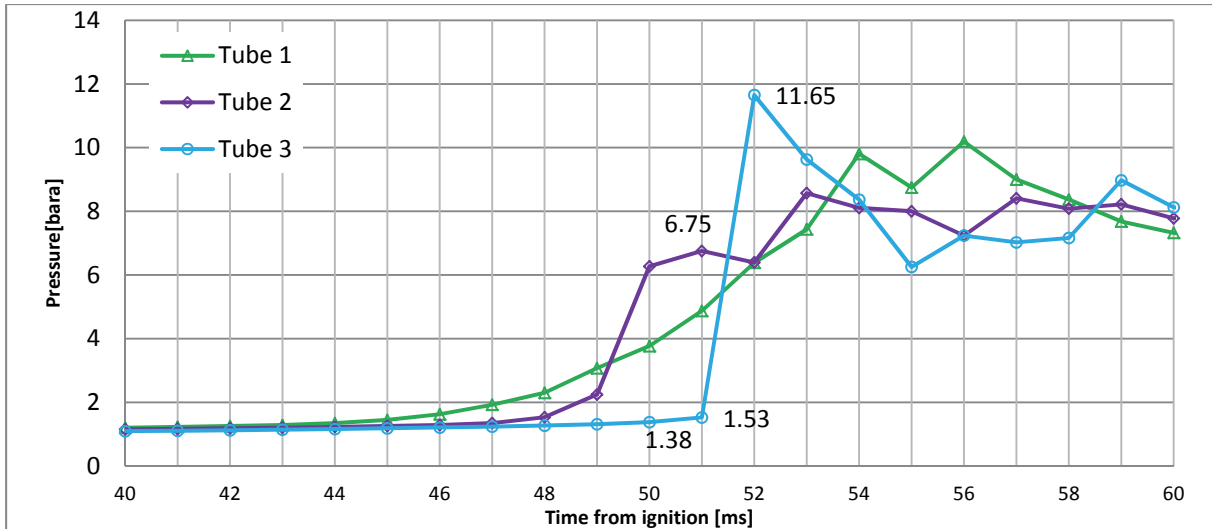
Figure 4.18: *Pressure time history for test 91, 5.1% propane-air, with obstacle configuration number 2. The distance between the measuring sensors is 120 cm.*

Figure 4.18 illustrates that the pressure recorded at the two first sensors both have a more steady pressure increase compared to the third sensor. The pressure measured at the end of the FAT undergoes a rapid increase before it levels out at a pressure equal to the other sensors. Since the flame speed measurements are not sufficiently accurate, it is not straightforward to determine whether the mixture did undergo DDT. Regarding the geometry of the channel, the 30 cm between the baffle plates should be sufficient to allow DDT to occur based on the detonation cell size of the 5.1% propane-air mixture.

A second explanation to the extreme pressure measured is pressure piling. With the obstructions mounted along the interior of the FAT, the tube might be considered as a series of interconnected vessels. This introduces the possibility of a propagating flame causing pressure piling and jet ignition as the flame front enters a chamber. As seen in Figure 4.18, the pressure in the last measuring position is 1.53 bara at the start of the sudden pressure increase. Thus, assuming a maximum pressure of 9 bar for the 5.1% propane-air mixture according to Figure 2.2, the resulting pressure would be 17.7 bar. Unfortunately, this pressure peak could not be measured as outlined in section 4.1.3.

Selected frames from the video recordings of test number 91 can be seen in Figure 4.19. The position of the last obstruction is marked in the upper picture. The shear violence of the explosion can especially be seen in the last photos where the flame starts to emit light with a much stronger intensity backwards toward the already reacted part of the mixture. By simple calculations, this radiation seems to move backwards towards the already reacted mixture with a velocity approaching 3000 m/s.
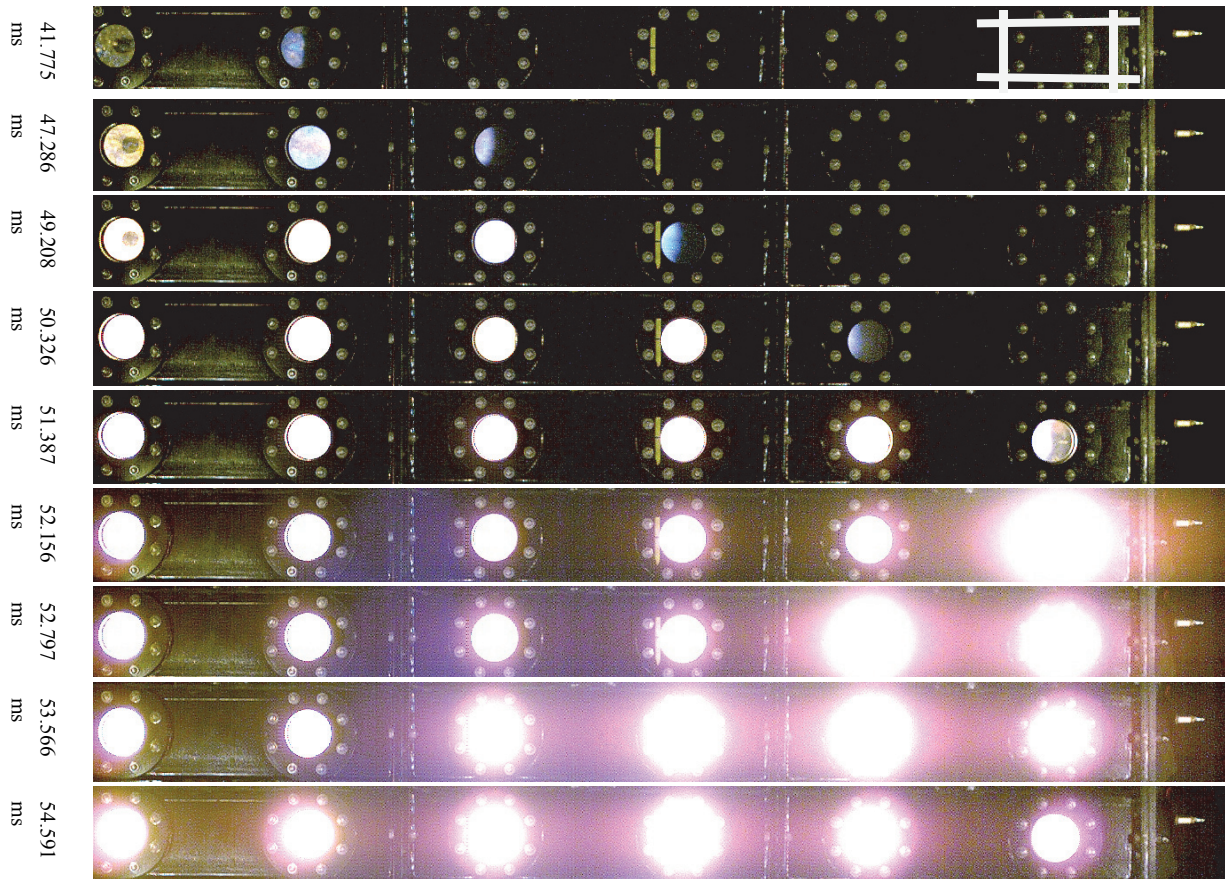
Figure 4.19 *: Selected frames from test number 91, 5.1%propane in air with obstruction configuration number 2, the flame seems to travel backwards after reaching the closed end wall, location of the last obstruction as shown in Figure 4.17 indicated in the top picture.*

Figure 4.20 summarizes the maximum pressure measured in experiments with different obstruction configurations and mixtures of both propane and maize starch.

For the gaseous mixtures, the added turbulence due to the obstructions, affects the maximum pressure severely with maximum values way above those previously encountered by Skjold and Castellanos[45] without obstructions in the FAT. There are some uncertainties with the pressure measurements for the experiments with obstruction configuration number 2 (orange curve). One should expect that the curve had a similar shape as the one reported by Skjold and Castellanos (Blue curve), but this is not the case. A possible reason for this odd behavior could be related to the measuring system as explained in section 4.1.3. The reactivity of the mixtures is at the highest around the stoichiometric concentration, thus implying that the highest rate of pressure rise would be found for these concentrations. This disturbance goes in both the positive and negative direction, thus being limited by the threshold of 15.6 bara, but not downwards. This would then result in a lower measured pressure than for less reactive mixtures. This could then explain why the theoretically worst case mixtures, reported lower pressures compared to leaner or richer mixtures. Another possible reason for this could be that the turbulence level generated by the speed of the reaction front causes the reaction to reach turbulent intensities where quenching occur, but this is not supported by the visually observed flame speeds.

The constant volume dust explosions, recorded similar maximum pressures as in previously conducted constant volume experiments, without obstructions, performed by Skjold and Castellanos[45]. It

should be noted that Skjold and Castellanos used a 1000J chemical igniter, while the igniter used in the present work was only 40J. Since both Skjold and Castellanos, and results obtained in the present work are done with the same maize starch and the same nominal dust concentration of 500 g/m³, one would expect the same explosion pressure. This comes from that the stoichiometric concentration for maize starch is 235g/m³[8] which means that air is the limiting agent in the 500 g/m³ experiments. The modest deviation in peak pressure may be explained by the heat lost to the walls of the FAT and the obstructions, and water vapor may condense on solid surfaces, causing a decrease in pressure. The added surface area of the obstructions, result in an enhanced heat transfer to the walls. This becomes a competition between the speed of the reaction, to reach the end of the tube, and heat transfer to the walls. Water vapor generated in the combustion will also generate a heat loss as it reaches the walls and undergoes a phase change to liquid water as it gets cooled, this also decreases the volume of total gas in the system. This cooling effect is less pronounced for experimental tests conducted in spherical or close to spherical vessels, like the USBM-vessels. This can be seen in Figure 4.20, where the experimental data, including the corrected value for the 1m³ ISO-vessel is shown, the experimental data for the *Meritena A* maize starch is extracted from the tests conducted at UiB by Skjold[39].
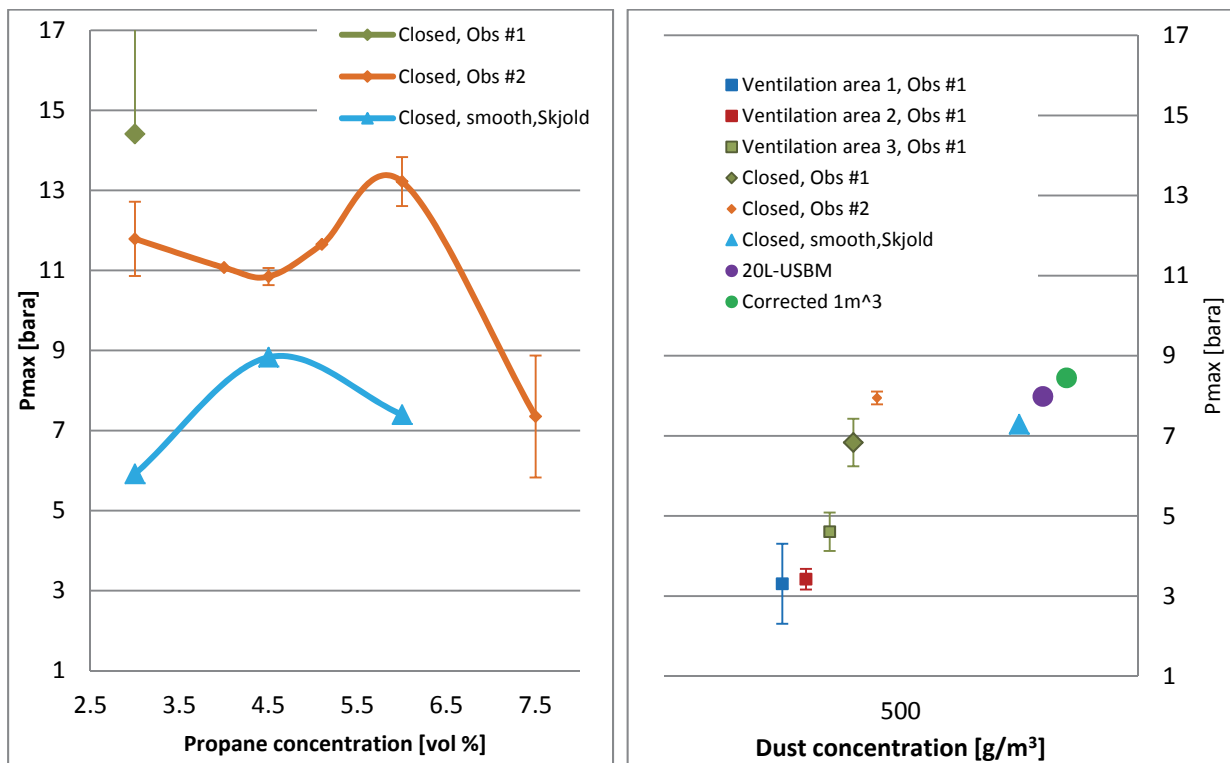
Figure 4.20 : *Maximum pressure for obstructed experiments with gaseous and solid fuel. Experimental data with smooth experiments from Skjold[45] and values from the modified 20-L USMB-vessel including the corrected/scaled pressure for the 1m³vessel.*

As seen in Figure 4.20, the pressure from the vented explosions with obstruction configuration number 1 are higher than the ones without obstructions, as shown in Figure 4.12. To summarize the information, the pressures measured without obstructions were 1.5, 1.7 and 1.9 bara for vent panel 1, 2 and 3, respectively. This shows that the obstacles induce turbulence, which greatly increase the maximum pressure reached for vented explosions.

4.4 Comparison of Experimental Data

4.4.1 Vented explosions without obstructions

Flame propagation in dust clouds can be characterized as premixed combustion with non-premixed substructures[7]. With respect to modeling, it is particularly interesting to quantify the degree of volumetric combustion in dust clouds, relative to combustion in premixed gaseous mixtures. The flame thickness can be expected to have strong influence on the pressure-time history curves from the different explosion scenarios. This phenomenon has been investigated by a comparison of the position of the flame front relative to the pressure rise for both gaseous and dust flames.

In the figures on the following pages, the position of the flame front is normalized by the length of the tube and indicated by both visual observation and thermocouple readings at the windows. The pressure is normalized with the maximum explosion pressure, where 0.0 indicates atmospheric pressure.
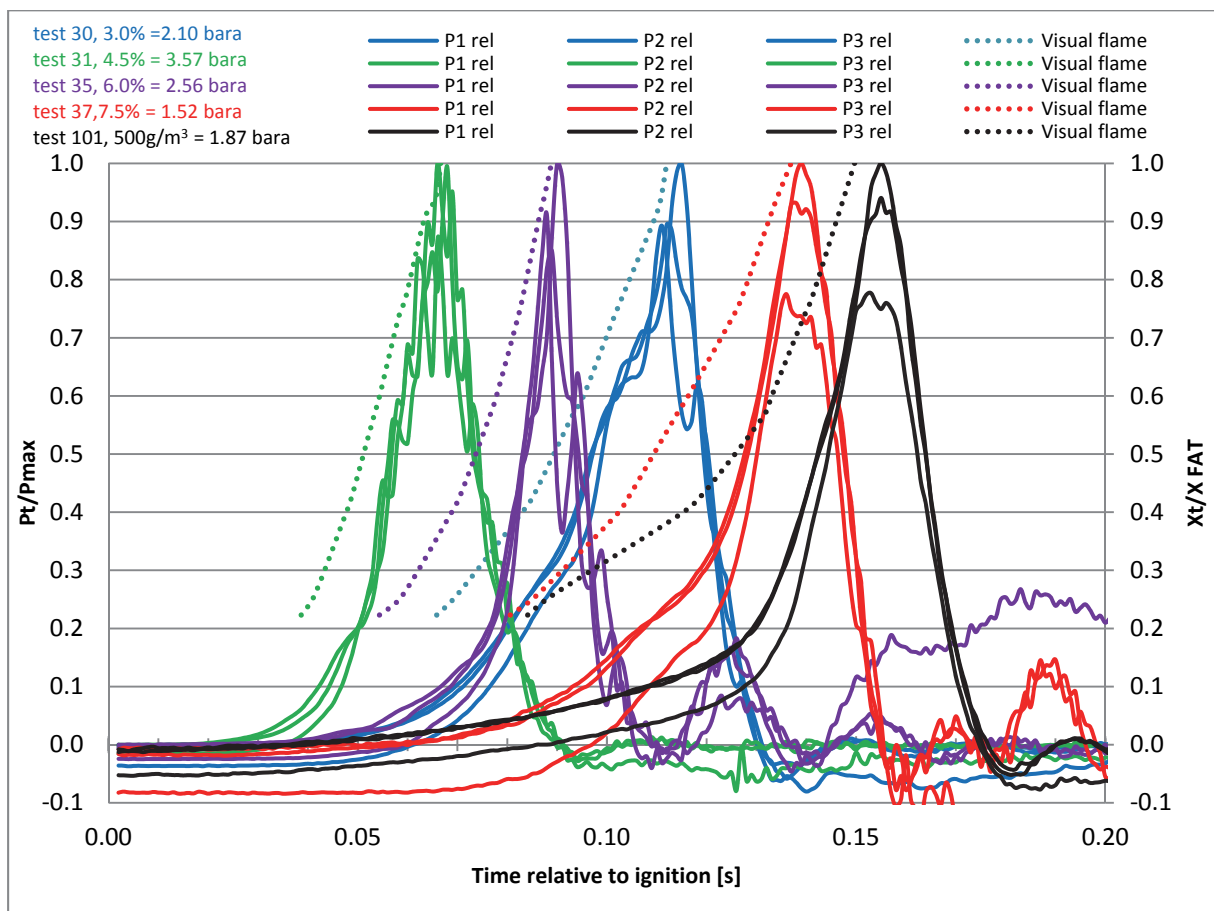
Figure 4.21 : *Comparison of flame propagation in reference to the pressure developed in test with vent panel number 2 (medium), for both propane and maize starch experiments. Solid curves represent the pressure measured by the Kistler measurement system, while the dotted lines represent the visual flame front observations. Thermocouple measurements are not included.*

As illustrated by Figure 4.21, showing the pressure time curves for experiments performed with venting area number 2(medium), the reactivity of the different combustible mixtures varies with concentration. By comparison of the gradient to the pressure rise, one can assume that the most reactive, are the propane mixtures, with 4.5% on the top, followed by the 6.0%, 3.0%, 7.5%, respectively, the least reactive mixture is the 500 g/m^3 maize starch cloud.

By looking at the dotted lines, indicating the flame front position in the tube, one can estimate how the energy release occurs. Steepest curves are found in the gaseous mixtures, where all the mixtures have a close to uniform pressure increase, where the only variation appears to be the slope of the curves.

As illustrated by the flame position and pressure curves in Figure 4.21, the 7.5% propane-air mixture seems best suited for comparison to the dust clouds, other mixtures have therefore not been included in this section. A summary of experiments with the different vent areas for the 7.5% mixtures can be seen in Figure 4.22.

Figure 4.22 : *Comparison of flame propagation in reference to the pressure developed in test 24(blue), 37(red) and 47 (green), vented, 7.5% propane.*

As illustrated in Figure 4.22, the experiments conducted without obstructions with vent area number 1(large), and 7.5% propane, produced a great deal of disturbance in the pressure signals, the reason for this discrepancy, compared to the other configurations were not found. On a general basis, the pressure increase produced by the flame propagation of a propane flame is a steady process, where the pressure build-up starts as soon as the mixture ignites. The highest pressure in vented explosions without obstructions is commonly measured at the closed end of the FAT for both propane and maize starch mixtures.

However, the pressure curve for the maize starch experiment, do not seem to follow the characteristic shape as shown for the propane experiments. The pressure for the dust explosion has a more moderate increase in the initiating phase of flame propagation, as the front reach the middle of the tube, suddenly the pressure increase becomes a much more rapid process.

Figure 4.23 : *Comparison of flame propagation in reference to the pressure developed in test 99(blue),101(red) and 104(green), vented, 500g/m³ maize starch. Vertical dotted line indicates the time of sudden pressure increase for the given experiments, the process of finding the time of the sudden pressure increase is done manually.*

As illustrated in Figure 4.23, the maize starch experiments, for the different vent areas, all have this characteristic shape. The effect of the vent area can be seen in Figure 4.23, where the smallest vent area has the largest area under the curve, hence the longest time period for the release of the energy. The distance the flame travels, before the sudden pressure increase (vertical lines) are quite constant for the vented dust experiments without obstructions, as shown in Table 4-5.

Table 4-5 : *Flame length before the sudden pressure increase for vented dust explosions without obstructions.*

	Test	Time [ms]	Rel. Distance	Length [m]
	98	160	0,50	1,80
Vent area #1	99	123	0,50	1,80
	100	118	0,45	1,62
	101	125	0,48	1,73
Vent area #2	102	163	0,52	1,87
	103	136	0,48	1,73
	104	153	0,53	1,91
Vent area #3	105	185	0,57	2,05
	106	135	0,44	1,58
	Average		**0,50**	**1,79**
	Std. Dev.		**0,04**	**0,15**

The values in

Table 4-5 are based on the visual flame only, and are therefore only an approximated distance since the flame front is hidden from sight at the largest fraction of the length of the tube. The fact that this estimated distance is approximately equal, for all of the experiments (small standard deviation), could indicate that the maize starch has a quite wide burning zone in the initial phase of flame propagation.

This could indicate that the flame of the *Meritena A* maize starch needs to build up a characteristically wide burning zone before the release of chemical energy is at its highest. A possible reason for this observation is that the maize starch needs to release the volatile components through devolatilization before it can burn. This rate of devolatilization depends on the temperature difference between the particles and the surrounding fluid, and the particles require a certain induction time before the volatiles are released. This is not the case for the gaseous mixtures, where the oxygen and propane molecules are mixed on a molecular level. Other explanations could be that the dust flame experiences local quenching, and hence, the area behind the flame front gets reignited as the temperature in the burned zone might be higher than the auto-ignition temperature of the dust. This is an observation which was observed in figure 15 in the constant pressure balloon experiments shown in Appendix E : Here, the flame appears to be disturbed in the early stages of the flame propagation, the internal radiation in the flame was reduced before the balloon suddenly ruptured.

4.4.2 Obstructed experiments

For the vented obstructed experiments, the pressure measured was significantly higher than for the experiments without obstructions. A summary of some vented experiments with maize starch for obstruction configuration number 1(20 baffle plates) are shown in Figure 4.24.
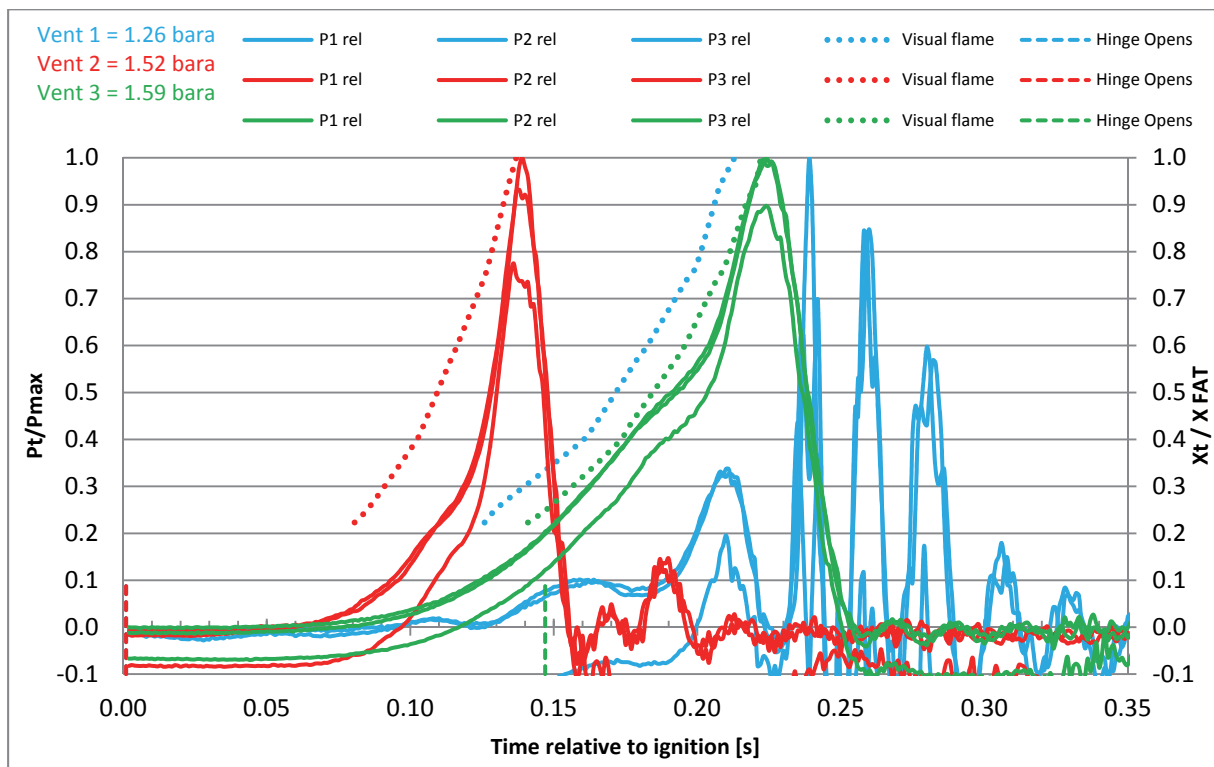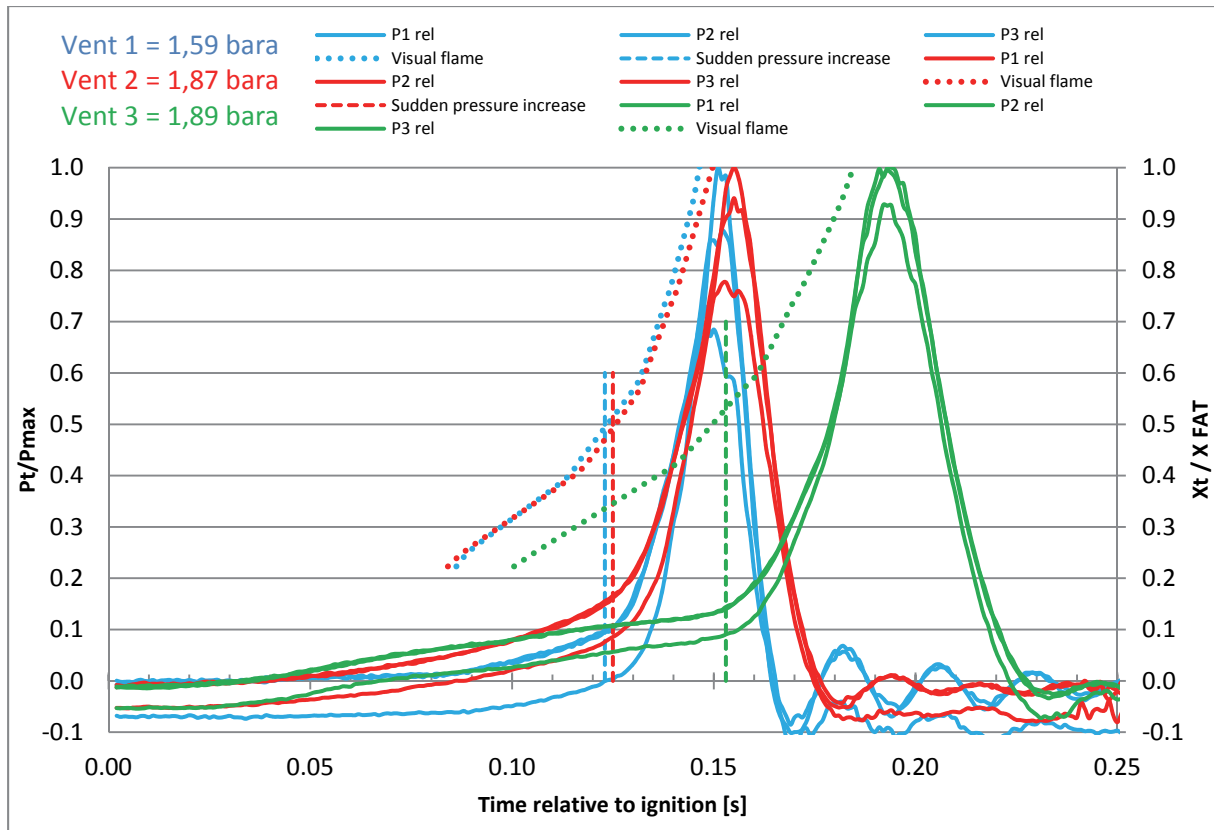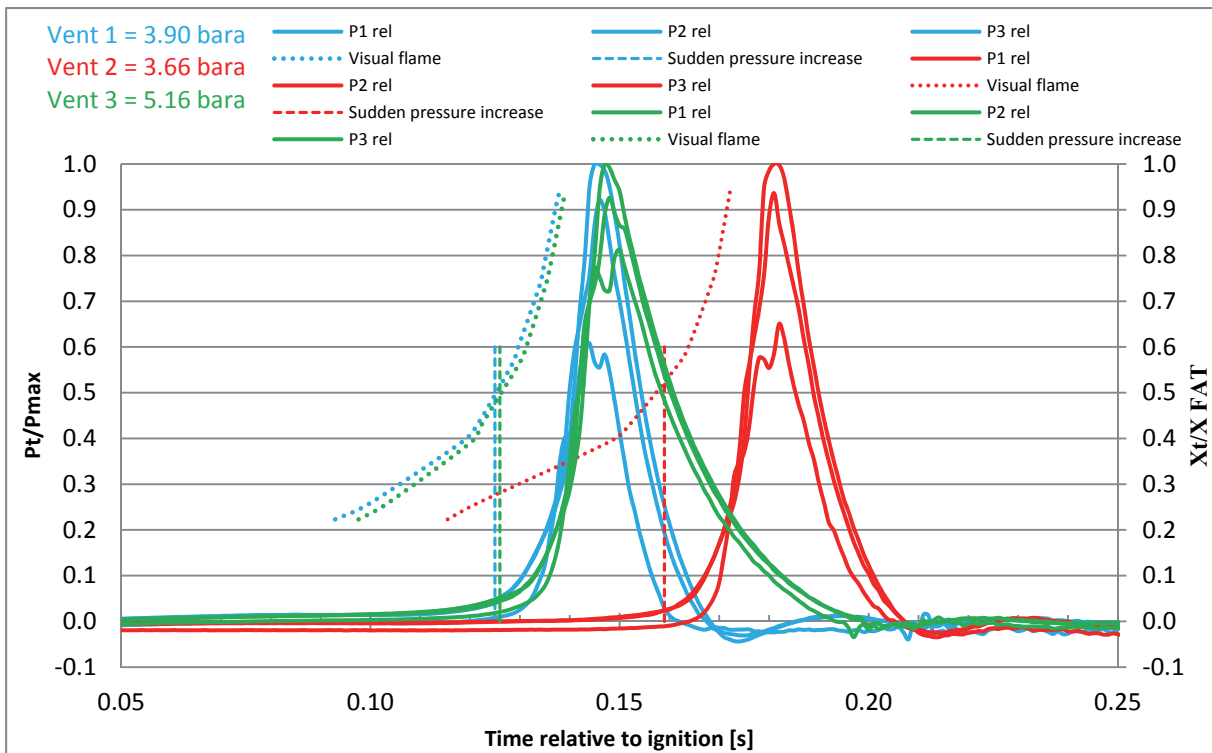

Figure 4.24 : *Comparison of flame propagation in reference to the pressure developed in test 64(blue),68(red) and 71(green), vented with obstruction configuration number 1(20 baffle plates), 500g/m³ maize starch. The time of sudden pressure increase corresponds to the pressure rise of 10 bar/s.*

The same observation with an induction length before the sudden pressure increase was found with the vented obstructed explosions, as with the explosions without obstructions. The time of the sudden pressure increase, was set to the time where the pressure rise exceeded 10 bar/s. As seen in Figure 4.24, this criterion worked well for the onset of sudden pressure rise in the pressure curves. The distance traveled by the flame front at this criterion, was roughly halfway through the tube, as in the previous experiments without the obstructions.
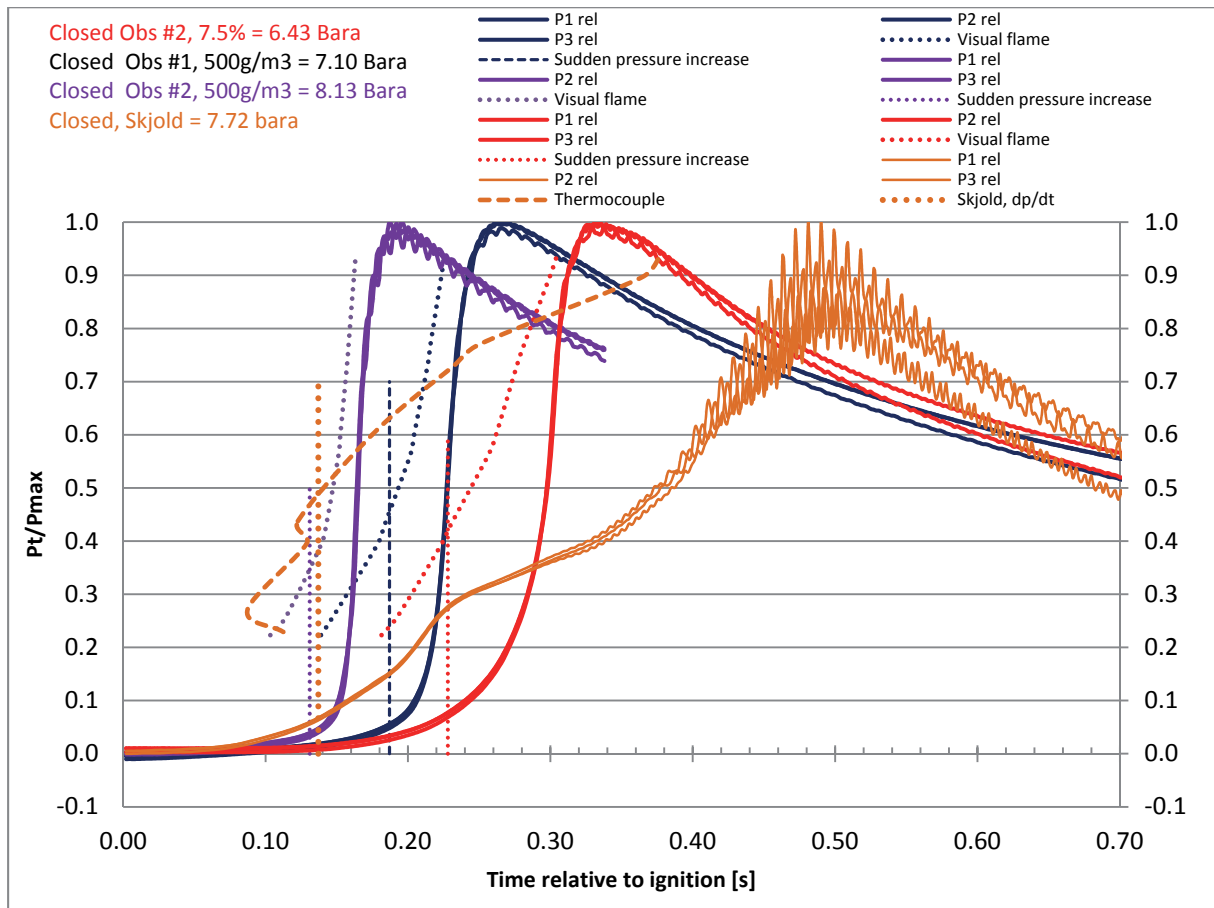
Figure 4.25 : *Constant volume, Test 75(dark blue) and 93(purple), 500g/m³ maize starch, conducted at constant volume with obstacle configuration 1 and 2, respectively. Test 88 (red) is 7.5% propane, conducted with configuration number 2. Orange curves represent test number 50 conducted by Skjold without obstructions (1000J chemical igniter). The time of sudden pressure increase corresponds to the pressure rise of 10 bar/s.*

For the constant volume experiments with obstructions, some typical pressure curves are presented in Figure 4.25. As seen here, the distance traveled by the flame front at the time of sudden pressure increase is somewhat lower than for the vented tests. The reason for this might the fact that the volume is constant, resulting in greater resistance applied to the flame front, from the slightly compressed unreacted mixture ahead.

The pressure from Skjold and Castellanos[45] (orange curve) do not follow the same characteristic as the pressures measured in the present work. By comparison of the present work and the pressure measured without obstructions in the tube[45], one can see that the obstacles dramatically enhance the rate of pressure rise and further accelerates the flame front.

An observation worth noticing is that the tests conducted with 10 baffle plates produced higher flame speeds than the tests with 20 baffles, as illustrated in Figure 4.14 and Figure 4.15. The pressure rise in

the 10 baffle plate experiments was also higher. This might indicate that the turbulence levels generated by the baffle plates might reach such high levels that local quenching might occur if the spacing in between the baffles is too short.

To summarize the observations mentioned above. There seems to be a clear difference between flame propagation and the accompanying pressure build-up for gaseous mixtures and dust clouds. There can be several reasons for the observed local phenomena, such as:

- A higher degree of volumetric combustion in dust clouds compared to the propane mixtures.
- Local quenching during the initial stages of flame propagation for dust mixtures.
- Influence by the degree of radiated energy in dust clouds compared to gas mixtures.

Hence, the results should be well suited for validation of CFD codes.

In CFD, the usual approach for increasing the accuracy of the simulations is to decrease the grid size. In DESC and FLACS, the modeled flame thickness is about three grid cells, and hence grid dependent. It is not obvious that the simulation results of a dust explosion will converge for finer grid resolutions. Hence, the model for the turbulent flame thickness used in the DESC code in the initial stages of flame propagation should be reviewed and tested in reference to the observations above.

5.   Conclusions

A comparative study on the influence of obstacles on constant volume explosions, and of obstacles and vent size on vented explosions, for gaseous mixtures and suspensions of maize starch in air, have been conducted in a 3.6 meter flame acceleration tube (FAT) with square cross section. The unique design of the flame acceleration tube allows for comparative studies of flame propagation in gaseous mixtures and dust clouds under the same initial, slightly turbulent, conditions. The experimental data has been analyzed with an aim to identify fundamental differences between gaseous flames and dust flames, suited for research purposes and validation work of computational fluid dynamic codes for both gas and dust explosions. A dump tank for the vented explosion experiments were acquired and fitted with a water deluge system and an entry tube.

In addition to the experiments in the flame acceleration tube, a series of experiments in a near constant pressure balloon experiment was conducted to investigate basic dust explosion phenomena, and also to test the data acquisition system and high speed video camera prior to the experiments in the FAT. The results from the balloon experiments shed light on the initial phase of flame propagation in dust clouds and made it possible to explore some of the challenges encountered when conducting dust explosions in the flame acceleration tube.

As predicted by theory, the introduction of additional obstacles in the tube resulted in enhanced flame acceleration and for both gaseous and dust mixtures. The obstructions induced sufficiently high turbulence levels to give a strong indication of local quenching of the dust flames. The experiments performed with gaseous mixtures and obstacles produced such high explosion pressures that it was decided to abort the remaining gaseous experiments due to both safety reasons and the damage inflicted on the experimental apparatus.

The effect of the different venting areas was as foreseen, where reduced vent area resulted in an increase in the reduced explosion pressure, for both fuel types. The gaseous mixtures generally produced the highest explosion pressures and the highest rate of pressure rise. It was found that the hinged vent panel opened somewhat late due to its relative high inertia, and another solution should be sought for further experiments.

Flame propagation in dust clouds can be characterized as premixed combustion with non-premixed substructures. With this in mind, it is of interest to investigate the degree of volumetric combustion in clouds of maize starch, relative to rich propane mixtures. A clear difference in behavior during the early stages of flame propagation was found. A comparison between the measured pressure-time histories and recorded flame front positions suggested that flame fronts in dust clouds require a certain induction length before a relative sudden increase in the rate of pressure rise takes place.

The present work demonstrates that dust explosions, similar to gas explosions, are accelerated by the presence of turbulence generating obstructions in a channel. The characteristics of the flame acceleration during dust explosions however differ somewhat from those of the gas explosions:

- Combustion rates are considerably lower than those shown for gas explosions, with an exception for rich gaseous mixtures, confirming earlier observations for laminar burning velocities and maximum rate of pressure rise measured under constant volume conditions.
- The flame thickness, or turbulent combustion zone, for a dust flame appears to be considerably larger than for the turbulent gaseous flames.
- Although not observed explicitly, local quenching of dust flames may play a role in flame propagation in obstacle laden geometries.

6. Recommendations for Further Work

To ensure a safe workplace and minimize the possible error sources of conducting experiments alone, it is recommended that the operation of the flame acceleration tube should be conducted by at least two people.

To decrease the inaccuracy of the time of ignition and greatly reduce the work for the operator of the experiment, one should implement an extra signal at the time of ignition that signalizes when the spark goes in the spark gap. This could then be implemented as a criterion for ignition in the MatLab script that analyses and compresses the raw data. A new smoothing criterion for removing the static disturbance from the pressure time history should also be directed some attention towards.

A new pressure measuring system for the high pressure reservoirs should be acquired to accurately evaluate the evacuation process of the high pressure reservoirs.

To increase the accuracy of the internal flame detection method, experimentation with ionization probes could be conducted and implemented in the measuring system.

To eliminate the uncertainties regarding the opening pressure and the time taken for the vent panel to fully open. It is recommended to design a new mechanism of lighter weight that will allow the exiting shock and reaction front to enter the secondary tank and not be diverted upwards by the vent panel.

To be able to distinguish if the insertion of obstructions increase the turbulence level to such high levels that DDT happens or just results in pressure piling, it is recommended to try to use the soot foil technique in the last section of the FAT to be able to visually observe if detonation cells form.

To validate the pressure data measured for the experiments with obstructions, new measurements with a higher measuring criterion should be conducted.

Experiments with different chemical compositions and a variety of dust concentrations should be conducted for further analysis and validation work for the DESC code.

References

1.   Vijayaraghavan, G., *Emerging emergency due to dust explosions in process industry.* Journal of Engineering Research and Studies, 2011.

2.   CSB, U.S.C.S.a.H.I.B., *Combustible Dust Hazard Study.* Investigation Report, 2006(Report No. 2006-H-1).

3.   Proust, C., *A few fundamental aspects about ignition and flame propagation in dust clouds.* Journal of Loss Prevention in the Process Industries, 2006. **19**(2–3): p. 104-120.

4.   CSB, U.S.C.S.a.H.I.B., *West Pharmaceutical Services Dust Explosion and Fire.* Investigation Report, 2003.

5.   Abbasi, T. and S.A. Abbasi, *Dust explosions–Cases, causes, consequences, and control.* Journal of Hazardous Materials, 2007. **140**(1–2): p. 7-44.

6.   Kauffman, C.W., *Agricultural dust explosions in grain handling facilities.* Fuel-Air Explosions, Proceedings of the International Conference on Fuel-Air Explosions.;Montreal, Que, Can;Code2766, 1982(Conference Paper).

7.   Williams, F.A., *Lectures on applied mathematics in combustion: Past contributions and future problems in laminar and turbulent combustion.* Physica D, 20D, 21-34., 1986.

8.   Eckhoff, R.K., *Dust Explosions in the Process Industries.* Textbook, 2003.

9.   Eckhoff, R.K., *Explosion hazards in the process industries.* Textbook, 2005.

10.   Management, B.B.P.S., *Industrial Explosion Protection.* Product Catalogue, 2012.

11.   CEN, E.C.f.S., *NS-EN 14994:2007. Systemer for trykkavlastning av gasseksplosjoner.* 2007.

12.   CEN, E.C.f.S., *NS-EN 14491:2006 : Beskyttende ventilasjonssystemer for støveksplosjoner.* 2006.

13.   Nolan, D.P., *handbook of fire and explosion protection engineering principles, for oil, gas, chemical and related facilities.* 2011(second edition).

14.   Skjold, T., *Review of the DESC project.* Journal of Loss Prevention in the Process Industries, 2007. **20**(4–6): p. 291-302.

15.   Arntzen, B.J., *Modelling of turbulence and combustion for simulation of gas explosions in complex geometries. .* Dr. Ing. Thesis, NTNU, Trondheim., 1998.

16.   Griffiths, J.E. and J.A. Barnard, *Flame and Combustion, Third Edition.* Textbook, 1995.

17.   Warnatz, J., U. Maas, and R.W. Dibble, *Combustion, 4th edition.* 2006.

18.   Babrauskas, V., *Ignition Hnadbok.* 2003.

19.   Lee, J.H.S., *Fundamentals of explosion.* A lecture presented at the Fourth European Summer School on Hydrogen Safety, 2009(7-16 September 2009).

20.   Ranzi, E., et al., *Hierarchical and comparative kinetic modeling of laminar flame speeds of hydrocarbon and oxygenated fuels.* Progress in Energy and Combustion Science, 2012. **38**(4): p. 468-501.

21.   Razus, D., et al., *Temperature and pressure influence on explosion pressures of closed vessel propane–air deflagrations.* Journal of Hazardous Materials, 2010. **174**(1–3): p. 548-555.

22.   Palmer, K.N., *Dust Explosions and fires.* 1973.

23.   Bartknecht, W., *Explosions. Course Prevention Protection.* Textbook, 1980(Second edition).

24.   Eckhoff, R.K., *Does the dust explosion risk increase when moving from µm-particle powders to powders of nm-particles?* Journal of Loss Prevention in the Process Industries, 2012. **25**(3): p. 448-459.

25.   papirleksikon, K., *hår - zoologi.* Store norske leksikon, 2011.

26.   Mannan, S., *Lees' Loss Prevention in the Process Industries, Volumes 1-3 (3rd Edition)*, Elsevier.

27.   Dahoe, A.E., et al., *Dust explosions in spherical vessels: The role of flame thickness in the validity of the 'cube-root law'.* Journal of Loss Prevention in the Process Industries, 1996. **9**(1): p. 33-44.

28. Borghi, R., *Turbulent combustion modelling.* Progress in Energy and Combustion Science, 1988. **14**(4): p. 245-292.

29. Lee, J.H.S. and I.O. Moen, *The mechans of transition from deflagration to detonation in vapor cloud explosions.* Progress in Energy and Combustion Science, 1980. **6**(4): p. 359-389.

30. Bjerketvedt, D., J.R. Bakke, and K. van Wingerden, *Gas explosion handbook.* Journal of Hazardous Materials, 1997. **52**(1): p. 1-150.

31. Shepherd, J.E., *Detonation Waves.pdf.*

32. Knystautas, R., J.H. Lee, and C.M. Guirao, *The critical tube diameter for detonation failure in hydrocarbon-air mixtures.* Combustion and Flame, 1982. **48**(0): p. 63-83.

33. Dorofeev, S.B., *Flame acceleration and explosion safety applications.* Proceedings of the Combustion Institute, 2011. **33**(2): p. 2161-2175.

34. Johansen, C.T. and G. Ciccarelli, *Visualization of the unburned gas flow field ahead of an accelerating flame in an obstructed square channel.* Combustion and Flame, 2009. **156**(2): p. 405-416.

35. Moen, I.O., et al., *Pressure development due to turbulent flame propagation in large-scale methane‧air explosions.* Combustion and Flame, 1982. **47**(0): p. 31-52.

36. Chao, J. and J.H.S. Lee, *The propagation mechanism of high speed turbulent deflagrations.* Shock Waves, 2003. **12**(4): p. 277-289.

37. Eckhoff, R.K., K. Fuhre, and G.H. Pedersen, *Dust explosion experiments in a vented 236 m3 silo cell.* Journal of Occupational Accidents, 1987. **9**(3): p. 161-175.

38. Eckhoff, R.K., et al., *Maize starch explosions in a 236 m3 experimental silo with vents in the silo wall.* Journal of Loss Prevention in the Process Industries, 1988. **1**(1): p. 16-24.

39. Skjold, T., et al., *Simulation of dust explosions in complex geometries with experimental input from standardized tests.* Journal of Loss Prevention in the Process Industries, 2006. **19**(2–3): p. 210-217.

40. Pu, Y.K., et al., *Comparative study of the influence of obstacles on the propagation of dust and gas flames.* Symposium (International) on Combustion, 1989. **22**(1): p. 1789-1797.

41. Pu, Y.K., et al., *Determination of the maximum effective burning velocity of dust–air mixtures in constant volume combustion.* Journal of Loss Prevention in the Process Industries, 2007. **20**(4–6): p. 462-469.

42. Skjold, T., K.L. Olsen, and D. Castellanos, *A Constant Pressure Dust Explosion Experiment.* 14 annual somposium, Texas A&M University, 2011.

43. Enstad, G.A., *Experimental Investigation of the Impedance Measurement Method for Detecting Dust and Gas Flames in a Flame Acceleration Tube.* Master thesis, 2009.

44. Kalvatn, I.B., *Experimental investigation of optical measurement method for detecting dust and gas flames in a flame acceleration.* Master thesis, 2009.

45. Skjold, T., *Experimental investigation of flame propagation in turbulent propane-air mixtures and dust-air suspensions.* 2011.

46. Skjold, T., *Selected aspects of turbulence and combustion in 20-litre explosion vessels.* Master thesis, 2003.

Appendices

Appendix A :   Calibration of the New Measuring Equipment

To get a better understanding of the performance of the new pressure measuring equipment from PCB Piezotronics, there was decided to do some calibration tests and compare the measured pressures with an accurate manometer and the existing measuring system. The reason for this validation was some deviations that were found while conducting propane gas explosion experiments with both the existing system and the new at the same radial distance from the ignition source.

Our new system consists of two PCB 482C05 signal conditioners, paired with three PCB 113B21 pressure transducers and three PCB 113B26 pressure transducers.

The reference system consists of three Kistler 5011 Charge amplifiers and three Kistler 701A Pressure transducers. The result from one of the tests is shown in figure Figure 6.1.
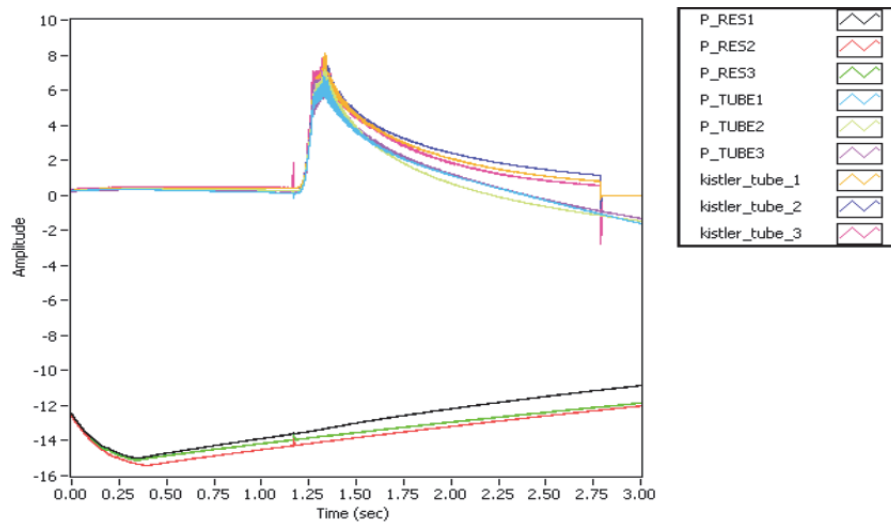
Figure 6.1 : *Closed volume explosion experiment with both pressure measuring systems*
Table 6-1 *: Chanel list in reference to the figure Figure* 6.1

Channel	Sensor model
P_Tube1	113B21
P_Tube2	113B21
P_tube3	113B21
P_RES1	113B26
P_RES2	113B26
P_RES3	113B26

As seen in figure Figure 6.1, there is a deviation in the order of 0.5-2 bar between the PCB and Kistler system. The signal received with the new system also seems to drift towards zero at a steady pace, while the old system does not. The disturbance observed at 2.75 seconds at the Kistler sensors is due to longer logging time than what the logging program was intended to.

Figure 6.2 : *Experimental setup for calibration of pressure transducers*

The experimental setup for the experiment is illustrated in figure Figure 6.2. The calibration system is built around an air reservoir fitted with a manometer with sensitivity 0.02bar, shown in figure Figure 6.2. Three PCB pressure sensors and three Kistler sensors are mounted on the same small volume, separated from the 3.37 liter reservoir by a manual valve. The data acquisition system used to measure the signals from the pressure transducers consists of a National Instruments NI CAD 6259 card and a LabView program. The tests are being conducted by filling the reservoir to a given pressure using compressed air until the pressure stabilizes at a given pressure. In the tests performed, this pressure was varied from 2-4 barg. The volume of the pressure transducers is in advance evacuated to atmospheric conditions. By opening the ball valve we generate a rapid increase in pressure inside the little volume which is then measured by the sensors.
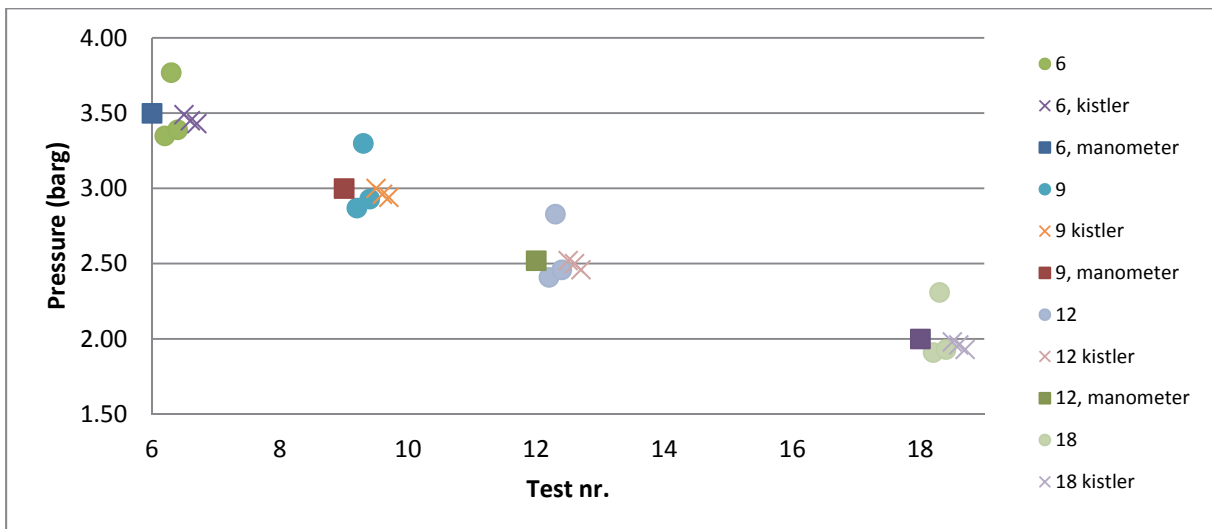
Figure 6.3 : *Calibration for PCB 113B21*
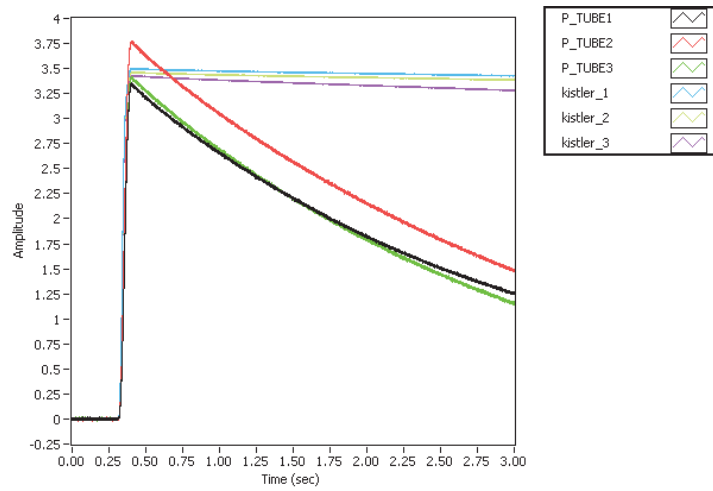
Figure 6.4 : *Recorded pressure test #6*
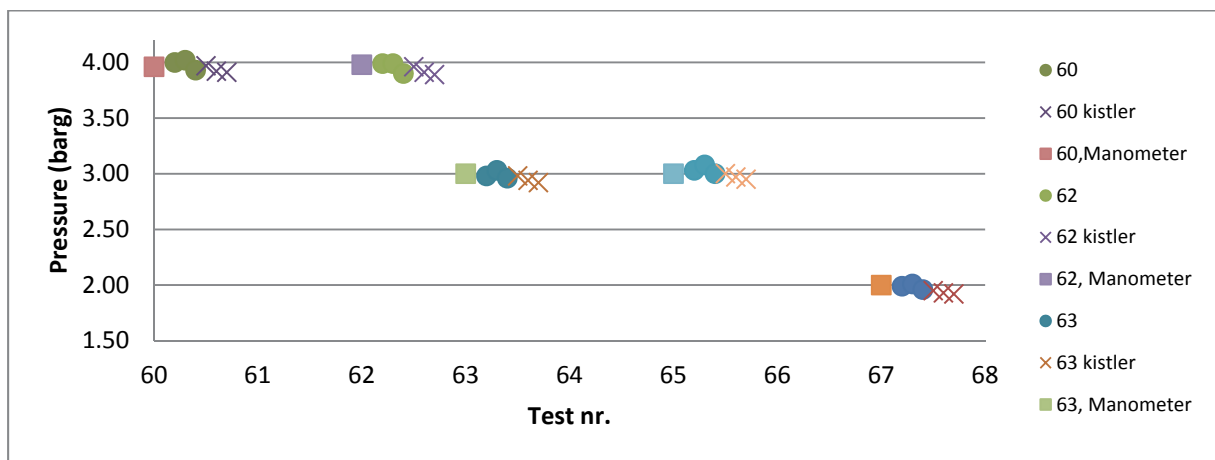
Figure 6.5 : *Calibration of PCB 113B26*
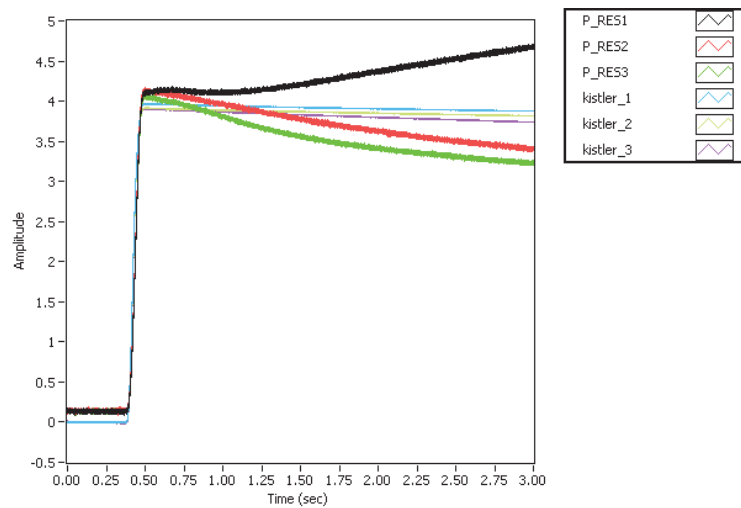
Figure 6.6 : *Recorded pressure test #60*

Based on the results, it was decided to use the PCB 113B26 sensors in the high pressure reservoirs while using the Kistler system inside the flame acceleration tube.

Appendix B : NI-CAD Channel List

Channel and cable list for the NI-CAD data card with input values for the amplification of the different measuring channels can be found below:

Channel name	Physical Channel	Connecting Cable	Sensor nr	Amplifier channel	Sensor model	Serial nr	mV/kPA Sensitivity <50	mV/Mpa Sensitivity >100	10 v = X bar labwiev input
P_RES1	Ai0	green A	1	1..1	113B26	22920	1.466	1476	±67,75067751
P_RES2	Ai1	yellow A	2	1..2	113B26	22923	1.447	1446	±69,15629322
P_RES3	Ai2	red A	5	1..3	113B26	22924	1.475	1479	±67,6132522
P_Tube1	Ai3	green B			701A				±15.0
P_Tube2	Ai4	yellow B			701A				±15.0
P_Tube3	Ai5	red B			701A				±15.0
TF1_2a	Ai6	green C							±15.0
TF1_2b	Ai7	green D							±15.0
TF2_1a	Ai8	yellow C							±15.0
TF2_1b	Ai9	yellow D							±15.0
TF2_2a	Ai10	yellow E							±15.0
TF2_2b	Ai11	yellow F							±15.0
TF3_1a	Ai12	red C							±15.0
TF3_1b	Ai13	red D							±15.0
TF3_2a	Ai14	red E							±15.0
TF3_2b	Ai15	red F							±15.0

Appendix C : MATLAB Program Used for the Analysis of the Raw Data

From previous experiments in the FAT, a MATLAB script for the interpretation of the raw data has been made. This script smoothes and resample the data so that it can be used later on in programs like Microsoft Excel. This script has been improved to be able to cope with different logging times and unpredictable events where the thermocouple broke etc. A transcript of the script is seen below:

If a thermocouple is broken, this test will assign it a given value:

```
function [value]=Failure_test(D1SG,nign, fcri, matrixIndex,  defaultValue, timerange)
value = find(D1SG(nign:timerange,matrixIndex) >= fcri);
if (isempty(value))
  value = defaultValue;
else
  value = value(1)+ nign;
end
if (value < 1)
  value  = 1;
end
```

The main script in MatLab:

```
function ni2FATvent_V1(test,tign,prin,ptin,fcri,nsmo)
% - - - - - - - - - - - - - - - - - - - - - - - - - - - - - - - - - - - - - -|
%|  Reading, processing, plotting and exporting NI data from vented FAT experiments  |
%|    Input variables:                                  |
%|            test: test number     [-]     (must be specified)    |
%|            prin: reservoir pressure[bara]    (default value 17.2
%|            ptin: initial FAT pressure[bara]    (default value 0.6
%|            fcri: flame arrival    [C/s]    (default value 1500 C/s ) |
%|            tign: time of ignition  [s]     (default value   1  s  ) |
%|            nsmo: Smoothing range  [-]     (default value   20   ) |
%|    File name:    46033-propane-*.txt                    |
%|- - - - - - - - - - - - - - - - - - - - - - - - - - - - - - - - - - - - -|
%|    Version 1.0  Last revision 02.05.2012
%|    Edited by Kjetil Lien Olsen             No copyright whatsoever!    |
%|_____
%
% Step 1: AMENITIES
% -------------------------------------------------------------------------------|
% Default values:
if nargin < 1; error('Test number must be specified'); end;
if nargin < 2; tign = 1;   end;
if nargin < 3; prin = 17.39;      end;
if nargin < 4; ptin = 0.600;   end;
if nargin < 5; fcri = 1500;    end;
if nargin < 6; nsmo = 20;      end;
% Error statements:
if (test < 0) | (test > 2000) | (ceil(test) ~= floor(test));
  error('Test number must be an integer between 0 and 200');
end;
% - - - - - - - - - - - - - - - - - - - - - - - - - - - - - - - - - - - -
% Initial pressure, additional delay, presampling, pressure calculation constants:
```

```
%if tign == 1;
  % prin = 17.20;
   % ptin = 0.600;
%elseif tign == 0;
 %  prin =  1.00;
  % ptin =  1.00;
%end;
prin                        % Initial pressure [bara] in reservoir
ptin                        % Initial pressure [bara] in tube
% - - - - - - - - - - - - - - - - - - - - - - - - - - - - - - - - - - - - - - -

% Step 2: DATA IMPORT FROM FILE
% -------------------------------------------------------------------------------|
ftxt = num2str(test);
if test < 10;
  fname = strcat('46033-propane-00',ftxt,'.txt'); % File name
  elseif test < 100;
  fname = strcat('46033-propane-0',ftxt,'.txt');  % File name
  elseif test <9000;
  fname = strcat('46033-propane-',ftxt,'.txt');   % File name
end; fname
fid  = fopen(fname);                % Importing data from file
DATA = fscanf(fid, '%g\n %g\n %g\n %g\n %g\n %g\n %g\n %g\n %g\n %g\n %g\n %g\n %g\n %g\n
%g\n %g\n', [17 inf]);
DATA = DATA';
DATA = DATA(:,2:17);
fclose(fid);
[rows cols] = size(DATA);
fsamp = 50000;              %sampling rate
tsamp = (rows-1)/fsamp;
rows
cols
tsamp
% Scaling:
TIME = [0:0.00002:tsamp]' - tign;
DATA(:, 1) = DATA(:, 1) + prin;
DATA(:, 2) = DATA(:, 2) + prin;
DATA(:, 3) = DATA(:, 3) + prin;
DATA(:, 4) = DATA(:, 4) + ptin;
DATA(:, 5) = DATA(:, 5) + ptin;
DATA(:, 6) = DATA(:, 6) + ptin;
DATA(:, 7) = DATA(:, 7) * 100;
DATA(:, 8) = DATA(:, 8) * 100;
DATA(:, 9) = DATA(:, 9) * 100;
DATA(:,10) = DATA(:,10) * 100;
DATA(:,11) = DATA(:,11) * 100;
DATA(:,12) = DATA(:,12) * 100;
DATA(:,13) = DATA(:,13) * 100;
DATA(:,14) = DATA(:,14) * 100;
DATA(:,15) = DATA(:,15) * 100;
DATA(:,16) = DATA(:,16) * 100;


% Step 4: SMOOTHING AND DIFFERENTIATING MEAN PRESSURE
% -------------------------------------------------------------------------------|
% Savitzky, A. & Golay, J.E. (1964), Analytical Chemistry, 36(8): 1627-1639: 'sago.m'
dsmo = 2;                     % Degree of smoothing polynomial
% Coefficients:
```

```
SGC0 = sago(nsmo,dsmo,0);              % S-G coeff. for smoothing
SGC1 = sago(nsmo,dsmo,1);              % S-G coeff. 1st derivative
% SGC2 = sago(nsmo,dsmo,2);              % S-G coeff. 2nd derivative
% Smothed data:
D0SG = zeros(rows,16);
D1SG = zeros(rows,16);
% D2SG = zeros(rows,16);
for i=1:16;
  for j=nsmo+1:rows-nsmo;
    SAMP = DATA(j-nsmo:j+nsmo,i);
    D0SG(j,i) = (SAMP'*SGC0);          % Smoothed values in D0SG
    D1SG(j,i) = (SAMP'*SGC1)*fsamp;       % 1st derivative  in D1SG
%     D2SG(j,i) = (SAMP'*SGC2)*fsamp^2;     % 2nd derivative  in D2SG
  end;
end;
clear SAGO;                    % Saving memory
_____
% Step 9: FLAME ARRIVAL TIMES AND EXPLOSION PRESSURES
% -----------------------------------------------------------------------------|
if tign == 1;
  nign = 50000;
elseif tign == 0;
  nign = 200;
else
   nign = tign * fsamp;% +200;
end;
%flame arrival temperature criteria values:                      ######
%added new variables 29.03.2012
%        fcri is given in the input to the function ni2FATvent(), default 2000 C/s     ######
%        fcri1 is default at 100                        ######
%        fcri2 is default at 200                        ######
%        fcri3 is default at 300                        ######
%        change theese values if the temperature at the latest
%        temperature probes never reach the given value, start with
%        "fcri3"
fcri1 = 100;
fcri2 = 200;
fcri3 = 300;
timerange = rows;% - nign;          %value that tells the program how manny time is should look for an extremal
value
        % Derivative dT/dt > fcri:
defaultValue = 1;              %if the programs don't find the given critical values, it will replace it with this one
ntf1b1_0 = Failure_test(D1SG, nign, fcri, 7, defaultValue,timerange);
  ttf1b1_0 = TIME(ntf1b1_0,1);
  ftf1b1_0 = D0SG(ntf1b1_0,7);
  dtf1b1_0 = D1SG(ntf1b1_0,7);
  ptf1b1_0 = (D0SG(ntf1b1_0,4)+D0SG(ntf1b1_0,5)+D0SG(ntf1b1_0,6))/3;

ntf1b2_0 = Failure_test(D1SG, nign, fcri, 8, defaultValue,timerange);
  ttf1b2_0 = TIME(ntf1b2_0,1);
  ftf1b2_0 = D0SG(ntf1b2_0,8);
  dtf1b2_0 = D1SG(ntf1b2_0,8);
  ptf1b2_0 = (D0SG(ntf1b2_0,4)+D0SG(ntf1b2_0,5)+D0SG(ntf1b2_0,6))/3;

ntf2a1_0 = Failure_test(D1SG, nign, fcri, 9, defaultValue,timerange);
  ttf2a1_0 = TIME(ntf2a1_0,1);
  ftf2a1_0 = D0SG(ntf2a1_0,9);
```

```
  dtf2a1_0 = D1SG(ntf2a1_0,9);
  ptf2a1_0 = (D0SG(ntf2a1_0,4)+D0SG(ntf2a1_0,5)+D0SG(ntf2a1_0,6))/3;

  ntf2a2_0 = Failure_test(D1SG, nign, fcri, 10, defaultValue,timerange);
  ttf2a2_0 = TIME(ntf2a2_0,1);
  ftf2a2_0 = D0SG(ntf2a2_0,10);
  dtf2a2_0 = D1SG(ntf2a2_0,10);
  ptf2a2_0 = (D0SG(ntf2a2_0,4)+D0SG(ntf2a2_0,5)+D0SG(ntf2a2_0,6))/3;

ntf2b1_0 = Failure_test(D1SG, nign, fcri, 11, defaultValue,timerange);
  ttf2b1_0 =  TIME(ntf2b1_0,1);
  ftf2b1_0 =  D0SG(ntf2b1_0,11);
  dtf2b1_0 =  D1SG(ntf2b1_0,11);
  ptf2b1_0 =  (D0SG(ntf2b1_0,4)+D0SG(ntf2b1_0,5)+D0SG(ntf2b1_0,6))/3;

ntf2b2_0 = Failure_test(D1SG, nign, fcri, 12, defaultValue,timerange);
  ttf2b2_0 = TIME(ntf2b2_0,1);
  ftf2b2_0 = D0SG(ntf2b2_0,12);
  dtf2b2_0 = D1SG(ntf2b2_0,12);
  ptf2b2_0 = (D0SG(ntf2b2_0,4)+D0SG(ntf2b2_0,5)+D0SG(ntf2b2_0,6))/3;

ntf3a1_0 = Failure_test(D1SG, nign, fcri, 13, defaultValue,timerange);
  ttf3a1_0 = TIME(ntf3a1_0,1);
  ftf3a1_0 = D0SG(ntf3a1_0,13);
  dtf3a1_0 = D1SG(ntf3a1_0,13);
  ptf3a1_0 = (D0SG(ntf3a1_0,4)+D0SG(ntf3a1_0,5)+D0SG(ntf3a1_0,6))/3;

ntf3a2_0 = Failure_test(D1SG, nign, fcri, 14, defaultValue,timerange);
  ttf3a2_0 = TIME(ntf3a2_0,1);
  ftf3a2_0 = D0SG(ntf3a2_0,14);
  dtf3a2_0 = D1SG(ntf3a2_0,14);
  ptf3a2_0 = (D0SG(ntf3a2_0,4)+D0SG(ntf3a2_0,5)+D0SG(ntf3a2_0,6))/3;

ntf3b1_0 = Failure_test(D1SG, nign, fcri, 15, defaultValue,timerange);
  ttf3b1_0 = TIME(ntf3b1_0,1);
  ftf3b1_0 = D0SG(ntf3b1_0,15);
  dtf3b1_0 = D1SG(ntf3b1_0,15);
  ptf3b1_0 = (D0SG(ntf3b1_0,4)+D0SG(ntf3b1_0,5)+D0SG(ntf3b1_0,6))/3;

ntf3b2_0 = Failure_test(D1SG, nign, fcri, 16, defaultValue,timerange);
  ttf3b2_0 = TIME(ntf3b2_0,1);
  ftf3b2_0 = D0SG(ntf3b2_0,16);
  dtf3b2_0 = D1SG(ntf3b2_0,16);
  ptf3b2_0 = (D0SG(ntf3b2_0,4)+D0SG(ntf3b2_0,5)+D0SG(ntf3b2_0,6))/3;

        % Temperature T > 100 degC:

ntf1b1_1  =  Failure_test(D0SG, nign, fcri1, 7, defaultValue,timerange);  %find(D0SG(nign:100000,7)  >=  fcri1);
ntf1b1_1 = ntf1b1_1(1)+ nign;

  ttf1b1_1 = TIME(ntf1b1_1,1);
  ftf1b1_1 = D0SG(ntf1b1_1,7);
  dtf1b1_1 = D1SG(ntf1b1_1,7);

ntf1b2_1 = Failure_test(D0SG, nign, fcri1, 8, defaultValue,timerange);
  ttf1b2_1 = TIME(ntf1b2_1,1);
  ftf1b2_1 = D0SG(ntf1b2_1,8);
```

```
  dtf1b2_1 = D1SG(ntf1b2_1,8);

ntf2a1_1 = Failure_test(D0SG, nign, fcri1, 9, defaultValue,timerange);
  ttf2a1_1 = TIME(ntf2a1_1,1);
  ftf2a1_1 = D0SG(ntf2a1_1,9);
  dtf2a1_1 = D1SG(ntf2a1_1,9);

ntf2a2_1 = Failure_test(D0SG, nign, fcri1, 10, defaultValue,timerange);
  ttf2a2_1 = TIME(ntf2a2_1,1);
  ftf2a2_1 = D0SG(ntf2a2_1,10);
  dtf2a2_1 = D1SG(ntf2a2_1,10);

ntf2b1_1 = Failure_test(D0SG, nign, fcri1, 11, defaultValue,timerange);
  ttf2b1_1 = TIME(ntf2b1_1,1);
  ftf2b1_1 = D0SG(ntf2b1_1,11);
  dtf2b1_1 = D1SG(ntf2b1_1,11);

ntf2b2_1 = Failure_test(D0SG, nign, fcri1, 12, defaultValue,timerange);
  ttf2b2_1 = TIME(ntf2b2_1,1);
  ftf2b2_1 = D0SG(ntf2b2_1,12);
  dtf2b2_1 = D1SG(ntf2b2_1,12);

ntf3a1_1 = Failure_test(D0SG, nign, fcri1, 13, defaultValue,timerange);
  ttf3a1_1 = TIME(ntf3a1_1,1);
  ftf3a1_1 = D0SG(ntf3a1_1,13);
  dtf3a1_1 = D1SG(ntf3a1_1,13);

ntf3a2_1 = Failure_test(D0SG, nign, fcri1, 14, defaultValue,timerange);
  ttf3a2_1 = TIME(ntf3a2_1,1);
  ftf3a2_1 = D0SG(ntf3a2_1,14);
  dtf3a2_1 = D1SG(ntf3a2_1,14);

ntf3b1_1 = Failure_test(D0SG, nign, fcri1, 15, defaultValue,timerange);
  ttf3b1_1 = TIME(ntf3b1_1,1);
  ftf3b1_1 = D0SG(ntf3b1_1,15);
  dtf3b1_1 = D1SG(ntf3b1_1,15);

ntf3b2_1 = Failure_test(D0SG, nign, fcri1, 16, defaultValue,timerange);
  ttf3b2_1 = TIME(ntf3b2_1,1);
  ftf3b2_1 = D0SG(ntf3b2_1,16);
  dtf3b2_1 = D1SG(ntf3b2_1,16);

          % Temperature T > 200 degC:

ntf1b1_2 = Failure_test(D0SG, nign, fcri2, 7, defaultValue,timerange);
  ttf1b1_2 = TIME(ntf1b1_2,1);
  ftf1b1_2 = D0SG(ntf1b1_2,7);
  dtf1b1_2 = D1SG(ntf1b1_2,7);
ntf1b2_2 = Failure_test(D0SG, nign, fcri2, 8, defaultValue,timerange);
  ttf1b2_2 = TIME(ntf1b2_2,1);
  ftf1b2_2 = D0SG(ntf1b2_2,8);
  dtf1b2_2 = D1SG(ntf1b2_2,8);
ntf2a1_2 = Failure_test(D0SG, nign, fcri2, 9, defaultValue,timerange);
  ttf2a1_2 = TIME(ntf2a1_2,1);
  ftf2a1_2 = D0SG(ntf2a1_2,9);
  dtf2a1_2 = D1SG(ntf2a1_2,9);
ntf2a2_2 = Failure_test(D0SG, nign, fcri2, 10, defaultValue,timerange);
```

x

```
  ttf2a2_2 = TIME(ntf2a2_2,1);
  ftf2a2_2 = D0SG(ntf2a2_2,10);
  dtf2a2_2 = D1SG(ntf2a2_2,10);
ntf2b1_2 = Failure_test(D0SG, nign, fcri2, 11, defaultValue,timerange);
  ttf2b1_2 = TIME(ntf2b1_2,1);
  ftf2b1_2 = D0SG(ntf2b1_2,11);
  dtf2b1_2 = D1SG(ntf2b1_2,11);
ntf2b2_2 = Failure_test(D0SG, nign, fcri2, 12, defaultValue,timerange);
  ttf2b2_2 = TIME(ntf2b2_2,1);
  ftf2b2_2 = D0SG(ntf2b2_2,12);
  dtf2b2_2 = D1SG(ntf2b2_2,12);
ntf3a1_2 = Failure_test(D0SG, nign, fcri2, 13, defaultValue,timerange);
  ttf3a1_2 = TIME(ntf3a1_2,1);
  ftf3a1_2 = D0SG(ntf3a1_2,13);
  dtf3a1_2 = D1SG(ntf3a1_2,13);
ntf3a2_2 = Failure_test(D0SG, nign, fcri2, 14, defaultValue,timerange);
  ttf3a2_2 = TIME(ntf3a2_2,1);
  ftf3a2_2 = D0SG(ntf3a2_2,14);
  dtf3a2_2 = D1SG(ntf3a2_2,14);
ntf3b1_2 = Failure_test(D0SG, nign, fcri2, 15, defaultValue,timerange)
  ttf3b1_2 = TIME(ntf3b1_2,1);
  ftf3b1_2 = D0SG(ntf3b1_2,15);
  dtf3b1_2 = D1SG(ntf3b1_2,15);
ntf3b2_2 = Failure_test(D0SG, nign, fcri2, 16, defaultValue,timerange);
  ttf3b2_2 = TIME(ntf3b2_2,1);
  ftf3b2_2 = D0SG(ntf3b2_2,16);
  dtf3b2_2 = D1SG(ntf3b2_2,16);


        % Temperature T > 300 degC:

ntf1b1_3 = Failure_test(D0SG, nign, fcri3, 7, defaultValue,timerange);
  ttf1b1_3 = TIME(ntf1b1_3,1);
  ftf1b1_3 = D0SG(ntf1b1_3,7);
  dtf1b1_3 = D1SG(ntf1b1_3,7);
ntf1b2_3 = Failure_test(D0SG, nign, fcri3, 8, defaultValue,timerange);
  ttf1b2_3 = TIME(ntf1b2_3,1);
  ftf1b2_3 = D0SG(ntf1b2_3,8);
  dtf1b2_3 = D1SG(ntf1b2_3,8);
ntf2a1_3 = Failure_test(D0SG, nign, fcri3, 9, defaultValue,timerange);
  ttf2a1_3 = TIME(ntf2a1_3,1);
  ftf2a1_3 = D0SG(ntf2a1_3,9);
  dtf2a1_3 = D1SG(ntf2a1_3,9);
ntf2a2_3 = Failure_test(D0SG, nign, fcri3, 10, defaultValue,timerange);
  ttf2a2_3 = TIME(ntf2a2_3,1);
  ftf2a2_3 = D0SG(ntf2a2_3,10);
  dtf2a2_3 = D1SG(ntf2a2_3,10);
ntf2b1_3 = Failure_test(D0SG, nign, fcri3, 11, defaultValue,timerange);
  ttf2b1_3 = TIME(ntf2b1_3,1);
  ftf2b1_3 = D0SG(ntf2b1_3,11);
  dtf2b1_3 = D1SG(ntf2b1_3,11);
ntf2b2_3 = Failure_test(D0SG, nign, fcri3, 12, defaultValue,timerange);
  ttf2b2_3 = TIME(ntf2b2_3,1);
  ftf2b2_3 = D0SG(ntf2b2_3,12);
  dtf2b2_3 = D1SG(ntf2b2_3,12);
ntf3a1_3 = Failure_test(D0SG, nign, fcri3, 13, defaultValue,timerange);
  ttf3a1_3 = TIME(ntf3a1_3,1);
  ftf3a1_3 = D0SG(ntf3a1_3,13);
```

```
  dtf3a1_3 = D1SG(ntf3a1_3,13);
ntf3a2_3 = Failure_test(D0SG, nign, fcri3, 14, defaultValue,timerange);
  ttf3a2_3 = TIME(ntf3a2_3,1);
  ftf3a2_3 = D0SG(ntf3a2_3,14);
  dtf3a2_3 = D1SG(ntf3a2_3,14);
ntf3b1_3 = Failure_test(D0SG, nign, fcri3, 15, defaultValue,timerange);
  ttf3b1_3 = TIME(ntf3b1_3,1);
  ftf3b1_3 = D0SG(ntf3b1_3,15);
  dtf3b1_3 = D1SG(ntf3b1_3,15);
ntf3b2_3 = Failure_test(D0SG, nign, fcri3, 16, defaultValue,timerange);
  ttf3b2_3 = TIME(ntf3b2_3,1);
  ftf3b2_3 = D0SG(ntf3b2_3,16);
  dtf3b2_3 = D1SG(ntf3b2_3,16);
%
%
FLAT_0 = [ttf1b1_0 ttf1b2_0 ttf2a1_0 ttf2a2_0 ttf2b1_0 ttf2b2_0 ttf3a1_0 ttf3a2_0 ttf3b1_0 ttf3b2_0]; % Flame arrival
dT/dt > fcri
FLTM_0 = [ftf1b1_0 ftf1b2_0 ftf2a1_0 ftf2a2_0 ftf2b1_0 ftf2b2_0 ftf3a1_0 ftf3a2_0 ftf3b1_0 ftf3b2_0]; % Temperature
DTDT_0 = [dtf1b1_0 dtf1b2_0 dtf2a1_0 dtf2a2_0 dtf2b1_0 dtf2b2_0 dtf3a1_0 dtf3a2_0 dtf3b1_0 dtf3b2_0]; % dT/dt
PFAT_0 = [ptf1b1_0 ptf1b2_0 ptf2a1_0 ptf2a2_0 ptf2b1_0 ptf2b2_0 ptf3a1_0 ptf3a2_0 ptf3b1_0 ptf3b2_0]; % Average
pressure
FLAT_1 = [ttf1b1_1 ttf1b2_1 ttf2a1_1 ttf2a2_1 ttf2b1_1 ttf2b2_1 ttf3a1_1 ttf3a2_1 ttf3b1_1 ttf3b2_1]; % Flame arrival
dT/dt > fcri
FLTM_1 = [ftf1b1_1 ftf1b2_1 ftf2a1_1 ftf2a2_1 ftf2b1_1 ftf2b2_1 ftf3a1_1 ftf3a2_1 ftf3b1_1 ftf3b2_1]; % Temperature
DTDT_1 = [dtf1b1_1 dtf1b2_1 dtf2a1_1 dtf2a2_1 dtf2b1_1 dtf2b2_1 dtf3a1_1 dtf3a2_1 dtf3b1_1 dtf3b2_1]; % dT/dt
FLAT_2 = [ttf1b1_2 ttf1b2_2 ttf2a1_2 ttf2a2_2 ttf2b1_2 ttf2b2_2 ttf3a1_2 ttf3a2_2 ttf3b1_2 ttf3b2_2]; % Flame arrival
dT/dt > fcri
FLTM_2 = [ftf1b1_2 ftf1b2_2 ftf2a1_2 ftf2a2_2 ftf2b1_2 ftf2b2_2 ftf3a1_2 ftf3a2_2 ftf3b1_2 ftf3b2_2]; % Temperature
DTDT_2 = [dtf1b1_2 dtf1b2_2 dtf2a1_2 dtf2a2_2 dtf2b1_2 dtf2b2_2 dtf3a1_2 dtf3a2_2 dtf3b1_2 dtf3b2_2]; % dT/dt
FLAT_3 = [ttf1b1_3 ttf1b2_3 ttf2a1_3 ttf2a2_3 ttf2b1_3 ttf2b2_3 ttf3a1_3 ttf3a2_3 ttf3b1_3 ttf3b2_3]; % Flame arrival
dT/dt > fcri
FLTM_3 = [ftf1b1_3 ftf1b2_3 ftf2a1_3 ftf2a2_3 ftf2b1_3 ftf2b2_3 ftf3a1_3 ftf3a2_3 ftf3b1_3 ftf3b2_3]; % Temperature
DTDT_3 = [dtf1b1_3 dtf1b2_3 dtf2a1_3 dtf2a2_3 dtf2b1_3 dtf2b2_3 dtf3a1_3 dtf3a2_3 dtf3b1_3 dtf3b2_3]; % dT/dt


pmaxt1 = max(D0SG(nign:rows,4));
nmaxt1 = find(D0SG(nign:rows,4) >= pmaxt1);
  nmaxt1 = nmaxt1(1) + nign;
  tmaxt1 = TIME(nmaxt1,1);
pmaxt2 = max(D0SG(nign:rows,5));
  nmaxt2 = find(D0SG(nign:rows,5) >= pmaxt2);
  nmaxt2 = nmaxt2(1) + nign;
  tmaxt2 = TIME(nmaxt2,1);
pmaxt3 = max(D0SG(nign:rows,6));
  nmaxt3 = find(D0SG(nign:rows,6) >= pmaxt3);
  nmaxt3 = nmaxt3(1) + nign;
  tmaxt3 = TIME(nmaxt3,1);

pmax = (pmaxt1 + pmaxt2 + pmaxt3)/3; pmax
tmax = (tmaxt1 + tmaxt2 + tmaxt3)/3; tmax
% _____|
%
% Step 9: RESAMPLING
% -------------------------------------------------------------------------------|
%
```

```
tjump = 0.001;                       % Time steps for resampling [s]          change from 50kHz to 1000Hz
njump = round(tjump*fsamp);          % Index steps for resampling
tstpr = -1;                  %
tstfl =  0;                  %
nstpr = find(TIME >= tstpr); nstpr=nstpr(1);      %
nstfl = find(TIME >= tstfl); nstfl=nstfl(1);      %
tndpr =  0.99;                   %
tndfl =  0.99;                   %
nndpr = find(TIME >= tndpr); nndpr=nndpr(1);      %
nndfl = find(TIME >= tndfl); nndfl=nndfl(1);      %
TIMEPR = TIME(nstpr:njump:nndpr);           % Resampled time for pressure
TIMEFR = TIME(nstfl:njump:nndfl);           % Resampled time for flame arrival
D0SGPR = D0SG(nstpr:njump:nndpr,1:6);          % Resampled pressure data
D0SGFR = D0SG(nstfl:njump:nndfl,7:16);          % Resampled temperature data
D1SGFR = D1SG(nstfl:njump:nndfl,7:16);          % Resampled dT/dt data
%
% clear TIME;                % Saving memory
% clear DATA;                % Saving memory
% clear D0SG;                % Saving memory
% clear D1SG;                % Saving memory
[rowp colp] = size(D0SGPR);
[rowf colf] = size(D0SGFR);
% _____|
%
% Step 9: PLOTTING
% ----------------------------------------------------------------------|
%
% Plotting range parameters:
mintp = tstpr;                   % Time range pressure
maxtp = tndpr;
mintf = tstfl;                   % Time range pressure
maxtf = tndfl;
minpr =   0.000;                 % Pressure range, reservoir
maxpr =  18.000;
minpt =   0.000;                 % Pressure range, tube
maxpt =  15.000;
minft =   0.000;                 % Temperature range, flame tube
maxft = 1000.000;
min1t =   0.000;
max1t = 5000.000;
% _____|
%
%   Figure 1: Pressure measurements
% ----------------------------------------------------------------------|
h=1; figure(h);
% Scaling of figure:
set(h,'PaperUnits','centimeters');
set(h,'PaperType','A4');
set(h,'PaperPosition',[3 2 16 25]);
set(h,'Position',[40 40 700 700]);
zoom on;
% ----------------------------------------------------------------------|
% Plot 1a) Pressure in reservoirs
subplot(2,1,1);
% Title
title(['\fontsize{11}9
 Pressure measurements for test _{ }',num2str(test)]);
```

```
% Label
xlabel('\fontsize{11} Time relative to ignition (s)');
ylabel('\fontsize{11} Reservoir pressure (bara)');
hold on;
% Main data series:
plot(TIME,DATA(:,1),'*y','MarkerSize',2);     % P_RES1 measured
plot(TIME,DATA(:,2),'*m','MarkerSize',2);      % P_RES2 measured
plot(TIME,DATA(:,3),'*c','MarkerSize',2);      % P_RES3 measured
plot(TIMEPR,D0SGPR(:,1),'-g','MarkerSize',3);  % P_RES1 smoothed & resampled
plot(TIMEPR,D0SGPR(:,2),'-r','MarkerSize',3);  % P_RES2 smoothed & resampled
plot(TIMEPR,D0SGPR(:,3),'-b','MarkerSize',3);  % P_RES3 smoothed & resampled
% Axes:
axis([mintp maxtp minpr maxpr]);
% Vertical and horizontal lines
plot([mintp maxtp],[1 1],'-k'); % Atmospheric pressure, black horizontal line
plot([0 0],[minpr maxpr],'-r'); % Time of ignition, red vertical line
hold off;
%
% ------------------------------------------------------------------------------|
% Plot 1b) Pressures in vessel
subplot(2,1,2);
% Label
xlabel('\fontsize{11} Time relative to ignition (s)');
ylabel('\fontsize{11} Pressure in vessel (bara)');
hold on;
% Main data series:
plot(TIME,DATA(:,4),'*y','MarkerSize',2);      % P_TUBE1 measured
plot(TIME,DATA(:,5),'*m','MarkerSize',2);      % P_TUBE2 measured
plot(TIME,DATA(:,6),'*c','MarkerSize',2);      % P_TUBE3 measured
%plot(TIMEPR,D0SGPR(:,4),'-g','MarkerSize',3);   % P_TUBE1 smoothed & resampled
%plot(TIMEPR,D0SGPR(:,5),'-r','MarkerSize',3);   % P_TUBE2 smoothed & resampled
%plot(TIMEPR,D0SGPR(:,6),'-b','MarkerSize',3);   % P_TUBE3 smoothed & resampled
plot(TIME,D0SG(:,4),'-g','MarkerSize',3);    % P_TUBE1 smoothed
plot(TIME,D0SG(:,5),'-r','MarkerSize',3);    % P_TUBE2 smoothed
plot(TIME,D0SG(:,6),'-b','MarkerSize',3);    % P_TUBE3 smoothed

% Axes:
axis([mintp maxtp minpt maxpt+1]);
% Vertical and horizontal lines
plot([mintp maxtp],[1 1],'-k');               % Atmospheric pressure
plot([0 0],[minpt maxpt],'-r');              % Time of ignition
%plot([tmax],[pmax],'Ok','MarkerSize',6);       % Maximum pressure
%plot([tmaxt1],[pmaxt1],'Or','MarkerSize',10);
%plot([tmaxt2],[pmaxt2],'Or','MarkerSize',10);
%plot([tmaxt3],[pmaxt3],'Or','MarkerSize',10);
hold off;
%
% _____|
%
%   Figure 2: Temperature measurements
% ------------------------------------------------------------------------------|
h=2; figure(h);
% Scaling of figure:
set(h,'PaperUnits','centimeters');
set(h,'PaperType','A4');
set(h,'PaperPosition',[3 2 16 25]);
set(h,'Position',[120 120 740 700]);
```

```
zoom on;
% ---------------------------------------------------------------------------|
% Plot 2a) Temperature
subplot(2,1,1);
% Title
title(['\fontsize{11} Temperature measurements for Test _{ }',num2str(test)]);
xlabel('\fontsize{11} Time relative to ignition (s)');
ylabel('\fontsize{11} Temperature (C)');
hold on;
% Main data series:
plot(TIME,DATA(:, 7),'*m','MarkerSize',2);     % TF1_1a measured
plot(TIME,DATA(:, 8),'*y','MarkerSize',2);     % TF1_1b measured
plot(TIME,DATA(:, 9),'*c','MarkerSize',2);     % TF2_1a measured
plot(TIME,DATA(:,10),'*m','MarkerSize',2);     % TF2_1b measured
plot(TIME,DATA(:,11),'*y','MarkerSize',2);     % TF2_1a measured
plot(TIME,DATA(:,12),'*c','MarkerSize',2);     % TF2_1b measured
plot(TIME,DATA(:,13),'*m','MarkerSize',2);     % TF3_1a measured
plot(TIME,DATA(:,14),'*y','MarkerSize',2);     % TF3_1b measured
plot(TIME,DATA(:,15),'*c','MarkerSize',2);     % TF3_1a measured
plot(TIME,DATA(:,16),'*m','MarkerSize',2);     % TF3_1b measured
plot(TIMEFR,D0SGFR(:, 1),'-r','MarkerSize',3);   % TF1_1a smoothed & resampled
plot(TIMEFR,D0SGFR(:, 2),'-g','MarkerSize',3);   % TF1_1b smoothed & resampled
plot(TIMEFR,D0SGFR(:, 3),'-b','MarkerSize',3);   % TF2_1a smoothed & resampled
plot(TIMEFR,D0SGFR(:, 4),'-c','MarkerSize',3);   % TF2_1b smoothed & resampled
plot(TIMEFR,D0SGFR(:, 5),'-m','MarkerSize',3);   % TF2_1a smoothed & resampled
plot(TIMEFR,D0SGFR(:, 6),'-r','MarkerSize',3);   % TF2_1b smoothed & resampled
plot(TIMEFR,D0SGFR(:, 7),'-g','MarkerSize',3);   % TF3_1a smoothed & resampled
plot(TIMEFR,D0SGFR(:, 8),'-b','MarkerSize',3);   % TF3_1b smoothed & resampled
plot(TIMEFR,D0SGFR(:, 9),'-c','MarkerSize',3);   % TF3_1a smoothed & resampled
plot(TIMEFR,D0SGFR(:,10),'-m','MarkerSize',3);   % TF3_1b smoothed & resampled
plot(FLAT_0,FLTM_0,'Ok','MarkerSize',6);       % Flame arrival time
plot(FLAT_1,FLTM_1,'Ok','MarkerSize',6);       % Flame arrival time
plot(FLAT_2,FLTM_2,'Ok','MarkerSize',6);       % Flame arrival time
plot(FLAT_3,FLTM_3,'Ok','MarkerSize',6);       % Flame arrival time
% Axes:
axis([mintf maxtf minft maxft]);
% Vertical and horizontal lines
% plot([mintf maxtf],[0 0],'-k'); % Atmospheric pressure, black horizontal line
% plot([0 0],[minft maxft],'-r'); % Time of ignition, red vertical line
hold off;
%
% ---------------------------------------------------------------------------|
% Plot 2b) Temperature, first derivative
subplot(2,1,2);
% Title
xlabel('\fontsize{11} Time relative to ignition (s)');
ylabel('\fontsize{11} Temperature, first derivative (C/s)');
hold on;
% Main data series:
plot(TIMEFR,D1SGFR(:, 1),'-r','MarkerSize',3);  % TF1_1a smoothed & resampled
plot(TIMEFR,D1SGFR(:, 2),'-g','MarkerSize',3);  % TF1_1b smoothed & resampled
plot(TIMEFR,D1SGFR(:, 3),'-b','MarkerSize',3);  % TF2_1a smoothed & resampled
plot(TIMEFR,D1SGFR(:, 4),'-c','MarkerSize',3);  % TF2_1b smoothed & resampled
plot(TIMEFR,D1SGFR(:, 5),'-m','MarkerSize',3);  % TF2_1a smoothed & resampled
plot(TIMEFR,D1SGFR(:, 6),'-r','MarkerSize',3);  % TF2_1b smoothed & resampled
plot(TIMEFR,D1SGFR(:, 7),'-g','MarkerSize',3);  % TF3_1a smoothed & resampled
plot(TIMEFR,D1SGFR(:, 8),'-b','MarkerSize',3);  % TF3_1b smoothed & resampled
```

```
plot(TIMEFR,D1SGFR(:, 9),'-c','MarkerSize',3);  % TF3_1a smoothed & resampled
plot(TIMEFR,D1SGFR(:,10),'-m','MarkerSize',3);  % TF3_1b smoothed & resampled
plot(FLAT_0,DTDT_0,'Ok','MarkerSize',6);        % Flame arrival time
% Axes:
axis([mintf 0.5*maxtf min1t max1t]);
% Vertical and horizontal lines
plot([mintf maxtf],[0 0],'-k'); % Atmospheric pressure, black horizontal line
plot([0 0],[min1t max1t],'-r'); % Time of ignition, red vertical line
hold off;
%




%   Figure 3: Fast Fourier transformation
% -------------------------------------------------------------------------------|
h=3;
figure(h);
% Scaling of figure:
set(h,'PaperUnits','centimeters');
set(h,'PaperType','A4');
set(h,'PaperPosition',[3 2 16 25]);
set(h,'Position',[40 40 700 700]);
zoom on;


% -------------------------------------------------------------------------------|
Fs = fsamp;              % Sampling frequency
L = rows;               % Length of signal

P1 = DATA(:,4);
x = TIME;
y = P1;

plot(x,y);

title('Originalt uredigert signal')
xlabel('seconds')
ylabel('bara')
axis([0 2 0 8]);

%plot([0 2],[0 0],'-k');

h=4;
figure(h);
% Scaling of figure:
set(h,'PaperUnits','centimeters');
set(h,'PaperType','A4');
set(h,'PaperPosition',[3 2 16 25]);
set(h,'Position',[40 40 700 700]);
zoom on;




% Plot single-sided amplitude spectrum.
NFFT = 2^nextpow2(L); % Next power of 2 from length of y
Y = fft(y,NFFT)/L;
f = Fs/2*linspace(0,1,NFFT/2+1);
```

```
% Plot single-sided amplitude spectrum.
plot(f,2*abs(Y(1:NFFT/2+1)))
title('Single-Sided Amplitude Spectrum of y(t)')
xlabel('Frequency (Hz)')
ylabel('|Y(f)|')
axis([0 200 0 0.2]);



% ------------------------------------------------------------------------------|
% _____|
%
% Step 10: EXPORT
% _____|
%
% Step 10: EXPORT
% ------------------------------------------------------------------------------|
%
if test < 10;
  export_t = strcat('outFAT_t_propane_00',ftxt,'.txt'); % File name
  export_p = strcat('outFAT_p_propane_00',ftxt,'.txt'); % File name
  export_f = strcat('outFAT_f_propane_00',ftxt,'.txt'); % File name
  export_d = strcat('outFAT_d_propane_00',ftxt,'.txt'); % File name
 elseif test < 100;
  export_t = strcat('outFAT_t_propane_0',ftxt,'.txt');  % File name
  export_p = strcat('outFAT_p_propane_0',ftxt,'.txt');  % File name
  export_f = strcat('outFAT_f_propane_0',ftxt,'.txt');  % File name
  export_d = strcat('outFAT_d_propane_0',ftxt,'.txt');  % File name
 elseif test <1000;
  export_t = strcat('outFAT_t_propane_',ftxt,'.txt');   % File name
  export_p = strcat('outFAT_p_propane_',ftxt,'.txt');   % File name
  export_f = strcat('outFAT_f_propane_',ftxt,'.txt');   % File name
  export_d = strcat('outFAT_d_propane_',ftxt,'.txt');   % File name
end;
export_t
export_p
export_f
export_d
OUTDAT_t = zeros(12,10);
  OUTDAT_t(1,:) = FLAT_0;
  OUTDAT_t(2,:) = FLTM_0;
  OUTDAT_t(3,:) = DTDT_0;
  OUTDAT_t(4,:) = FLAT_1;
  OUTDAT_t(5,:) = FLTM_1;
  OUTDAT_t(6,:) = DTDT_1;
  OUTDAT_t(7,:) = FLAT_2;
  OUTDAT_t(8,:) = FLTM_2;
  OUTDAT_t(9,:) = DTDT_2;
  OUTDAT_t(10,:) = FLAT_3;
  OUTDAT_t(11,:) = FLTM_3;
  OUTDAT_t(12,:) = DTDT_3;
OUTDAT_p = zeros(rowp,colp+1);
  OUTDAT_p(:,1) = TIMEPR(:,1);
  OUTDAT_p(:,2:7) = D0SGPR(:,1:6);
OUTDAT_f = zeros(rowf,colf+1);
  OUTDAT_f(:,1) = TIMEFR(:,1);
  OUTDAT_f(:,2:11) = D0SGFR(:,1:10);
OUTDAT_d = zeros(rowf,colf+1);
```

```
  OUTDAT_d(:,1) = TIMEFR(:,1);
  OUTDAT_d(:,2:11) = D1SGFR(:,1:10);
save(export_t,'OUTDAT_t','-ascii');
clear OUTDAT_t;
save(export_p,'OUTDAT_p','-ascii');
clear OUTDAT_p;
save(export_f,'OUTDAT_f','-ascii');
clear OUTDAT_f;
save(export_d,'OUTDAT_d','-ascii');
clear OUTDAT_d;
%
_____THIS_____IS_____THE_____END_____MY_____FRIEND_____|
%
```

Appendix D :   Water deluge system in the dump tank

P

Fine Atomization

DESIGN FEATURES
- High energy efficiency
- One-piece construction
- No whirl vanes or internal parts
- Highly efficient laminar jet impinges on target pin generating fine fog
- Male connection

SPRAY CHARACTERISTICS
- Finest fog of any direct pressure nozzle
- Produces high percentage of droplets in the 25-400 micron range; ideal for dust suppression

Spray pattern: Cone-shaped Fog
Spray angle: 90°. For best 90° pattern operate nozzle at or above 4 bar
Flow rates: 0.153 to 30.3 l/min

Metal

MISTING
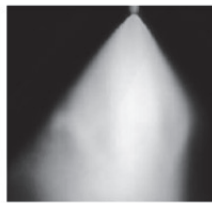
Fog
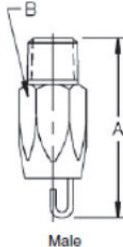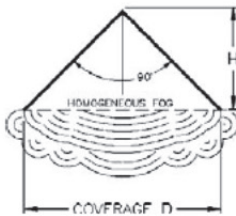
Male

Fog Pattern

Dimensions are approximate. Check with BETE for critical dimension applications.

P Flow Rates and Dimensions
Cone-Shaped Fog, 90° Spray Angle, 1/4" Pipe Size, BSP or NPT

Male Pipe Size	Nozzle Number	K Factor	LITERS PER MINUTE @ BAR								Approx. Orifice Dia. (mm)	Approx. Coverage (mm) D	Approx. Spray Height H (mm)	Approx. Dim. (mm) A	B	Wt. (g) Metal
			1 bar	2 bar	3 bar	5 bar	7 bar	10 bar	20 bar	30 bar						
1/4	P20	0.153	0.153	0.216	0.264	0.341	0.404	0.483	0.683	0.836	0.508	300	150			
	P24	0.228	0.228	0.322	0.395	0.510	0.603	0.721	1.02	1.25	0.610	400	200			
	P28	0.296	0.296	0.419	0.513	0.662	0.784	0.937	1.32	1.62	0.711	460	230			
	P32	0.410	0.410	0.580	0.710	0.917	1.09	1.30	1.83	2.25	0.813	560	280			
	P40	0.638	0.638	0.902	1.11	1.43	1.69	2.02	2.85	3.49	1.02	610	305	46.5	16.0	57
	P48	0.912	0.912	1.29	1.58	2.04	2.41	2.88	4.08	4.99	1.22	710	355			
	P54	1.21	1.21	1.71	2.09	2.70	3.20	3.82	5.40	6.62	1.37	760	380			
	P66	1.71	1.71	2.42	2.96	3.82	4.52	5.40	7.64	9.36	1.68	910	455			
	P80	2.46	2.46	3.48	4.26	5.50	6.51	7.78	11.0	13.5	2.03	1200	600			
	P120	5.54	5.54	7.83	9.59	12.4	14.7	17.5	24.8	30.3	3.05	1500	750			

TO ORDER: specify pipe size, connection type, nozzle number, spray angle, and material.

Flow Rate $(l/min) = K \sqrt{bar}$

Standard Materials: Brass, 303 Stainless Steel and 316 Stainless Steel.

Spray angle performance varies with pressure. Contact BETE for specific data on critical applications.

www.BETE.com

Appendix E :   A Constant Pressure Dust Explosion Experiment

A paper describing the balloon experiments, for both dust and gas explosions was presented at the 14th annual symposium, Mary Kay O'Connor Process Safety Center at Texas A&M University, College Station, Texas at the 25-27 of October, 2011.

The paper is called

A Constant Pressure Dust Explosion Experiment

A Constant Pressure Dust Explosion Experiment

Trygve Skjold [a,b]**, Kjetil L. Olsen** [b] **& Diana Castellanos** [c]

[a] GexCon AS, Bergen, Norway
[b] University of Bergen, Bergen, Norway
[c] Texas A&M University, College Station, Texas, USA
E-mail: *trygve@gexcon.com*

Abstract

This paper describes an apparatus for investigating dust explosions at near constant pressure conditions. The experimental approach is inspired by the classical soap bubble method for measuring burning velocities in gaseous mixtures. Combustible dust is dispersed with pressurised air from a reservoir to form an explosive mixture inside a transparent latex balloon. After a certain delay time, the turbulent dust cloud is ignited by a chemical igniter. A digital high-speed camera records the propagating flame and the expansion of the balloon. Experiments were performed with two types of dust, *Lycopódium* spores and maize starch, as well as with propane-air mixtures under initially quiescent and turbulent conditions. The results are primarily qualitative in nature, but they nevertheless demonstrate both similarities and differences between premised combustion of gaseous and solid fuels, and highlight some fundamental challenges for future dust explosion research.

Introduction

Dust explosions continue to cause serious accidents in the process industry, and the empirical correlations available in various standards and guidelines for design of explosion protection systems are still of limited value in many practical situations [1]. Current state-of-the-art in explosion protection entails the use of computational fluid dynamics (CFD), combined with empirically determined combustion parameters [2]. Further progress on the numerical modelling approach requires relevant and reliable data from repeated large-scale experiments, as well as improved understanding of the inherently complex phenomena involved in dust explosions: transient, turbulent, particle-laden, reactive flows in more or less complex geometries [3].

The conventional way of characterizing the explosion properties of a combustible dust sample entails the use of a constant volume explosion vessel. A certain mass of dust is injected into the vessel to form a mechanical suspension, and the turbulent dust cloud is ignited by a chemical igniter after a specified ignition delay time t_v. Measures for the energy content and the reactivity of the dust-air suspension are derived from the pressure-time history $P(t)$: the heat of combustion and specific heat of the solid fuel are reflected in the corrected maximum explosion pressure P_{max}, and the reactivity of the mixture is reflected in the size corrected maximum rate of pressure rise $K_{St} = V^{1/3}(dp/dt)_{max}$ ('cubic law'). Both P_{max} and K_{St} are determined from the same type of experiments in constant volume explosion vessels [4-7].

For CFD modelling it is convenient to introduce parameters such as turbulent burning velocity S_T and turbulent flame thickness δ_T, and to correlate these to more fundamental parameters characterizing the thermodynamic state, combustion properties and flow conditions in the mechanical suspension. Parameters of interest include pressure p and temperature T, dust concentration c_d, laminar burning velocity S_L, laminar flame thickness δ_L, root-mean-square of the turbulent velocity fluctuations u'_{rms}, and at least one representative turbulent length scale ℓ [2]. Unfortunately it is not straightforward to determine accurate and unambiguous values for these parameters from experiments performed in constant volume explosion vessels: flow in a mechanical suspension of fine particles dispersed in air is inherently turbulent; turbulence parameters in dust clouds are inherently difficult to measure; turbulent flow structures create local concentration gradients; parameters such as pressure, temperature, dust concentration and turbulence vary significantly during the course of the explosion; and finally, the use of strong chemical igniters violates the common assumption of a point-like ignition source, whereas the use of weak ignition sources may result in poor repeatability [8-11].

Most investigations of flame propagation in dust clouds at constant pressure have utilized various types of tubes, burners or open vessels [1, 12-13]. The purpose of the present study is to explore the possibility of utilizing an alternative experimental technique, inspired by the classical soap bubble method. Since the pioneering work by Stevens in 1923 [14], several researchers have used variations of the soap bubble method to measure burning velocities in gaseous mixtures [e.g. 15-18]. Others have performed similar experiments with gaseous fuels at larger scales, but with balloons rather than soap bubbles [e.g. 19-21].

The soap bubble method has certain advantages: it is well suited for mathematical analysis, the burning velocity calculations do not require consideration of pressure or wall effects, the flame propagates in the same direction as the flow, and the flame can be observed directly. Strehlow and Stuart [17] described a procedure for calculating burning velocities by assuming that the flammable mixture is contained in a spherical soap bubble with initial radius r_{b0} at the time of ignition. An infinitely thin spherical flame propagates at constant burning velocity S_u from the centre of the bubble after ignition. The volume of burned reactive gas at any instant t relative to ignition is then equal to the difference between the volume enclosed by the flame radius r_f and the increase in the volume of the bubble with radius r_b:

$$V_r = \frac{4}{3}\pi\left[r_f^3 - \left(r_b^3 - r_{b0}^3 \right) \right] \tag{1}$$

Provided the flame speed S_f is constant, it can be expressed as:

$$S_f = \frac{dr_f}{dt} = \frac{r_f}{t} \tag{2}$$

Assuming constant densities of unburned (ρ_{un}) to burned (ρ_{bu}) mixture, and introducing the expansion ratio Φ, conservation of mass over the flame front yields:

$$\rho_{bu}S_f = \rho_{un}S_u \quad \Rightarrow \quad S_f = \frac{\rho_{un}}{\rho_{bu}}S_u = \Phi S_u \tag{3}$$

For a spherical flame propagating at constant burning velocity S_u and flame speed S_f, the volume of burned mixture can also be expressed as:

$$V_r = S_u \int_0^t 4\pi r_f^2 dt = S_u \int_0^t 4\pi S_f^2 t^2 dt = \frac{4}{3}\pi S_f^2 S_u t^3 \qquad (4)$$

Combining equations (1) and (4) results in this expression for the burning velocity:

$$S_u = S_f \left[1 - \frac{r_b^3 - r_{b0}^3}{r_f^3} \right] \qquad (5)$$

One of the main disadvantages of this method is a rather strong sensitivity to small errors in the measurements of flame radius and bubble radius.

This paper describes an experimental apparatus for investigating flame propagation in dust clouds at near constant pressure conditions. Since soap bubbles presumably are too fragile to survive the dust dispersion process, as well as subsequent impingement of solid particles on the soap film, the dust was dispersed with air from a pressurized reservoir and released into a partly filled latex balloon prior to ignition. The apparatus has been modified in several stages, and some results have been presented previously [22-23].

There are several inherent limitations with this method, including [17, 22-23]:

- Afterburning of hot combustion products and interaction between the flame front and the balloon makes it difficult to determine the expansion ratio, and hence to estimate the burning velocity for mixtures where Φ is not known.
- The dead space in the dispersion system, balloon holder and spark gap, as well as heat loss from the flame kernel to the spark gap and dispersion nozzle, influence the results.
- Convective rise of hot combustion products becomes a problem for low flame speeds.
- The inertia of the balloon may become important for high flame speeds.
- The actual dust concentration inside the balloon is not known.
- It is not straightforward to identify the flame front for lean gaseous mixtures, as well as for dust flames that emit significant radiation.

Nevertheless, by performing dust and gas explosion experiments at near constant pressure, in an apparatus where flame propagation can be observed more or less directly, the aim is to complement observations from constant volume explosion vessels, and ultimately gain increased understanding of the dust explosion phenomenon.

Experiments

Figure 1 shows the experimental setup for the balloon experiment. The apparatus is placed on a shelf, about 1.5 metres above ground, with the balloon holder, dispersion nozzle and spark gap pointing downwards. Before a test, the ignition source is connected to either a spark gap or a special holder for weak chemical igniters, and the balloon is fixed to the balloon holder with tape. For dust explosion tests, the dust sample is added to the 0.95-litre dust reservoir. Compressed air for dispersion is charged to a 1.15-litre reservoir, and air for pre-filling the balloon is charged to a 1.05-litre reservoir. A Druck DPI 705 pressure indicator is used to monitor the pressure in both reservoirs. For tests involving gaseous fuels, the gases are mixed by

partial pressure in the 1.05-litre reservoir prior to pre-filling. Both reservoirs are charged to a total pressure of about 20 barg.

After pre-filling the balloon, a signal from the NI 6259 control unit triggers the fast-acting valve that separates the 1.15-litre air reservoir from the dust reservoir. A specially designed nozzle at the inlet to the dust reservoir creates swirling flow that entrains the dust and transports the suspension down the annular tube towards the dispersion nozzle. The inner tube serves as a cable gland for the spark gap. The dust is injected into the balloon through the dispersion nozzle. The default delay from onset of dispersion to activation of ignition by electric discharges or chemical igniters is 1 second. For tests with gaseous fuels at initially quiescent conditions, ignition is triggered several minutes after injecting air into the balloon.
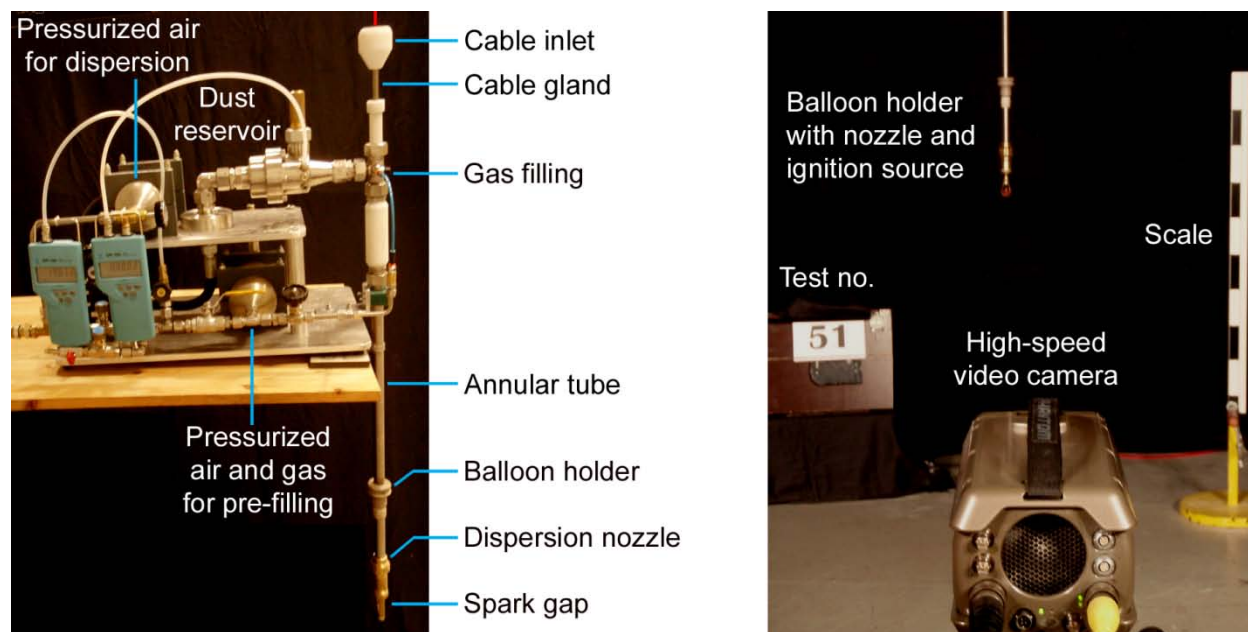
Figure 1 *Experimental apparatus and experimental setup for the balloon experiment.*

Figure 2 shows the dispersion nozzle, the spark gap, the holder for 40 J chemical igniters, and various ignition sources. Electrical discharges worked well for igniting gaseous fuels, but did not work for turbulent dust clouds. Experience from various demonstration experiments suggested that a glowing coil could be a reliable ignition source for dust. However, after several attempts it was concluded that flow induced during the dispersion process cooled the coil sufficiently to prevent ignition. It was possible to ignite some dust clouds with a heated metal sphere or ceramic tube, but hot surfaces were nevertheless abandoned as ignition sources because it was not possible to control the time of ignition.

The 2 x 5 kJ chemical igniters used in the 20-litre vessel could not be used: not only did the balloon rupture more or less instantaneously, but strong radiation from burning particles emitted by the igniter made observation of flame propagation inherently difficult. In the end, the dust explosion tests were ignited by triggering a 40 J chemical igniter, placed inside an open plastic cap to limit the extent of volumetric ignition. Figure 3 shows selected frames after firing a 40 J

chemical igniter in air, and for reason of comparison after firing two 5 kJ chemical igniters inside a balloon with nominal dust concentration 375 g m^{-3} maize starch.
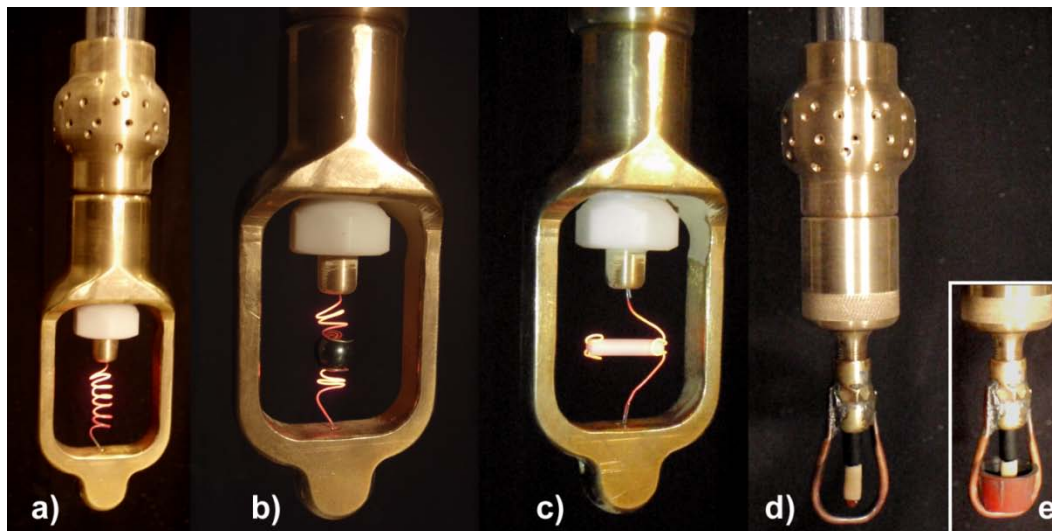

Figure 2 *Dispersion nozzle, spark gap and holder for chemical igniters. Ignition sources tested include: 50-100 mJ electrical discharges over a 3 mm spark gap (not shown); a glowing coil (a); a glowing coil with a metal sphere (b); a glowing coil with a ceramic tube (c); a 40 J chemical igniter (d); a 40 J chemical igniter with a plastic cap (e); two 5 kJ chemical igniters (not shown).*
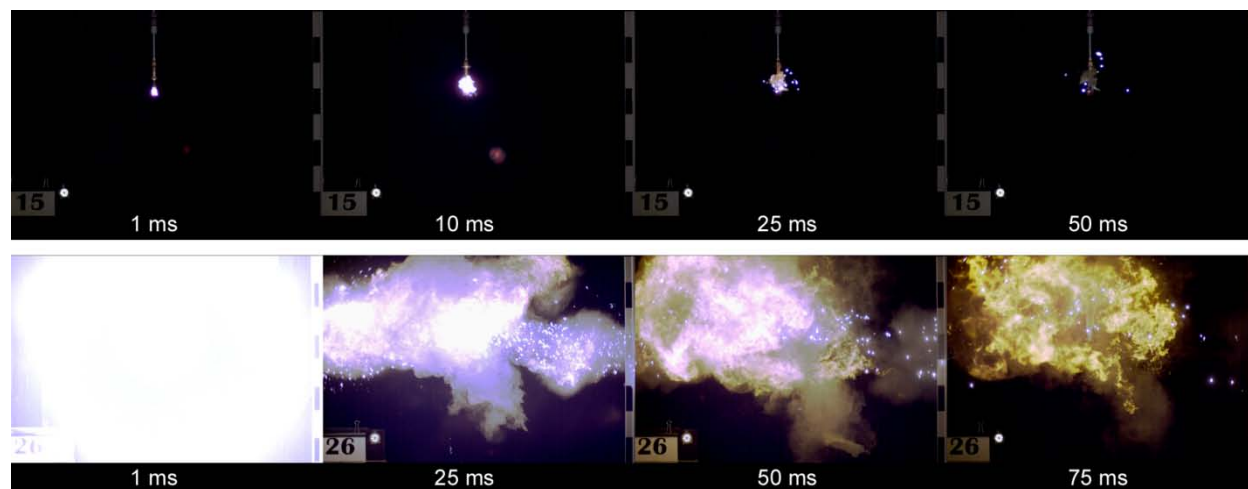
Figure 3 *Chemical igniters: 40 J igniter fired in open air (above), and two 5 kJ igniters fired inside a balloon with 375 g m^{-3} maize starch (below).*

A Phantom v210 digital high-speed video camera recorded the propagating flame and the expanding balloon at a temporal resolution of 2000 frames per second. The volume of both flame and balloon was estimated by counting pixels in selected frames, translating the pixel counts by means of the scale included in the pictures, assuming symmetry around the vertical axis, and assuming near spherical shape of flame and balloon. Figure 4 shows selected frames during an initial test where a balloon was gradually filled in order to compare the volume estimated from the procedure outlined above, to the volume estimated from the measured pressure drops in the reservoir during filling. Figure 5 summarizes the results, including pressure development in the

balloon. The camera observations under-predict larger balloon volumes, but since the test took about two hours to complete, some air may have escaped. For the relevant range of balloon volumes, the overpressure in the balloon is in the range 13-26 millibars.
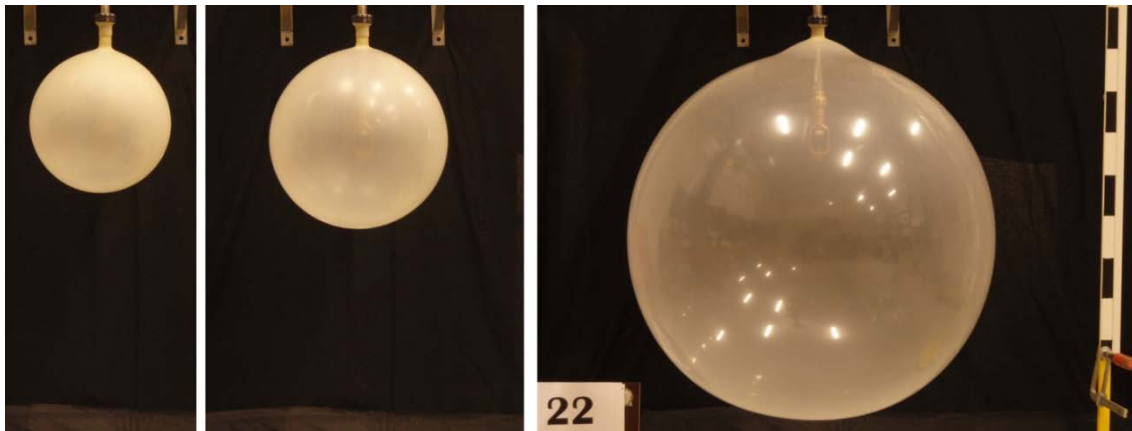

Figure 4 Selected frames during filling of a balloon: 20 liters, a typical volume after pre-filling, prior to dispersion; 40 liters, a typical volume at time of ignition; and 360 liters, nine times the volume at time of ignition.
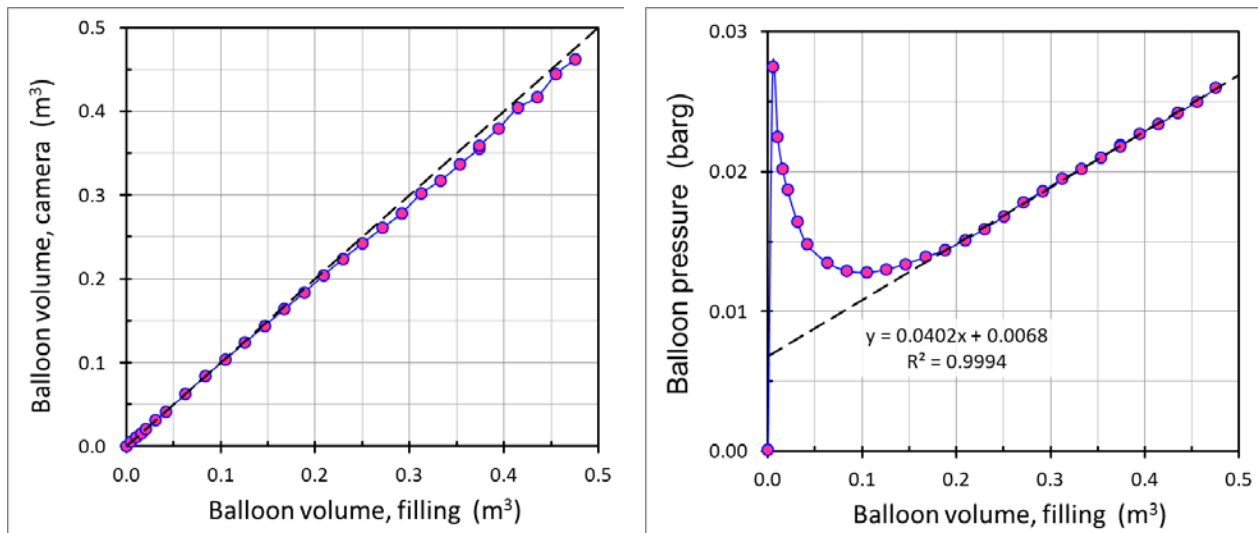

Figure 5 Balloon volume estimated from photographs (left) and balloon pressure (right), both as a function of balloon volume estimated from pressure differences in the high-pressure reservoir during stepwise filling of the balloon.

The experiments with gaseous fuel were performed with propane-air mixtures under initially quiescent or turbulent conditions, ignited one second after onset of dispersion with either an electrical discharge or a 40 J chemical igniter. The dust explosion experiments were performed under turbulent conditions and ignition with 40 J chemical igniters after a delay time of one second. Two types of dusts were used: spores of *Lycopódium clavátum* (Stag's-horn Clubmoss) [10] and maize starch (Meritena A) [24]. The *Lycopódium* spores are close to monodisperse, with mean particle diameter 32 μm [10]. The particle size distribution for the maize starch was measured by laser diffraction (Malvern Mastersizer X), and the standard percentile readings were 10, 13 and 20 μm for the 10, 50 and 90 percentile, respectively [24].

Results

Experiments with propane-air mixtures

Various propane-air mixtures were tested: lean (about 3.4 %), slightly over-stoichiometric (about 4.7 %) and rich (about 6.2 %). Eqs. 1-5 assumes an infinitely thin and spherical flame front, and the approach should therefore be best suited for calculating burning velocities in initially quiescent mixtures. Figure 6 shows some typical results for propane-air mixtures ignited by an electric discharge. The linear increase in flame radius up to the point where the flame starts to interact with the balloon makes it straightforward to calculate flame speed according to Eq. 2, and provided the expansion ratio is known the burning velocity can be calculated according to Eq. 3. The burning velocities plotted in Figure 6 illustrate how sensitive the results obtained directly from Eq. 5 are with respect to small errors in the measured flame and balloon radius.
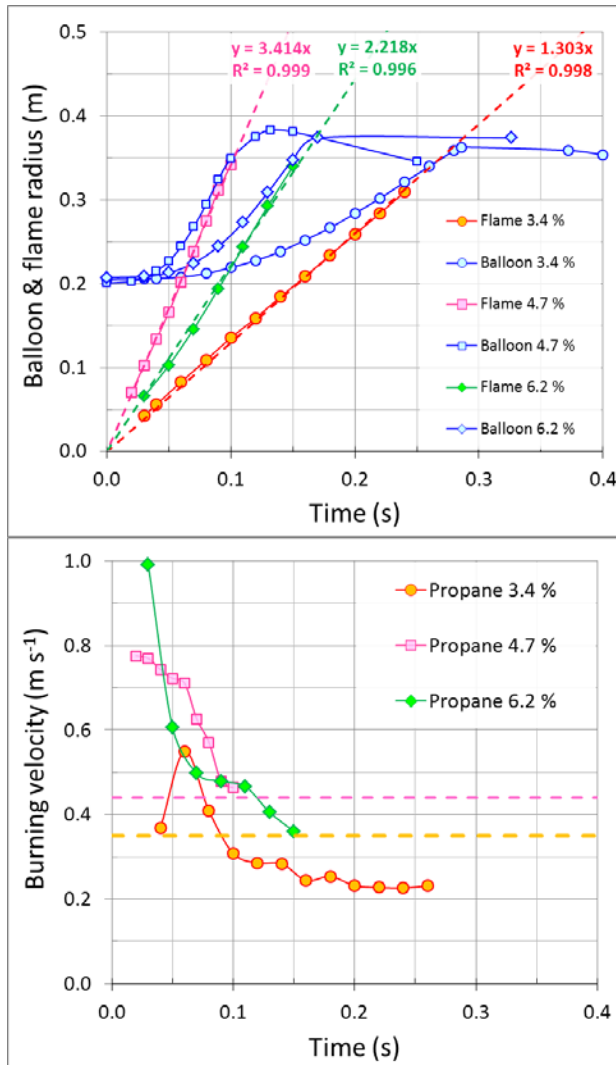
Figure 6 *Balloon and flame radius for various propane-air mixtures (left) and corresponding burning velocities according to Eq. 5 (right). The horizontal lines indicate literature values [25] for laminar burning velocity in 3.4 and 4.7 % propane-air mixtures.*
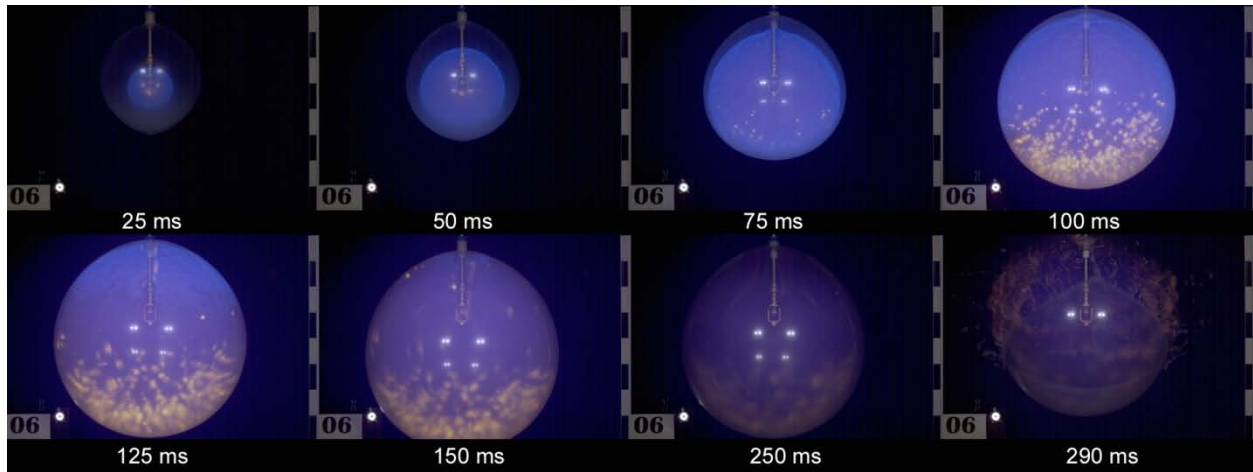
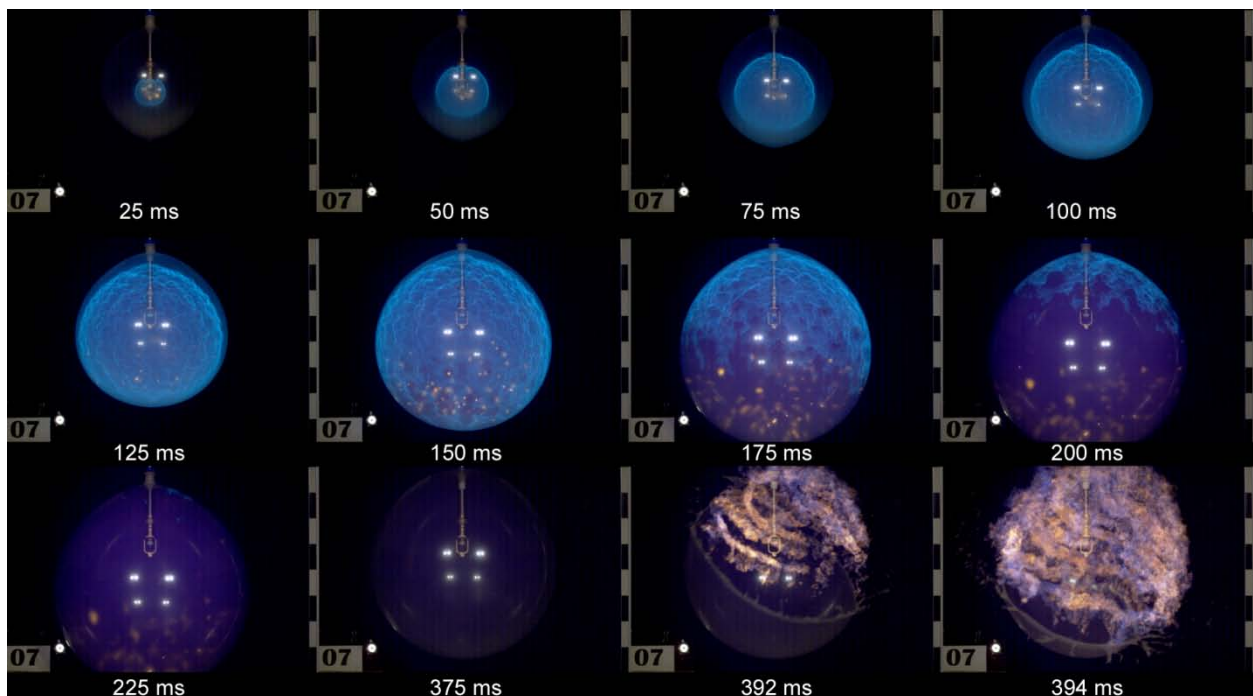***Figure 7*** *Selected frames from test no. 6: initially quiescent mixture of 4.7 per cent propane in air, ignited with a spark discharge.*
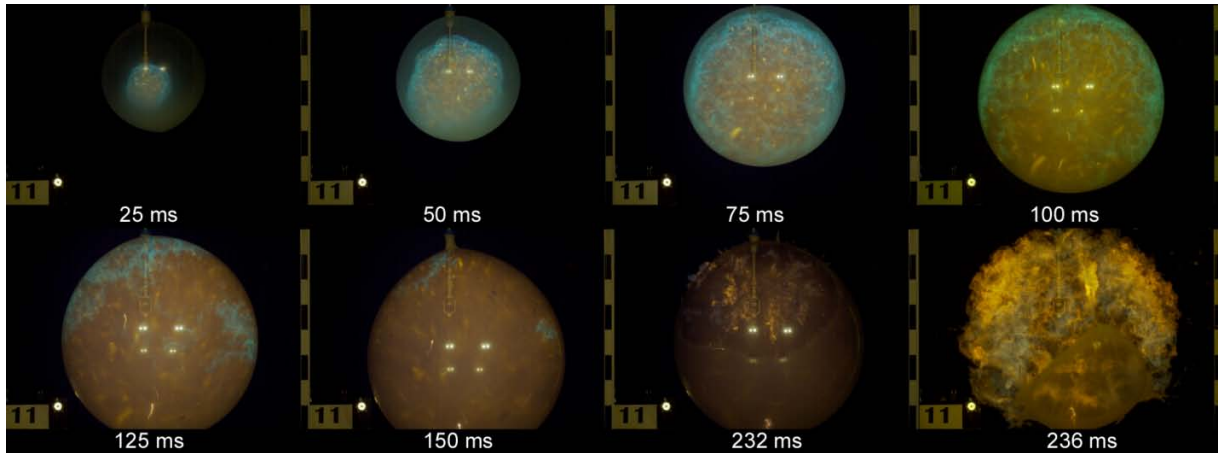
Figures 7 and 8 show selected frames from two tests with initially quiescent propane-air mixtures, ignited by an electric discharge. Flame wrinkling is significantly more pronounced for the rich mixtures. Figure 9 show results from a test with initial turbulence, and comparison with Figure 8 shows that both flame structure and burning velocity are significantly influenced by turbulence.

Figure 8 *Selected frames from test no. 7: initially quiescent mixture of 6.2 per cent propane in air, ignited with a spark discharge.*

Figure 9 *Selected frames from test no. 11: initially turbulent mixture of 6.2 per cent propane in air, ignited with a spark discharge.*

Dust explosion experiments

Figures 10 and 11 show selected frames from two tests with nominal concentration 140 g m^{-3} *Lycopódium clavátum* where the balloon only increased slightly in size, and did not rupture.
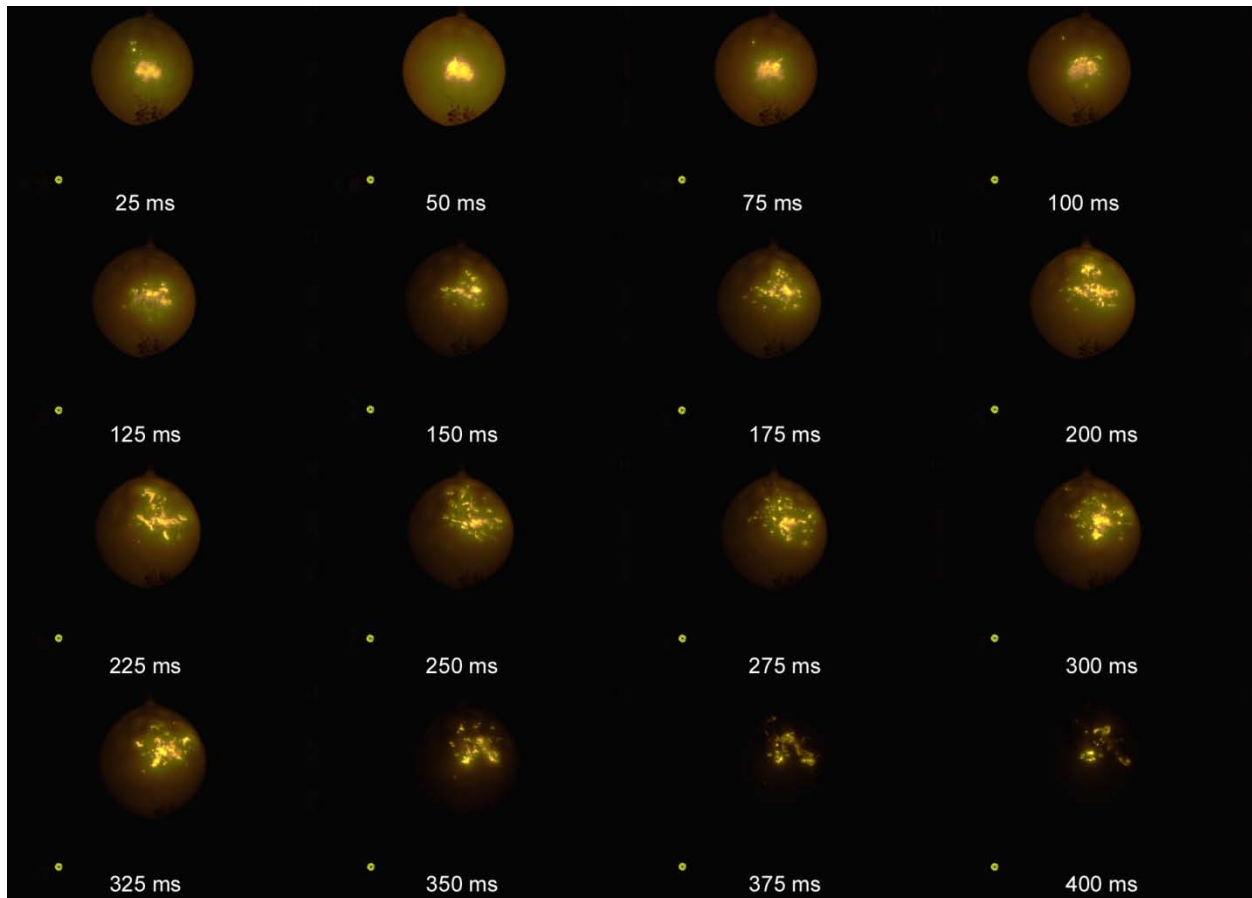

Figure 10 *Selected frames from test no. 17: Lycopódium clavátum, ignited by 40 J chemical igniter, nominal dust concentration 140 g m^{-3}.*
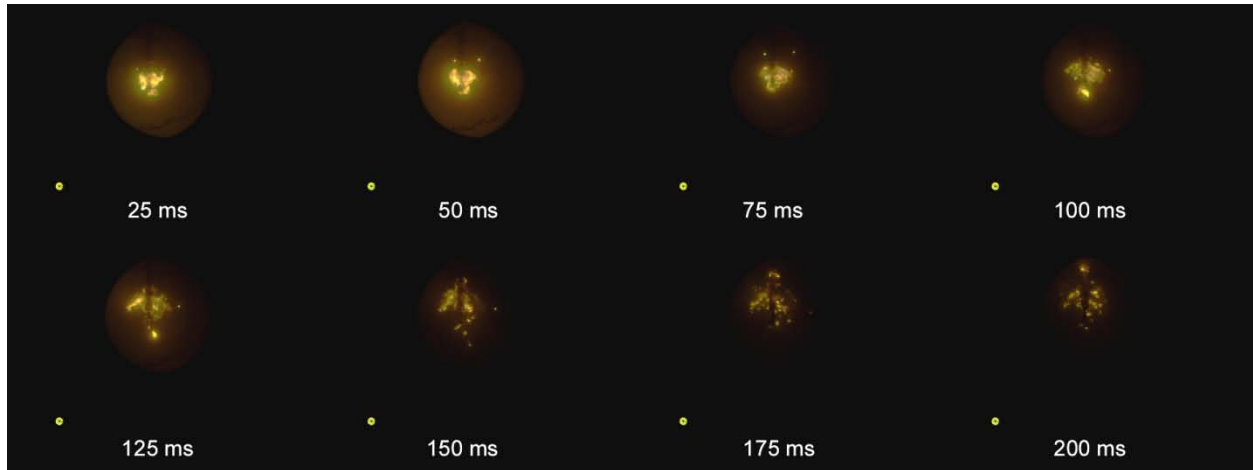
Figure 11 *Selected frames from test no. 56: Lycopódium clavátum, ignited by 40 J chemical igniter, nominal dust concentration 140 g m^{-3}.*

The visible flame in Figures 10 and 11, or at least combustion products emitting radiation, is observed significantly beyond the first 50 milliseconds when the ignition source is still active, see Figure 3. However, it appears the flame is sufficiently 'diluted' by the turbulent flow field to prevent regular flame propagation, and the flame eventually dies out. Similar behaviour was observed for tests with relatively low concentrations of maize starch dispersed in air. It should be pointed out that the average actual dust concentration is significantly lower than the nominal dust concentration, since significant amounts of dust settle in the bottom of the balloon.

Figures 12 and 13 illustrate flame propagation in clouds of *Lycopódium* spores dispersed in air, with nominal dust concentrations 140 and 210 g m^{-3}. Unfortunately it was rather difficult to follow the flame front from the video recording, since radiation from the flame is scattered in the dust cloud. Figure 14 indicates the estimated average radius of the flame front and the expansion of the balloon for the test illustrated in Figure 13. The behaviour differs significantly from the tests with gaseous mixtures summarized in Figure 5, but further analysis is required before any conclusions can be drawn from these results.

Figure 15 shows results from a test with nominal dust concentrations 425 g m^{-3} maize starch. The flame appears to be distributed throughout the balloon at a relatively early stage. The radiation is significant reduced, and the balloon shrinks somewhat, before the balloon ruptures. It is worth noticing the formation of turbulent flame balls when the balloons ruptures, and the similarity between tests with dust and rich mixtures of gaseous fuel.
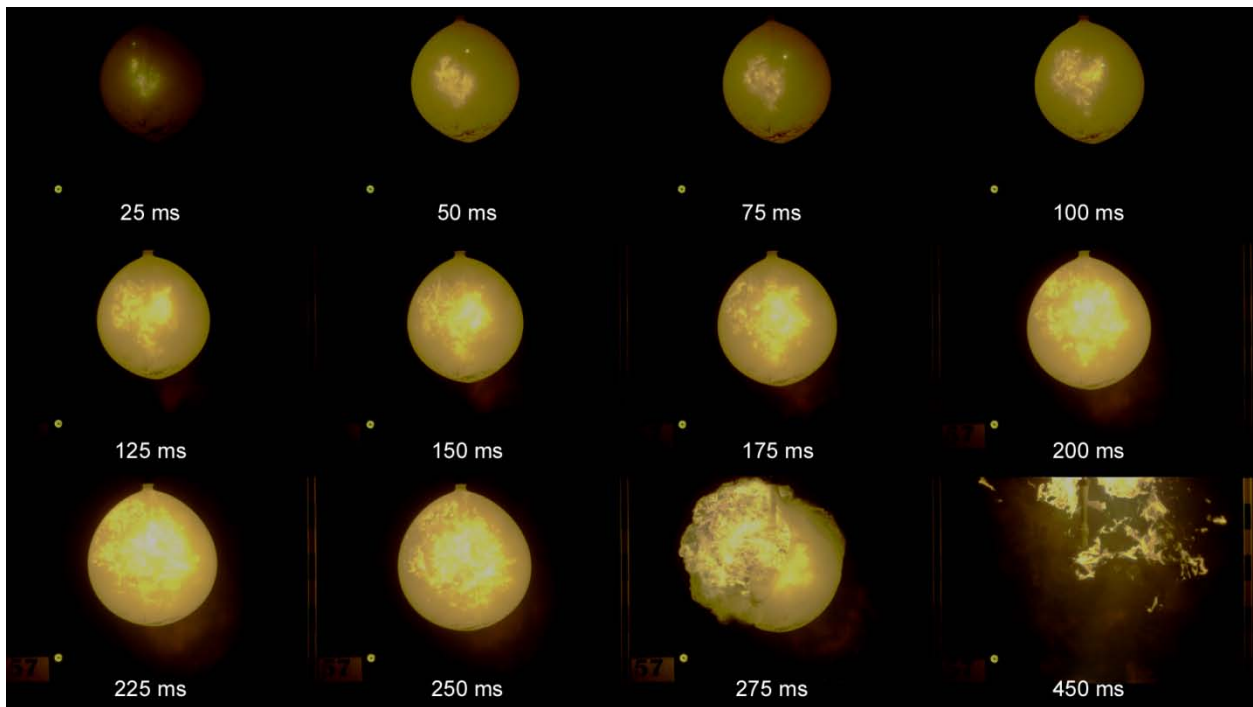

Figure 12 *Selected frames from test no. 57: Lycopódium clavátum, ignited by 40 J chemical igniter, nominal dust concentration 210 g m^{-3}.*
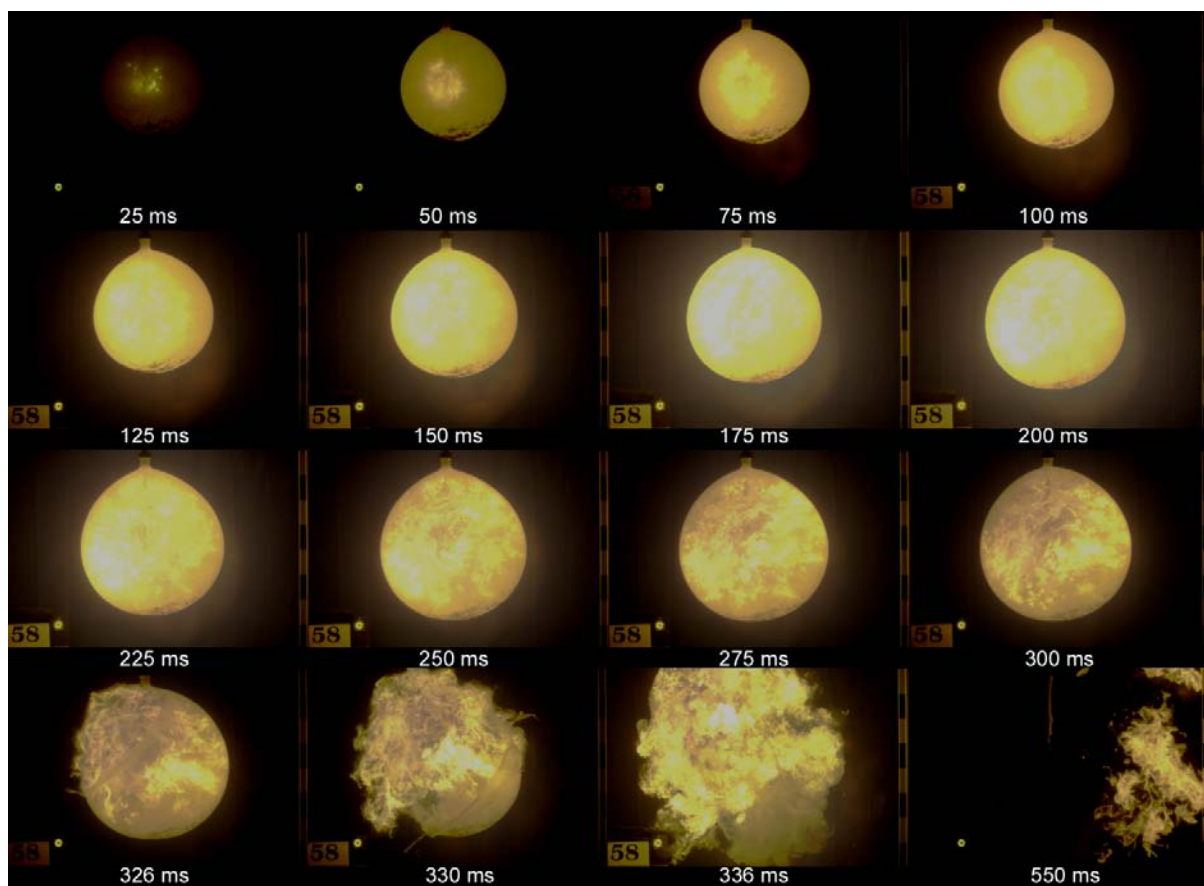
Figure 13 *Selected frames from test no. 58: Lycopódium clavátum, ignited by 40 J chemical igniter, nominal dust concentration 285 g m^{-3}.*
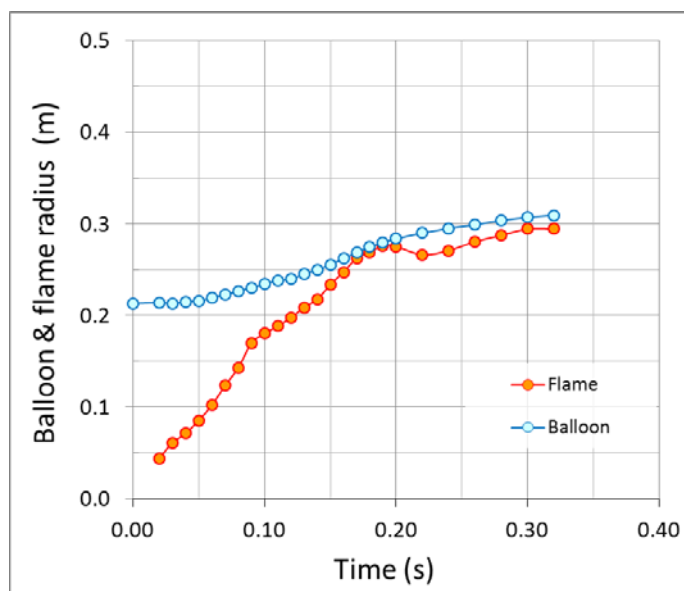

Figure 14 *Estimated balloon and flame radius for test no. 58: Lycopódium clavátum, ignited by 40 J chemical igniter, nominal dust concentration 285 g m^{-3}.*
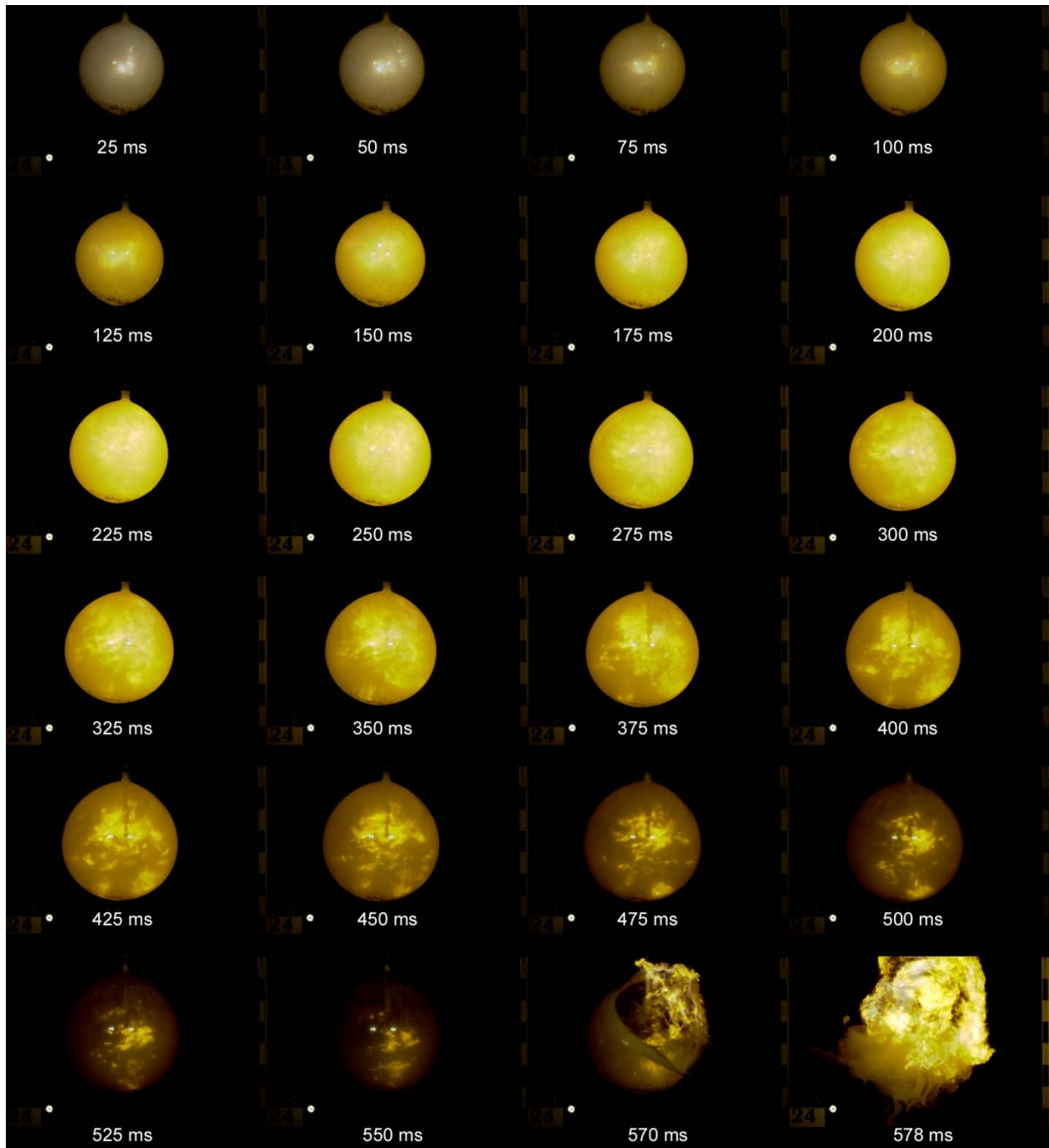
Figure 15 *Selected frames from test no. 58: Meritena A maize starch, ignited by 40 J chemical igniter, nominal dust concentration 425 g m^{-3}.*

Discussion and conclusions

A balloon experiment has been constructed for studying flame propagation in dust clouds at near constant pressure. It was not straightforward to perform sufficiently accurate measurements of flame speed to support reliable estimates of burning velocity and flame thickness in dust flames, and further improvement to the methodology is necessary. Several key parameters could not be measured or controlled in the experiments, including the actual dust concentration, relevant turbulence parameters, as well as pressure and temperature inside the balloon. The possibility of performing dust and gas explosion experiments at near constant pressure, in an apparatus where flame propagation and volumetric expansion can be observed more or less directly, nevertheless represents an interesting complement to established tests in constant volume explosion vessels. The results may also prove useful for validating the sub-grid models that various CFD codes use for describing the initial phase of flame propagation. On a final note, the balloon experiment is well suited for teaching and demonstration purposes: it is straightforward to set up, it is quite safe to operate, and it is a well-known fact that *"no one can be uncheered by a balloon"* [26].

References

[1] Eckhoff, R.K. (2003). *Dust explosions in the process industries*. Third edition. Gulf Professional Publishing, Amsterdam.

[2] Skjold, T. (2007). Review of the DESC project. *Journal of Loss Prevention in the Process Industries*, **20**: 291-302.

[3] Skjold, T. (2010). Flame propagation in dust clouds: challenges for model validation. *Eighth International Symposium on Hazards, Prevention and Mitigation of Industrial Explosions* (ISHPMIE), 5-10 September 2010, Yokohama, Japan: 11 pp.

[4] ISO 6184-1 (1985). Explosion Protection Systems – Part 1: Determination of explosion indices of combustible dusts in air. International Organization for Standardization (ISO).

[5] EN 14034-1 (2004). Determination of explosion characteristics of dust clouds – Part 1: Determination of the maximum explosion pressure P_{max} of dust clouds. European Committee for Standardization (CEN), Brussels, September 2004.

[6] EN 14034-1 (2006). Determination of explosion characteristics of dust clouds – Part 2: Determination of the maximum rate of explosion pressure rise $(\mathrm{d}p/\mathrm{d}t)_{max}$ of dust clouds. European Committee for Standardization (CEN), Brussels, May 2006.

[7] ASTM E-1226 (2010). Standard test method for pressure and rate of pressure rise for combustible dusts. American Society for Testing and Materials (ASTM), January 2010.

[8] Dahoe, A.E., Zavenbergen, J.F., Lemkowitz, S.M. & Scarlett, B. (1996). Dust explosions in spherical vessels: the role of flame thickness in the validity of the ´cube-root law´. *Journal of Loss Prevention in the Process Industries*, **9**: 33-44.

[9] Dahoe, A.E. (2000). Dust Explosions: A Study of Flame Propagation. PhD-thesis, Delft University of Technology, Delft, Holland.

[10] Skjold, T. (2003). Selected aspects of turbulence and combustion in 20-litre explosion vessels. MSc Thesis, Depart. Physics, University of Bergen, Bergen, Norway: 324 pp.

[11] Dyduch, Z. & Skjold, T. (2010). An assessment of the laminar burning velocity in dust/air mixtures based on a model for dust explosions in closed 20-litre vessels. *Eighth International Symposium on Hazards, Prevention and Mitigation of Industrial Explosions* (ISHPMIE), 5-10 September 2010, Yokohama, Japan: 11 pp.

[12] Brown, K.C. & James, G.J. (1962). Dust explosions in factories: a review of the literature. Safety in Mines Research Establishment (SMRE), Research Report No. 201: 67 pp.

[13] Dahoe, A.E., Hanjalic, K. & Scarlett, B. (2002). Determination of the laminar burning velocity and the Markstein length of powder-air flames. *Powder Technology*, **122**: 222-238.

[14] Stevens, F.W. (1923). A constant pressure bomb. National Advisory Committee for Aeronautics (NACA), Report No. 176: 305-310.

[15] Fiock, E.F. & Roeder, C.H. (1935). The soap-bubble method for studying the combustion of mixtures of CO and O_2. National Advisory Committee for Aeronautics (NACA), Report No. 532: 451-464.

[16] Pickering, H.S. & Linnett, J.W. (1951). Burning velocity determinations: Part VI – The use of Schlieren photography in determining burning velocities by the soap bubble method. *Transactions of the Faraday Society*, **47**: 989-992.

[17] Strehlow, R.A. & Stuart, J.G. (1953). An improved soap bubble method of measuring flame velocities. *Fourth International Symposium on Combustion*: 329-336.

[18] Leyer, J.-C., Guerraud, C. & Manson, N. (1974). Flame propagation in small spheres of unconfined and slightly confined flammable mixtures. *Fifteenth International Symposium on Combustion*: 645-653.

[19] Lind, C.D. & Whitson, J. (1977). Explosion hazard associated with spills of large quantities of hazardous materials, Phase II. United States Department of Transportation, Coast Guard Final Report, Report no. CG-D-85-77, (ADA 047585).

[20] Brossard, J., Desbordes, D., Difabio, N., Garnier, J.L., Lannoy, A., Leyer, J.C., Perrot, J. & Saint-Cloud, J.P. (1985). Truly unconfined deflagrations of ethylene-air mixtures. Tenth International Colloquium on the Dynamics of Explosions and Reactive Systems (ICDERS), Berkeley, California.

[21] Pedersen, G.H. (1994). Measurement of laminar burning velocity in balloons. Christian Michelsen Research (CMR), Report No. CMR-94-F25002, Bergen, Norway.

[22] Skjold, T. & Eckhoff, R.K. (2006). A balloon experiment for dust explosions. Poster *Thirty-first International Symposium on Combustion*, 6-11 August 2006, Heidelberg: 606.

[23] Skjold, T., Eckhoff, R.K., Enstad, G.E., Kalvatn, I.B., van Wingerden, M. & van Wingerden, K. (2008). A modified balloon experiment for dust explosions. Poster *Thirty-second International Symposium on Combustion*, 3-8 August 2008, Montreal, Canada.

[24] Skjold, T., Arntzen, B.J., Hansen, O.J., Storvik, I.E. & Eckhoff, R.K. (2006). Simulation of dust explosions in complex geometries with experimental input from standardized tests. *Journal of Loss Prevention in the Process Industries*, **19**: 210-217.

[25] Law, C.K. (1993) in: Peters, N. & Rogg, B. (Eds.): Reduced Kinetic Mechanisms for Application in Combustion Systems, Springer, Berlin.

[26] Milne, A.A. (1926). Winnie-the-Pooh. Methuen & Co, London.